STUDY REPORT

SR 304 (2013)

Post-Earthquake Performance of Passive Fire Protection Systems

P. C. R. Collier

The work reported here was funded by BRANZ from the Building Research Levy whose logo is shown above.

ISSN: 1179-6197

Preface

This a final report on the earthquake damage to passive fire protection (PFP) systems that was part of a larger collection of projects looking into the earthquake damage to fire protection systems in general. The broader findings of which have been disseminated in a series of reports and a nationwide seminar series.

The experimental investigation sought to determine the principal parameters that dictate how damaged PFP systems may behave in fire and the mechanisms for failures.

Acknowledgments

This work was funded by the Building Research Levy.

The assistance of building owners and managers in the City of Christchurch in granting access to their damaged buildings is greatly appreciated. Without their support, this project would not have been possible.

Brent Houston for his assistance with the preliminary assessment of the suitability of damaged buildings for more detailed internal surveys.

Note

This report is intended for building inspectors, engineers, architects, designers, builders, manufacturers and building owners.

Post-Earthquake Performance of Passive Fire Protection Systems

BRANZ Study Report SR 304 (2013)

P. C. R. Collier

Reference

Collier PCR, 2013. Post-Earthquake Performance of Passive Fire Protection Systems, BRANZ Study Report 304, BRANZ, Judgeford, New Zealand.

Abstract

Passive fire protection (PFP) systems that are damaged by earthquakes may suffer significant reductions in fire resistance, resulting in increased risks to life safety in the event of an outbreak of post-earthquake fire and subsequent spread. In the aftermath of the Canterbury (New Zealand) earthquake events, damage to PFP systems has been surveyed in moderately-damaged buildings. The degree of damage observed ranged from minimal to moderate damage where some fire resistance remains, to extensively damaged where no protection remains.

This paper focuses on damage in the low-to-moderate range where the majority of PFP systems protecting a fire compartment were largely intact, but one or two systems such as a doorset or a firewall were showing some degree of damage that compromised the protection of the whole fire compartment.

Following the building surveys, selected elements of damage to PFP systems were built into the fire resistance test specimens as defects and instrumented with thermocouples to assess the failure mechanisms. The reduction in fire resistance of the damaged systems was correlated to the degree of damage in such form as the size of gaps, furnace pressure and oxygen content of the fire gases, and then compared with fluid flow theory in restrictive openings.

Traditionally, the focus has been on the risk of fires immediately following an earthquake event when the occupants are evacuating and damaged PFP coupled with inoperable sprinklers due to loss of water supply and impeded egress routes are likely to impact life safety. It is now also acknowledged that PFP may be damaged in an otherwise structurally safe building that may be reoccupied post-earthquake; this research additionally provides a basis for building assessors to require that damaged PFP be restored to specification.

Looking to the future, methods of minimising damage to PFP systems by isolating them from the lower amplitude movements of the main building structure offer promising possibilities, not just from a perspective of ensuring the performance of PFPs post-earthquake. There is an economic benefit as well where a building deemed structurally sound for reoccupation requires only minimal if any repairs to PFPs.

Contents Page

Figures Page

Tables Page

1. INTRODUCTION

This project has provided a significant insight into the robustness of passive fire protection (PFP) systems in a major earthquake and what the implications are for post-earthquake fire safety in buildings.

On-site inspections of passive fire protection systems in commercial buildings in Christchurch were undertaken to ascertain the amount of damage that has occurred as a result of the earthquake events in 2011 followed by an experimental programme to determine the impact of similarly damaged systems on the overall fire performance.

The findings will provide clear guidance as to what regulatory changes are required, with the overall benefit from the research being improved social and economic outcomes in the event of serious post-earthquake fires in the New Zealand built environment.

2. BACKGROUND

The background to this study considered the characteristics of the initial earthquake and an aftershock, seismic design and the risks of post-earthquake fire (Baker, Collier, Abu, and Houston 2012). It is of significance that the active systems (sprinklers) were largely rendered inoperable by a combination of loss of storage tank water supplies, electricity supply to pumping systems and severing of sprinkler pipework in the earthquake events. Considering the 50% reduction in PFP protection permitted where sprinklers are installed, this represents a serious shortfall in the level of protection if the already reduced level of PFP is also damaged and unlikely to perform.

2.1 The Canterbury earthquakes of 2010-11

When earthquakes occur there are usually three key statistics quoted in the news media to characterise the event, namely the magnitude, the location (often referred to as the epicentre) and the depth of the earthquake below the earth's surface. It is generally the case that, the greater the magnitude, the closer the proximity of the epicentre, and the shallower the earthquake, then the greater the damage to buildings. The time of day that the earthquake occurs is also often quoted in news reports. While the former three parameters have a direct bearing on the damage that buildings will sustain and, indirectly, injuries and fatalities, the timing of an earthquake can have a dramatic bearing on the number of casualties.

The initial earthquake occurred at 4.35 am on Saturday 4 September 2010 was followed by a subsequent major aftershock, which occurred at 12.51 pm on Tuesday 22 February 2011. The September 2010 event had a magnitude of 7.1 and was centred 40 km to the west of the Christchurch central business district (CBD), near the rural town of Darfield, at a depth of 10 km. The aftershock in February 2011 had a magnitude of 6.3 and was centred 10 km south-east of the CBD near the port suburb of Lyttelton, at a depth of 5 km (DBH 2012).

The key difference between the two seismic events was the proximity to the CBD area and, to a lesser extent, the depth of the earthquakes, which had a dramatic effect on the level of ground shaking that occurred. Earthquake ground shaking is measured in terms of acceleration, which is expressed as a proportion of the gravitational acceleration, *g*. In the September 2010 event, the impact was widespread and severe, but no major modern buildings collapsed and there was no loss of life. There was substantial damage to unreinforced masonry buildings in the CBD area, with the major hazard being falling

masonry, but because of the time of day the earthquake occurred, there was no loss of life (DBH 2012).

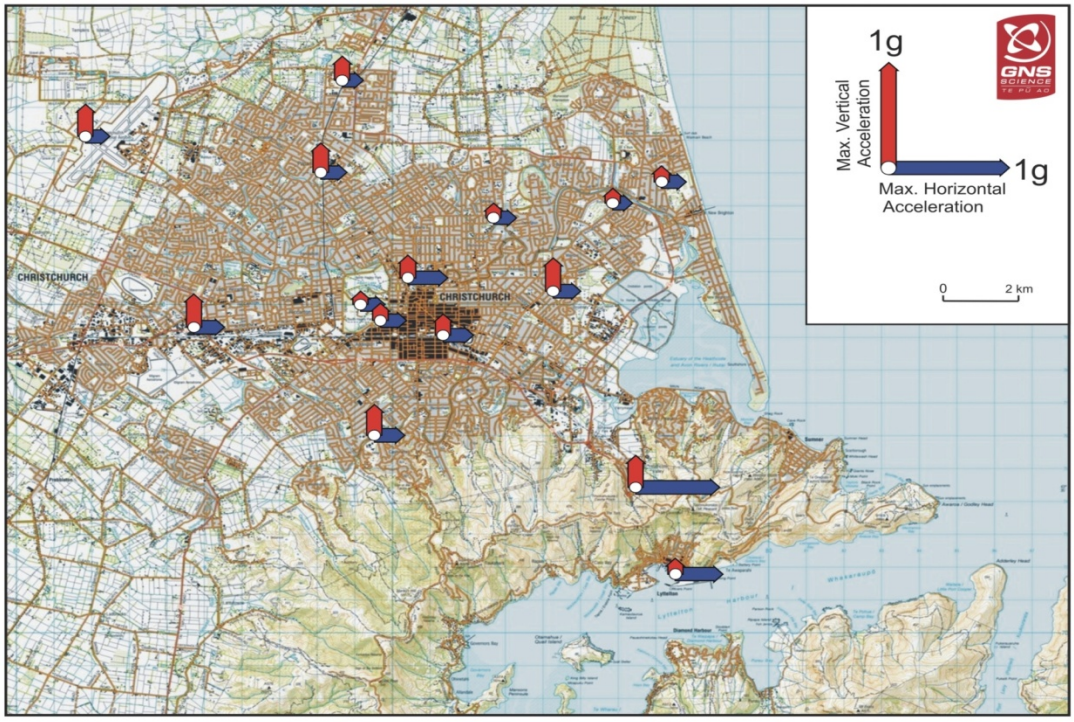

Figure 1: Peak ground accelerations – September 2010 (courtesy GNS Science)

Figure 1 shows the horizontal and vertical peak ground accelerations (PGAs), which were recorded by a network of accelerometer measuring stations in and around Christchurch, for the September 2010 event. In the CBD area (shaded black in the centre) the PGAs are approximately 0.2-0.3 g.

2.2 Lyttelton aftershock – February 2011

In the February 2011 aftershock, severe damage occurred to buildings in the CBD and in eastern and southern suburbs. A large proportion of modern commercial buildings in the CBD area were significantly damaged and many (older) unreinforced masonry buildings collapsed. At least two multi-storey buildings collapsed and precast concrete stairs collapsed in at least four modern multi-storey buildings (DBH 2012).

The vertical PGAs in the epicentral area were in the range 1.8-2.2 g – amongst the highest ever recorded in an urban area. The relatively short duration of the aftershock moderated the PGAs in the CBD area, where the vertical PGAs were in the range 0.5-0.8 g, as shown in Figure 2. The horizontal PGAs near the epicentre exceeded 1.6 g, and in the CBD were between 0.4-0.7 g (DBH 2012).

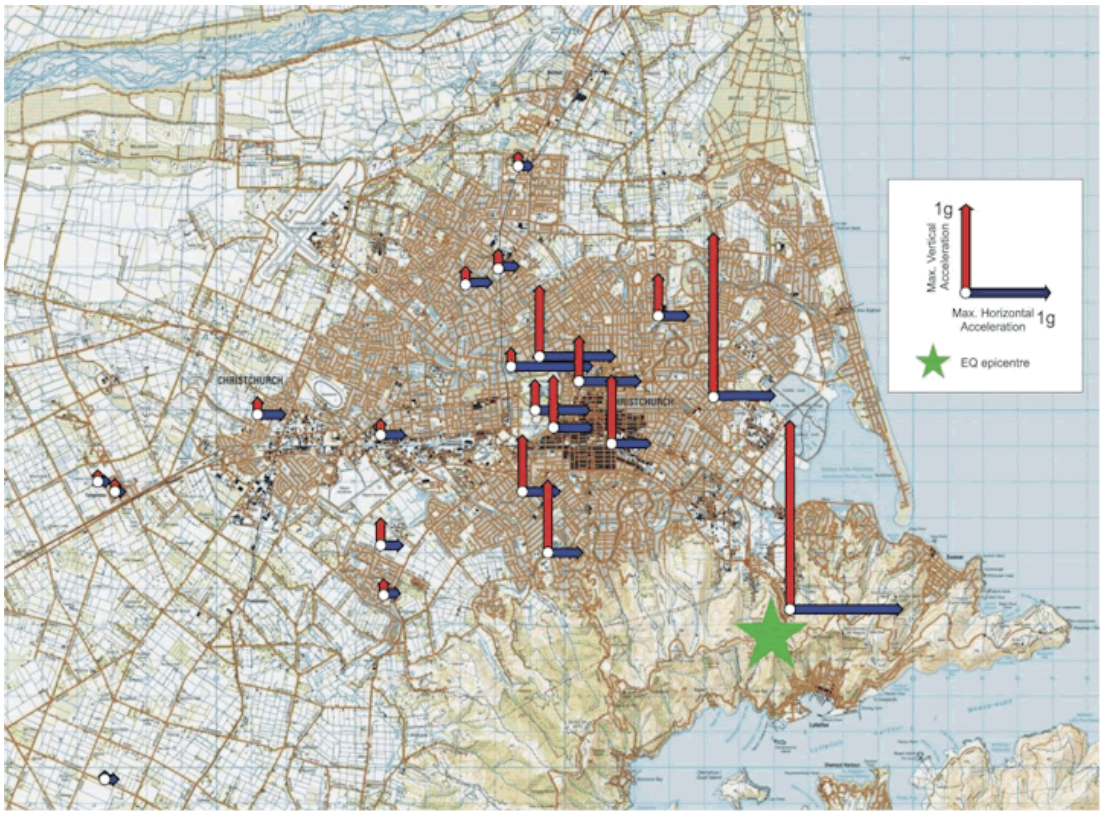

Figure 2: Peak ground accelerations – February 2011 (courtesy GNS Science)

2.3 Seismic design

In a structural engineering context, buildings are designed to resist a combination of actions such as self-weight (dead), superimposed (live), snow, wind and earthquake loads. When these design actions are dominated by seismic forces, the building design is known as "seismic design". Seismic loading is a low-likelihood/high-consequence scenario and it is therefore uneconomic to design buildings for the maximum likely ground motion. Generally therefore, buildings are designed to respond inelastically to the ground motion but allowing sufficient ductility to prevent collapse (Dhakal 2011). Essentially this design approach seeks to prevent structural collapse but accepting that significant, even irreparable, damage is likely to occur (DBH 2012).

In New Zealand, buildings are designed in accordance with the seismic loadings standard (NZS 1170.5:2004), which is cited in the compliance document for New Zealand Building Code (NZBC) clause B1 *Structure* (DBH 2011), using the limit state design method. The ultimate limit state (ULS) is achieved when there is a very low risk of: 1) structural collapse; 2) failure of parts or elements of the building that would be life threatening; or 3) failure of parts or elements whose function is critical for safe evacuation (NZS 1170.5 Supp 1:2004). The annual probability of exceedance (AS/NZS 1170.0:2002) for the ULS of a normal use building is 1/500 (500-year return period), i.e. these buildings are designed for earthquake ground shaking intensities expected to occur, on average, not more than once every 500 years [1]. For important buildings such as hospitals and the like, the corresponding threshold is 1/2500.

In Figure 3, the elastic design spectrum (horizontal) from the seismic loadings standard [3] are shown for both a 1/500 and a 1/2500 event for the ULS, as well as spectral accelerations (horizontal) for the February 2011 event from four measuring stations around the perimeter of the CBD area. It can be seen from Figure 3 that, for normal use buildings in particular, the ground accelerations in and around the CBD exceeded the

level required by the NZBC. The specific requirements in the seismic loadings standard to design for vertical acceleration are less stringent than the horizontal action. With regard to period, typical commercial/industrial buildings would be in the range 0.5-1.5 seconds.

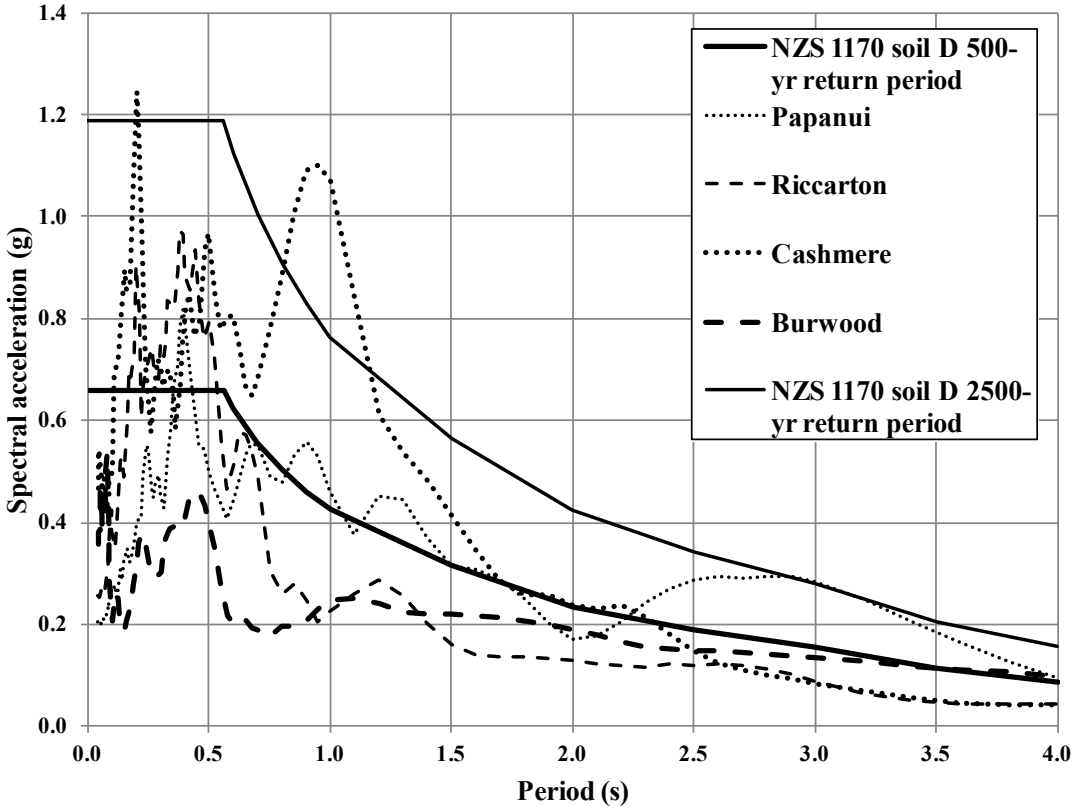

Figure 3: Design spectrum and recorded accelerations – February 2011 (recorded data courtesy GNS Science)

2.4 Post-earthquake fires

Large fires in urban areas following an earthquake are relatively rare events. The two largest post-earthquake fires in urban areas of the 20th Century occurred in San Francisco, US, in 1906 and Kanto, Japan, in 1923 (Scawthorn 1984 and Borden 1994). The 1906 San Francisco earthquake was magnitude 7.9 and there was a death toll of more than 3000 people. Fire caused 80% of the damage, amounting to a burnt area of 12.2 km^2 and 28,000 buildings. In the 1923 Kanto earthquake, the magnitude 8.2 event resulted in 140,000 fatalities and a burnt area of 38.3 km^2 (Scawthorn 1984).

After the recent earthquakes in Canterbury, virtually no earthquake-related fires occurred, which questions the need to consider the threat of fire following earthquakes. There were a number of factors, however, which contributed to the lack of fires occurring after the September 2010 and February 2011 seismic events. The two fundamentals which impact the occurrence of post-earthquake fires are fuel and ignition sources. Christchurch does not have extensive underground gas reticulation and in the more destructive February 2011 event there were breakages in the above-ground reticulation due to building collapses but the underground network remained intact. The reticulation was isolated at the four supply points around the city within two-three hours of the earthquake occurring. Gas would have been present for a few hours afterwards until lines depressurised. The reticulation system remained off for several weeks until it could be progressively tested and reinstated. There was no record of fires from gas leaks following the September 2010 and February 2011 events. The time of day for the first

earthquake in September 2010, in the early hours of the morning, meant typical ignition sources, such as those from gas heating, were virtually nonexistent. In February 2011, being the middle of a working day in mid-summer, the same conditions were present (Baker 2012).

Christchurch may be considered a lower post-earthquake fire risk due to its low level of gas reticulation, but the risk is much more serious for North Island cities with more extensive gas reticulation due to the ease of connections to the natural gas pipeline network throughout the island.

3. BUILDING SURVEYS

The focus of the building surveys was the PFP systems in order to gather data on the types of damage that occurred and to replicate typical damage in the laboratory for fire testing.

3.1 Passive fire protection systems

Following the February 2011 earthquake, a series of inspections of passive fire protection systems in buildings were carried out. In some buildings, the damage had been so extensive that the passive fire protection was destroyed. The focus of the investigation was on damage in the low-to-moderate range, i.e. where the building was structurally safe but where damage to passive fire protection had occurred, so that the impact of earthquake actions on passive fire protection could be quantified.

An example of a six-storey commercial building assessed in the building survey is shown in Figure 4. The ground floor comprised a retail outlet on the left side and an entrance lobby on the right, with an elevator and a stairwell servicing the five levels above that were open plan offices. A second stairwell servicing the upper five levels also connected to the ground level alley providing a second means of egress.

Figure 4: Six-storey office building surveyed

3.1.1 Firewalls

A close up of the 30/30/30 firewall between the retail store and the entrance lobby, as shown in Figure 5, separates the two tenancies and provides protected egress from the floors above through the lobby. Because the building is fitted with sprinklers a 50% reduction of the otherwise required fire resistance rating of 60 minutes is permitted thus

reducing it to 30 minutes and this is achieved with 13 mm of standard plasterboard each side of a timber or steel frame.

Figure 5: Fire wall between retail store and entrance lobby

Inside the entrance lobby the plasterboard is extensively cracked at end and top corner as shown in Figure 6.

Figure 6: Severe cracking at opposite ends of the 30/30/30 firewall inside the entrance lobby

The cracking and detachment of the plasterboard on the top edge of the lobby side of the wall is shown in Figure 7.

Figure 7: Top edge of entrance lobby firewall

On the retail store side of the wall the lining is cracked on opposite sides as shown in Figure 8.

Figure 8: Opposite sides of firewall left to right, retail store and lobby

The service penetration carrying electrical cabling through the lobby wall shown in Figure 9 had some cracking between the rack and the ceiling and it is unknown whether the

ceiling-to-plasterboard interface or the penetration is the cause of the plasterboard cracking. In this case the degree of damage is relatively minor compared with other parts of the same wall, so it is most likely the first failure of fire resistance would be at the more severely damaged locations. The upper side of the cable penetrations through the concrete floor was not located to assess the level of any damage there.

Figure 9: Service penetration though lobby firewall and floor above

The two stairwells servicing all levels provided a safe path for egress with Integrity and smoke control of -/30/- SM for the fire doors and the surrounding walls rated at FRR 30/30/30 for the protection between the occupied spaces on each floor and the stairwell. Inspections focused on the condition of the fire doors, the condition of the plasterboard surrounding the doors and the plasterboard in the stairwells.

Figure 10: Fire door between stairwell and floor, -/30/- SM view from the stairwell side, intumescent strip is included to achieve smoke control

Fire doors were one area of focus for the site inspections, with a range of damage being observed. In Figure 10, the gap down the door jamb has increased from 2-3 mm originally to 4-16 mm after the earthquakes and the gap at the top right corner had increased to 7 mm. For all but the smallest of increases in gap from the original 2-3 mm that the doorset passed the required fire resistance test, the intumescent seal is unlikely to expand enough to fill the gap and the fire resistance will be significantly compromised.

Figure 11: 1.5 mm gap between door stop and leaf

On the other side of the same door where the “leaf-to-frame” gap was 16 mm at the bottom there was a 1.5 mm gap (see-through) between the leaf and the door stop as shown in Figure 11. In exposure to fire, especially from the office space side, it is likely that only minimal deflection of the door leaf on heating will be required to result in a rapid opening of the gap, allowing smoke into stairwell. Integrity failure is also deemed to have occurred if the gap increases to greater than 6 mm.

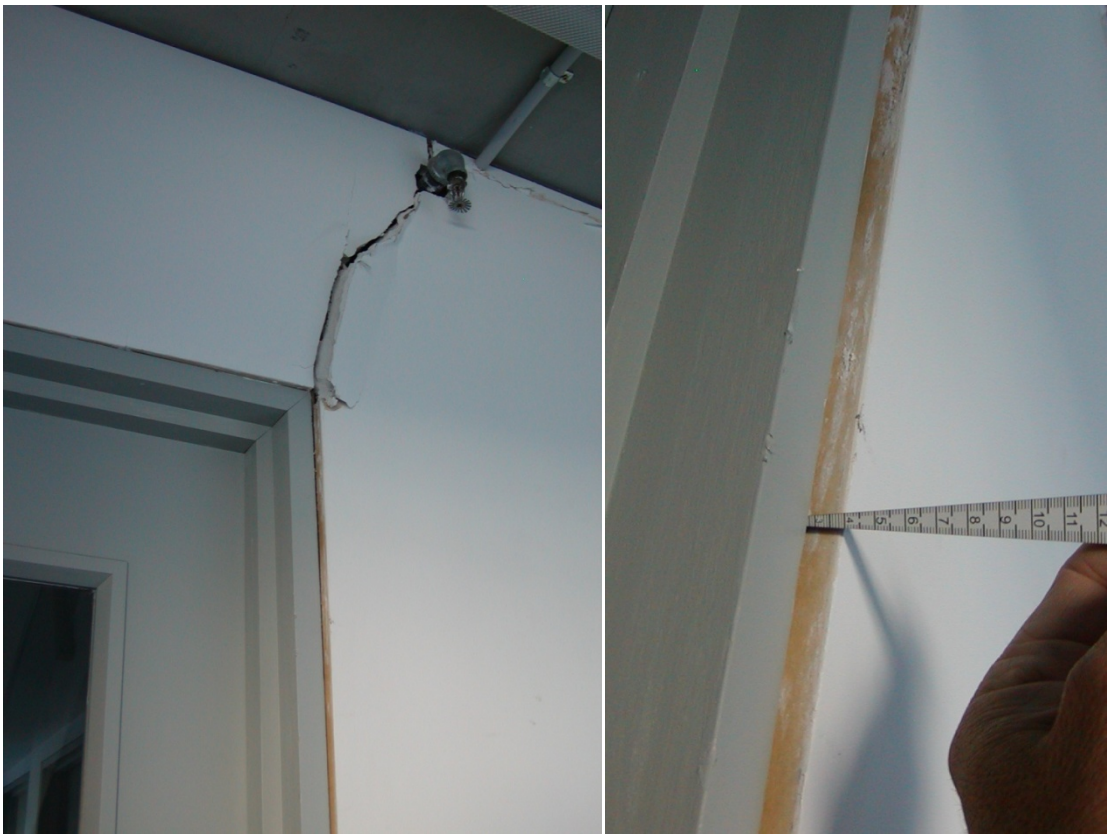

Figure 12: Cracked and displaced lining on stairwell side of door frames

Damage to plasterboard was also observed around door frames particularly at the top corners. Figure 12 shows damage to the fire-rated lining at the head of the door and a 7 mm displacement between the lining and door frame. If movement of the door frame is greater than clearances around the leaf, then the fracture and displacement of the plasterboard lining is more likely. In some cases the door leaf-to-frame clearances may return to their near original position but the displacements during the event have extensively damaged the plasterboard.

Figure 13: Vertical crack on plasterboard above door frame and 7 mm gap between plasterboard and door frame

Plasterboard tends to open gaps where there is a joint between sheets formed over double studs above door frames (Figure 13).

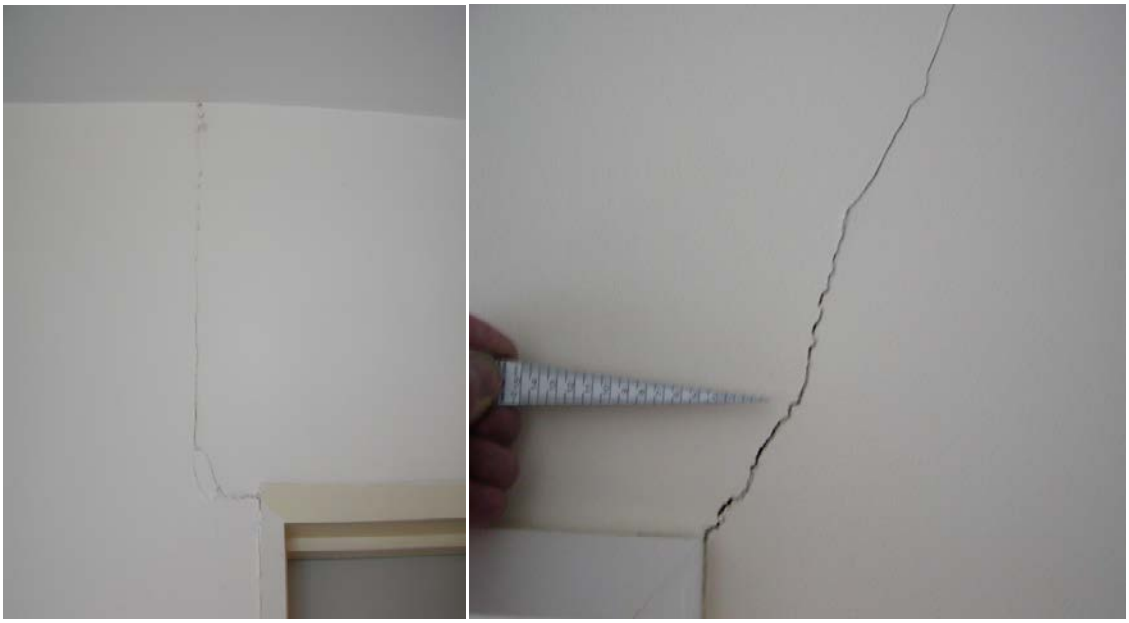

Figure 14: Lining sheets separating on one side and diagonal cracking on the other

In a number of instances a diagonal crack on one side of a door frame was matched by a vertical crack on the other and the gap opening size could be quite different, Figure 14 being a good example.

3.1.2 Stairwells

In the protected stairwells the plasterboard lining sustained some damage as well, typically it was in wall-to-wall internal corner junctions with gaps opening to up to 15 mm on landings between stair flights as well as tread-to-wall gaps opening 5 to 10 mm as shown in Figure 15.

Figure 15: Stairwell plasterboard damage in corner and on stair tread

Figure 16: Plasterboard damage under scissor stair flight

Figure 16 shows the underside of a precast concrete stair where the junction to the fire-rated wall beneath has been crushed or displaced by earthquake-induced motion.

Figure 17: Vertical crack of ~4 mm at lining junction over double studs and opening of gap between stair flight and wall

Although not necessarily confined to stairwells, some instances of vertical openings at plasterboard joints were observed where double studs are covered by lining sheets that also join over the double stud. This type of joint, also found above doors and windows, is particularly prone to opening up in normal service and more so in earthquakes as shown in Figure 17 and provides a ready path for the transport of hot gases and eventually fire.

3.1.3 Elevator shafts

Elevator shafts are protected by the fire-rated shaft walls and the doorset. In the six-level building most of the doorset-to-shaft wall junctions were essentially undamaged. The only exception was on the top level (level 5) which showed movement had left a 10 mm gap between the doorset and shaft wall as shown in Figure 18, representing a risk of smoke and fire movement into elevator shafts and spread to other floors.

The observation that only the level 5 elevator doorset showed noticeable damage not unexpectedly demonstrates that with different levels of building subjected to different displacements in earthquakes – and this concurs with the findings for the building surveys in general – the degree of damage on PFPs can vary considerably. Such is the randomness of earthquakes it is not possible to predict where the damage is going to occur.

Figure 18: Top floor elevator doorset and 10 mm gap on right hand side

Figure 19 shows an elevator doorset in an apartment building that has similar damage around the frame as recorded for swing doorsets.

Figure 19: Cracking of plasterboard surrounding an elevator doorset

3.1.4 Low rise industrial buildings

A broad and mainly external survey of low rise industrial buildings of predominantly concrete tilt slab construction in an industrial area south of the Christchurch CBD indicated that earthquake movement of the buildings and subsequent settlement due to liquefaction were jointly responsible for damage. The external view of a typical tilt slab building is shown in Figure 20 and a close up of the damaged joints in Figure 21 show an internal wall corner junction where the sealant has failed and the concrete fractured at the steel angle attachment. Also an external wall panel butt joint has opened, stretching the silicone sealant and causing it to tear, leaving an opening.

Figure 20: External view of typical concrete tilt slab building

Figure 21: Internal corner and external butt joint

Surveying around the perimeter of the same city block showed that the damage in Figure 22 was fairly typical, with openings such as that shown but also some joints that were compressed as the ground settled unevenly as a result of liquefaction.

Figure 22: Typical opening of butt joints in concrete tilt slab panels

The implications are that the opening of gaps on the external walls represents an increased risk of fire spread to neighbouring buildings. Although fire spread along a street is unlikely, some of the buildings are very close to each other and if gaps or fractures in tilt panels were to match up, then it would be relatively easy for fire to spread to an adjacent premises.

3.1.5 Loss of intumescent paint on steel beams

In a different multi-storey building that was not part of the BRANZ survey of PFP, the loss of intumescent paint was recorded in Figure 23. In this case paint had detached from the beam below the ceiling, most likely due to multiple cyclical deflections of the beam leading flaking of the relatively thick coating of brittle paint and potential exposure of unprotected steel in the event of a fire outbreak.

Figure 23: Loss of intumescent paint on steel beam post-earthquake

3.2 Summary of building surveys

Earthquake damage observed in the building surveys covered a wide spectrum.

The original objective was to focus on buildings in the moderate damage range in accordance with the three broad damage categories below:

- Extreme
    - Structurally unsafe and the state of the PFP is of secondary importance
- Moderate (survey focused on this)
    - Structurally safe in general but the PFP is damaged
- Superficial
    - Structurally safe, PFP generally intact and any damage is mainly cosmetic.

Within the moderately-damaged buildings a similar spread of damage was observed and although not in the structurally unsafe category, certain protocols were followed for access to be granted. In the buildings surveyed the degree of damage fell into the following three categories:

- PFP clearly damaged and totally ineffective
- PFP moderately damaged and performance clearly expected to be below specification
- PFP superficially damaged and maybe capable of performing to specification.

From the surveys of the moderately-damaged buildings the following generalised conclusions can be drawn:

- Observed that ~10% of PFP systems compromised in moderately-damaged buildings

- Given multiple PFP systems are protecting one firecell, protection only as good as weakest link
- Doorsets where the leaf-to-frame clearance is increased from the 2-3 mm required to meet the FRR were the most frequently encountered departure from specification and most likely PFP to fail first
- Given multiple PFP systems are protecting one firecell, protection only as good as weakest link
- A potential failure of PFP in 5 to 10% of the barriers protecting one firecell is a serious concern.

Figure 24 presents the probability of failure of any one PFP system when any number up to 25 are protecting a firecell and the probability of the failure of any one is 5 to 10%.

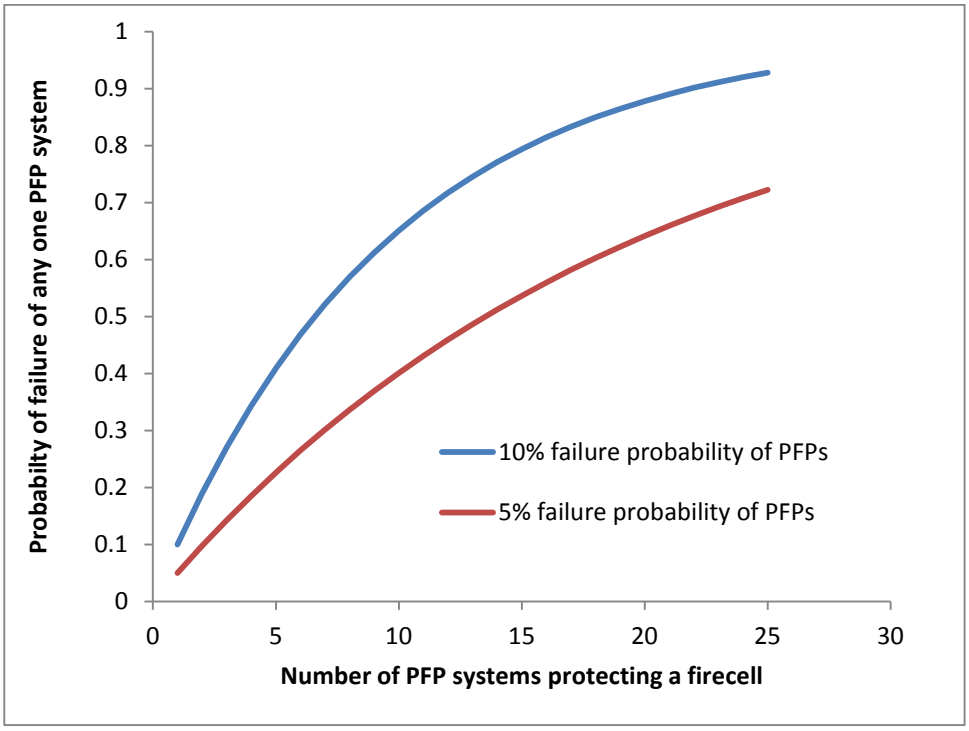

Figure 24: Probability of firecell failure as a result of a single PFP failure

The above concerns apply in the event of fires occurring immediately after an earthquake and also in reoccupied buildings deemed structurally safe but where the damage to PFP systems, mainly of a superficial nature, is not remedied. Furthermore, the ongoing settlement and liquefaction may have changed the damage status of some PFP systems weeks or months later.

4. PREVIOUS BRANZ RESEARCH

A previous BRANZ research project (Collier 2005, 2008) focused on simulating earthquake damage to walls and then subjecting them to a test to determine the reduction in fire resistance.

The earthquake damage was created by racking the test walls back and forth in a prescribed manner to simulate as closely as possible likely earthquake damage as shown in Figure 25. The walls were then subjected to a fire resistance test.

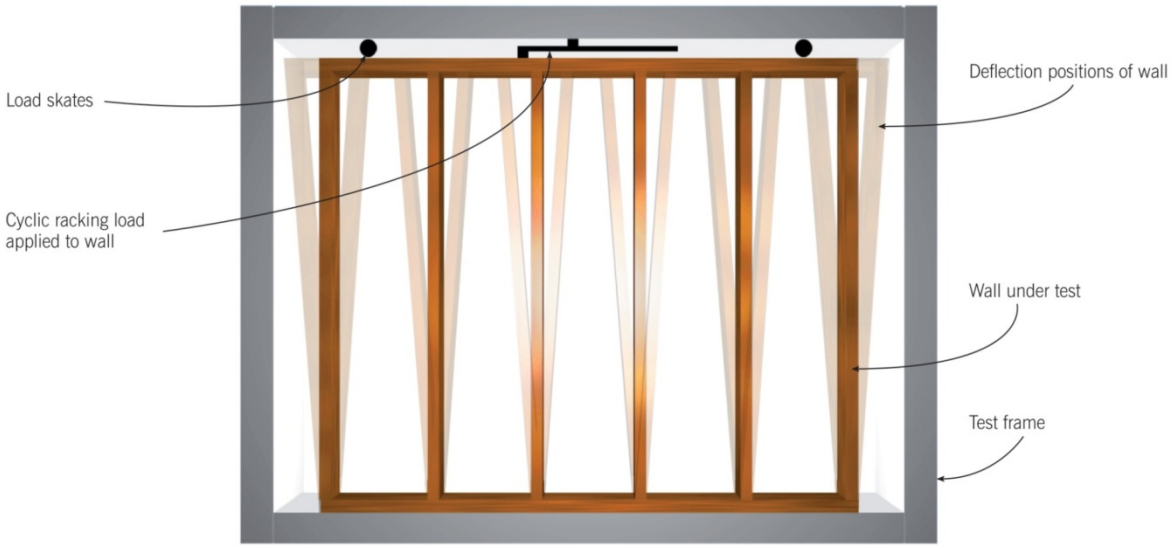

Figure 25: Racking of walls to simulate earthquake damage

The walls tested were five timber-framed and two steel-framed (one included a fire door) and the racking cycle in Figure 26 was intended to simulate a series of earthquake exposures progressively from 1 to 2.5% drift to get a range of damage for fire testing.

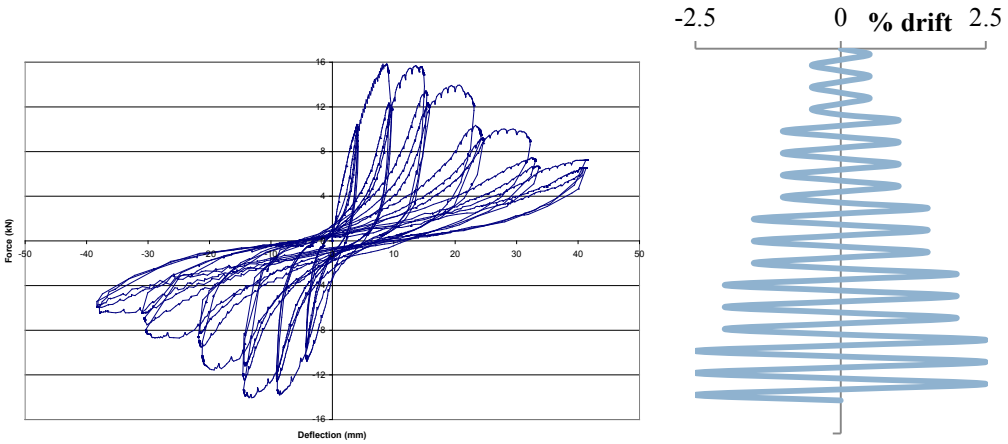

Figure 26: The racking process to simulate earthquake exposure

The walls were racked back and forth in a prescribed manner based on an equivalence of energy that would be imparted into a wall to simulate as closely as possible likely

earthquake damage. Racking started off small, built to a maximum and then back to 0% over typically about 30 cycles, back and forth. The time scale was much slower than an actual earthquake, racking taking place over several tens of minutes whereas an earthquake event may be over in a minute or less.

Following the fire resistance testing of the simulated earthquake damaged walls, these two aspects were examined:

- The reduction in FRR and how it was related to the level of simulated earthquake damage
- The modes of and reasons for failures of the fire resistance.

The reductions in fire resistance are shown in Figure 27, the majority of the reductions fall within a band of 30 to 70% of the base test fire resistance and in all of these tests the first mode of failure was Integrity. The only test not to fail by Integrity was Test C which failed by Insulation, in this case the lining remained attached to the framing after racking and throughout the fire test performing similarly to an undamaged test wall.

The typical damage that resulted in failures was due to:

- Detachment of linings particularly around the perimeter of the test wall
- Cracks on corners and joints.

Restraining the lining around the perimeter with skirting boards, corner details and other junctions was shown to improve performance by preventing detachment of the lining.

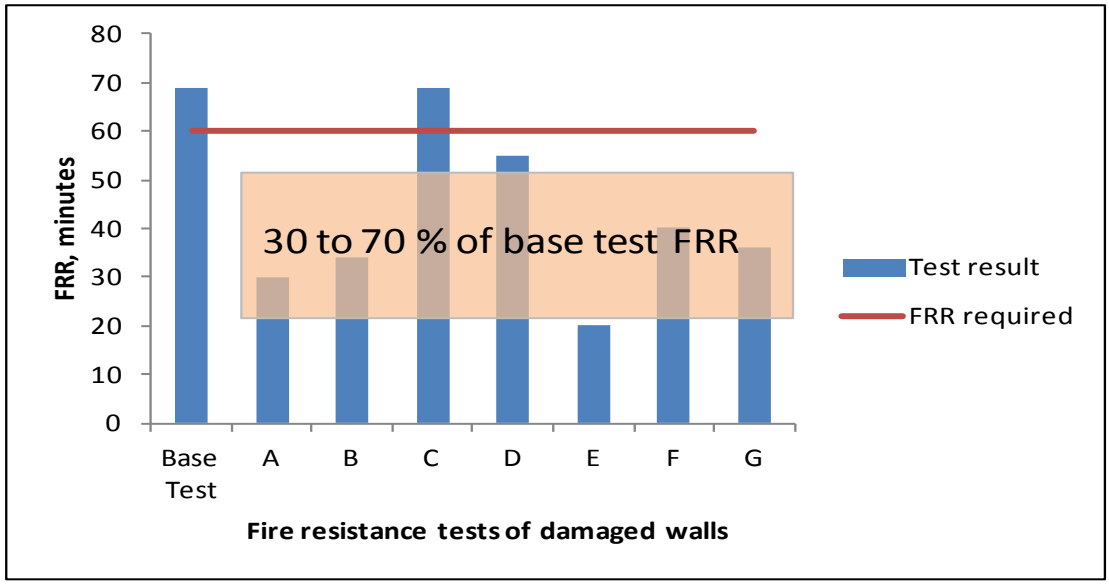

Figure 27: Comparing fire resistance of damaged walls

The Integrity and Insulation failure times for the test walls are compared in Figure 28 and Table 1. Clearly, Integrity predominates as the first failure and comparing Tests C, D and E where the perimeter of the lining was better secured with realistic detailing, there is clearly a “break point” after 1% drift in the racking process after which the fire resistance (Integrity) decreases rapidly.

Table 1: Relationship of drift ratio to Integrity and Insulation failures

Test	Base	A	B	C	D	E	F	G
Mean drift ratio, %	0	1.0	1.4	0.9	1.5	2.2*	1.2	1.3
Integrity failure	69	30	34	69NF	55	20	40	36
Insulation failure	69	47	62NF	67	64	60NF	51	54

* Wall E was fire tested at a 1.5% drift state, all others were returned to 0% for fire test

The types of damage sustained to the walls in the laboratory tests after earthquake simulation by racking were:

- Lining that had worked loose around the fixings to the frame, particularly around the perimeter and in the corners
- In the cases of greater racking, the lining was damaged in the corners, with gaps through the wall
- A door that had resisted racking when the leaf contacted the frame but the frame in turn damaged the surrounding plasterboard wall.

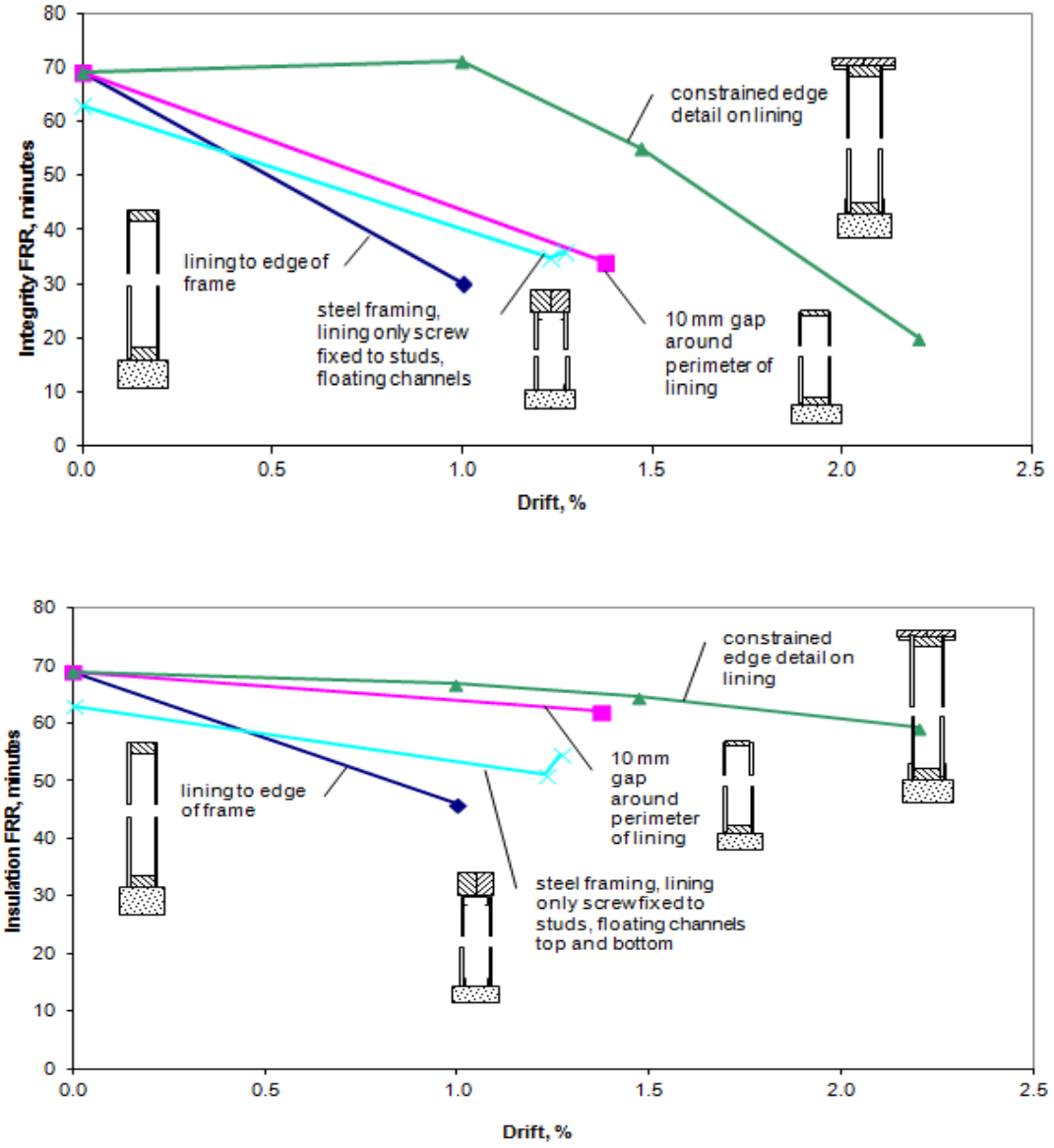

Figure 28: Comparing Integrity (top) and Insulation (bottom) failures versus drift ratio

Insulation failures (as determined by an average temperature rise of 140K or a maximum temperature rise of 180K) are relatively easy to predict. Models have been available for several decades and these can be manipulated by degrading the linings on the basis of damage incurred to show reductions in fire resistance.

Integrity failures (where flaming of greater than 10 seconds from a gap appears) are more difficult to predict and since it is most likely to be the first mode of failure in earthquake-damaged systems, this warrants gaining an increased understanding of the parameters that the fire resistance is sensitive to.

5. THEORY

Extensive modelling of the Insulation and Structural Adequacy modes of failure in fire resistance systems has been conducted over the last two-three decades, but the Integrity failure mode has not received nearly as much attention. Since it is likely the failure mode in earthquake-damaged systems will be Integrity, a theoretical basis needed to be established prior to the testing programme so that the test specimens could be instrumented accordingly. An extensive literature review was unable to find any informative studies of fire spread in gaps, except that by Nightingale and Sultan (1998) considered fire spread in wall cavities with fire stops to prevent fire spread from a floor below.

As a starting point the theory on flame spread on open surfaces was used on the basis that at least it offers some similarities to the process occurring in cavities. The difference being that it is applied to two surfaces facing each other in close proximity which may have an impact on heat transfer. In addition, there are differences in the physical properties of air at ambient and fire temperatures, and a significant one is viscosity, which markedly increases with temperature meaning a difference in resistance to flow depending on the direction. Hot gases flowing outwards from a fire compartment experience more resistance than inward flow of cool ambient air especially if the flow regime is laminar to the transition zone rather than turbulent, a situation more likely in narrow gaps. This phenomenon suggests that fire spread outward through gaps may be less than expected for increasing pressure and elevation, but for flow in the reverse direction the resistance is less. In instances of oscillating flow, fire spread may happen more rapidly if it is easier to draw in fresh air with ambient oxygen even momentarily that feeds the combustion process. The following sections more closely explore this mechanism.

5.1 Factors influencing Integrity failure

A mechanism for reductions in the Integrity fire resistance of timber panels (Craft, Desjardins and Mehaffey 2011) can be attributed to the inward flow of fresh air through small gaps in ~100 mm thick timber panels due to negative pressure inside the furnace. The inward flow of fresh air caused the oxidation of the char layer on the hot exposed surface subsequently leading to the loss of char in the vicinity of the air flow. Eventually, this reduction in char depth leads to an increase in the charring rate in that location and results in a cone-shaped void that slowly grows from the exposed surface to the unexposed surface as shown in Figure 29 (from Test 1 in this project). As the void reached the unexposed layer, the air flow increased due to the enlarging opening and the resulting surface flaming is deemed an Integrity failure.

Figure 29: Cone-shaped charring progression in 6 mm holes, left to right, reducing furnace pressure from 11 Pa to -11 Pa (top to bottom) in BRANZ tests

The failure mechanism described above can be compared with opposed-flow flame spread (Drysdale 1998), (Hasemi 2008). For opposed-flow flame spread, the Damkohler number (Da) characterises the competing effects of providing fresh air at a low velocity to assist with combustion compared with the cooling effect of higher velocity air, which if high enough, has a tendency to extinguish a flame. For air flow in the opposite direction, such as where positive furnace pressure causes hot gases to flow though gaps, it is the heat transfer by hot gases and high radiation (~55 kW/m^2) that determine charring and the influence of oxygen content (~10% in furnace) in reducing the charring rate is considered minimal (Mikola 1990), (Cedering 2006) and (Frequin 2011).

The flow rate and velocity through the narrow gaps in a fire barrier are dependent primarily on the pressure difference and gap size followed by the gas properties of density and viscosity. The density reduces with increasing temperature, but the viscosity increases with increasing temperature. So for hot gases, the resistance to flow is likely to increase more especially if the flow is laminar, as in small gaps, compared with larger gaps where the flow is turbulent (Gross. and Haberman 1989).

Although the pressure in fire resistance furnaces is prescribed to be set at a neutral pressure at say one-third of height, in reality, it is operationally difficult to maintain that pressure and oscillations are common. As a result, the flow through gaps above and below the neutral plane will undergo a cycle of ~10% oxygen hot furnace gases heating the internal surfaces and then cooler 21% oxygen supporting combustion of sufficiently heated surfaces. The potential of an oscillating flow introduces the possibility of a “whipsaw effect” that may, under certain conditions, further reduce the fire resistance due to cycling, thus sustaining more rapid charring and eventually burning on the ambient side.

The expected differences in flow velocity though a range of circular gaps for a range of pressure differences and temperatures are shown in Figure 30. It was assumed the flow into the furnace with negative pressures is ambient air at 20^{o}C and the outward flow with positive pressures is at 1000^{o}C. Comparing the hot (positive (+ve) pressure) and cold (negative (-ve) pressure) for flow out of and into the furnace, the resistance to inward flow of cold air is less than the outward flow of hot gases on the basis of the velocity.

For circular holes (gaps) of 3, 6 and 12 mm in diameter, the results show that the velocity tends to be greater for flow of ambient air into the furnace than for hot gases out of the furnace. All flow is laminar for these conditions. For the larger 24 mm diameter gap, the regime changes from laminar to turbulent for the flow into the furnace and is consequently slowed as the head loss changes with the square of the velocity. This

formulation used to calculate the velocity/pressure relationship agrees with the findings of Gross and Haberman (1989) for flow through door gaps at ambient and elevated temperatures, and it is anticipated that it can be used to give guidance on likely Integrity failures through gaps in the experimental programme related to actual earthquake-induced damage.

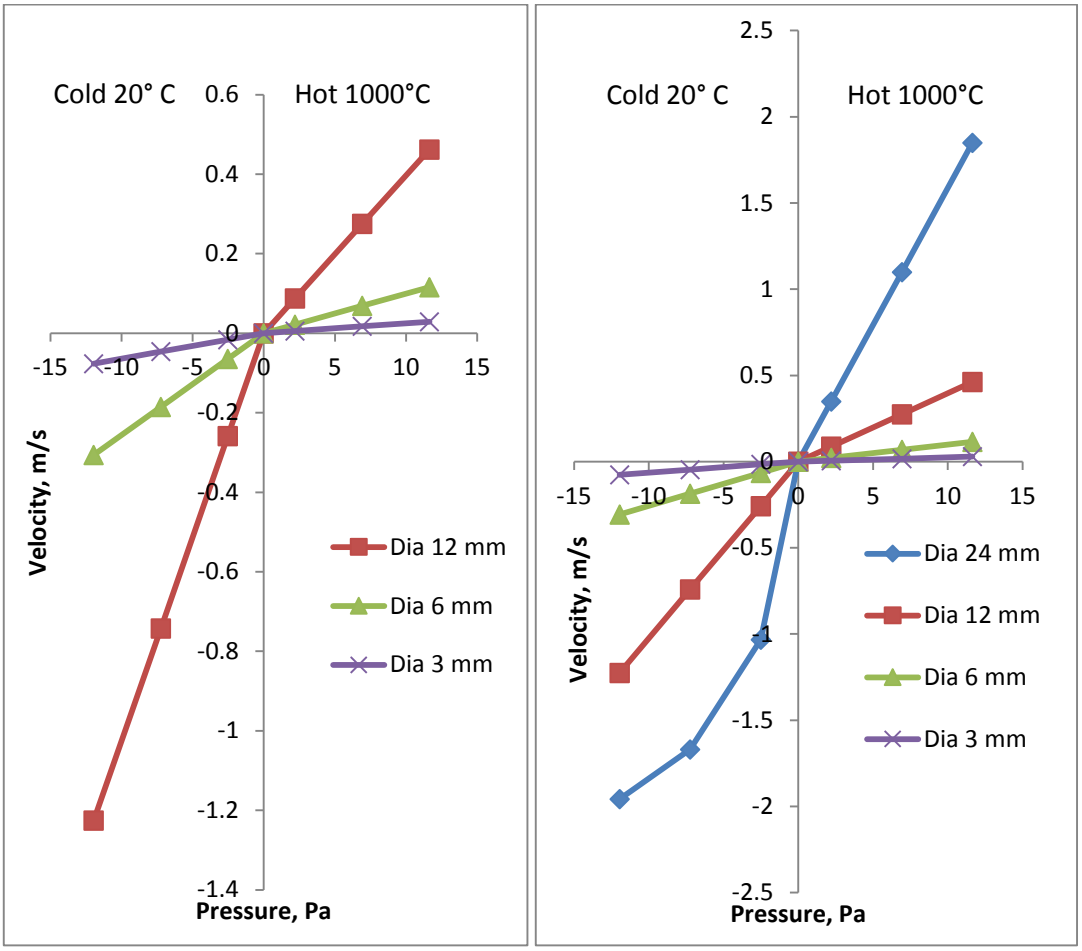

Figure 30: Predicted flow velocity through circular gaps versus furnace pressure

The calculations are based on fluid flow theory considering the Reynolds number (Re) based on velocity, viscosity, density and diameter (hole size) to determine the friction factor *f* for the flow from a Moody diagram to determine velocity versus pressure difference in accordance with Equation 1.

$$h_f = \frac{\Delta p^*}{\rho g} = \frac{4fl}{d}\frac{\bar{u}^2}{2g} \; or \; = \frac{fl}{m}\frac{\bar{u}^2}{2g} \quad \text{..... Equation 1}$$

The friction factor (*f*) is primarily determined by the Reynolds number (Re) in accordance with Equation 2 and a Moody diagram as shown in Figure 31 and Figure 32.

$$Re = \frac{\rho v d}{\mu} = \frac{v d}{\nu} \quad \text{..... Equation 2}$$

The area of the moody diagram of interest in this study is in the lower velocity laminar transition region with Reynolds numbers below 3 x 10^3. The friction factor for the laminar region is well defined by f = 16/Re, but exactly where the transition zone applies will depend to an extent on the roughness and Figure 32 shows some uncertainty as to the value of the friction factor (f).

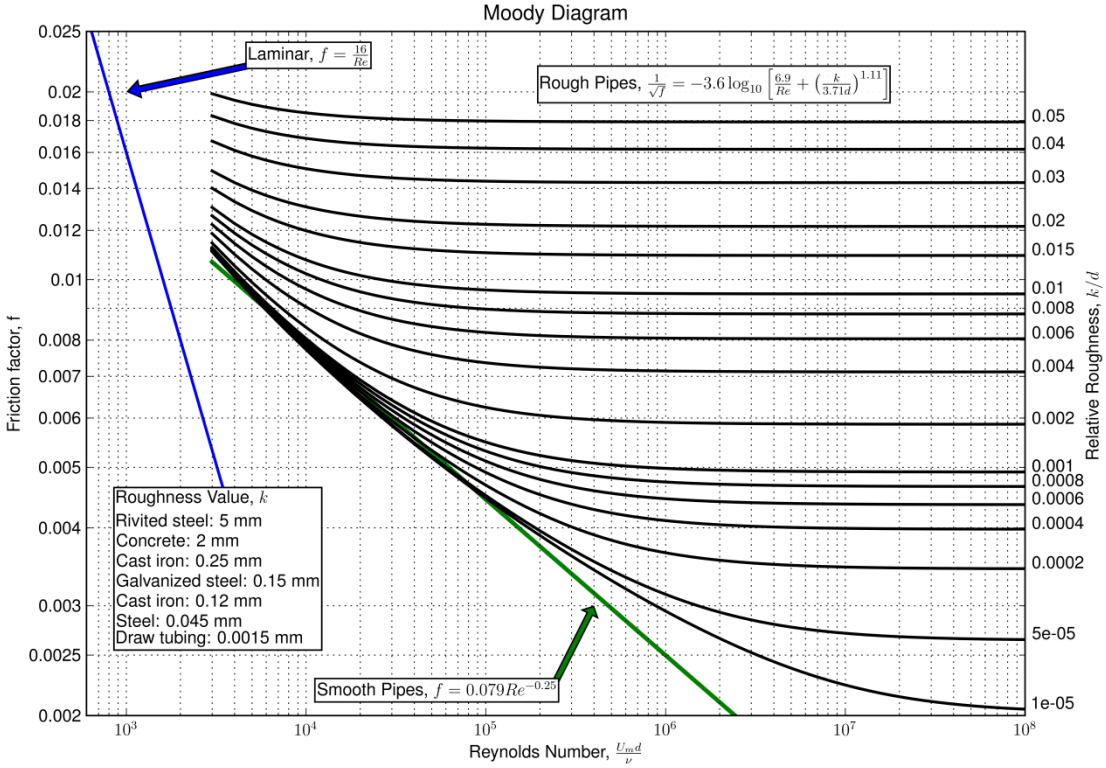

Figure 31: Moody diagram (1)

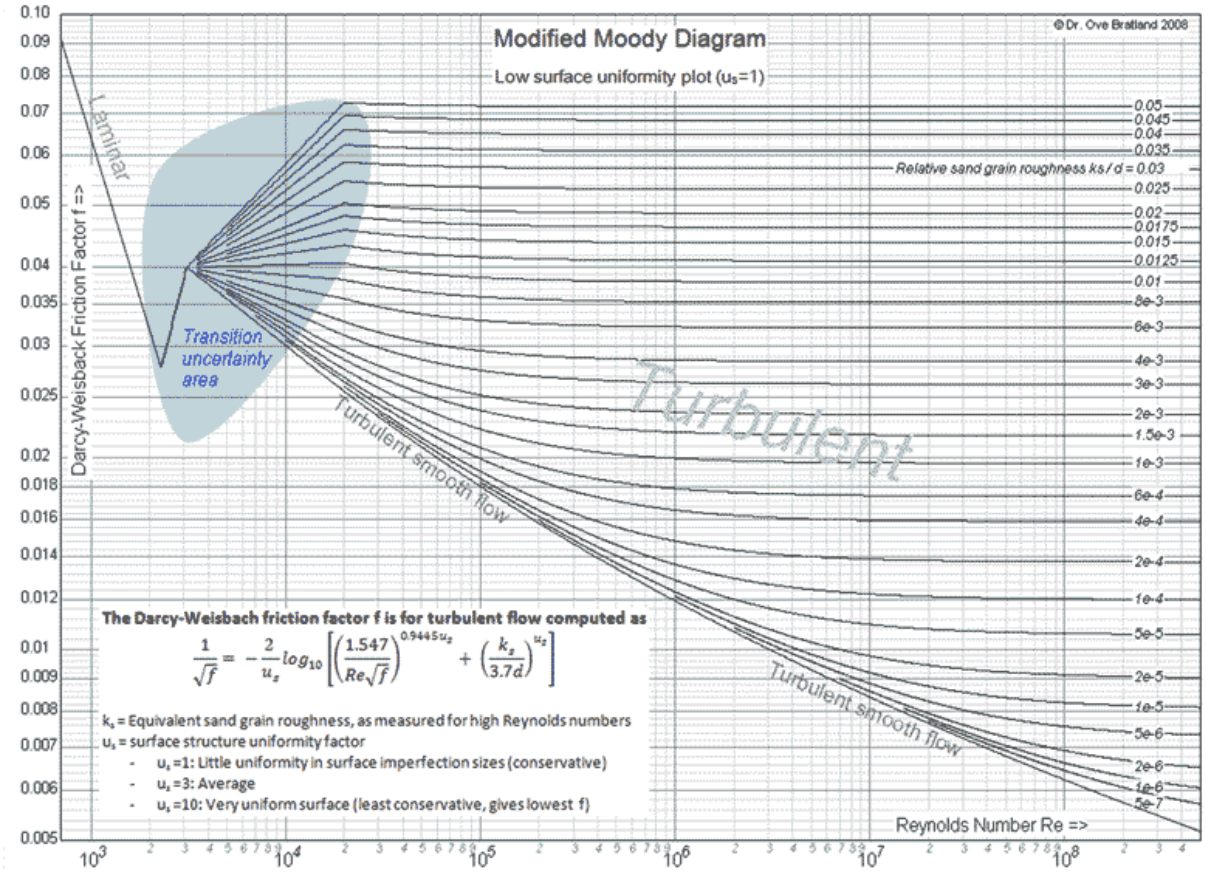

Figure 32: Moody diagram (2)

The effect of elevated temperatures may not normally be considered in flow calculations, but fire temperatures are expected to make a significant difference to the flow. It is well known that the density of air decreases with temperature as shown in Figure 33. On the other hand the dynamic viscosity increases with temperature and when this is divided into the density to get the kinematic viscosity as shown in Figure 34 the increase is an order of magnitude. Since the kinematic viscosity is the denominator in Equation 2, this reduces the Reynolds Number (Re) in the Moody diagram tending to keep the flow in the laminar/transition region and with a higher friction factor (*f*), the flow resistance will be greater with overall effects on flow, in particular when the gaps are small.

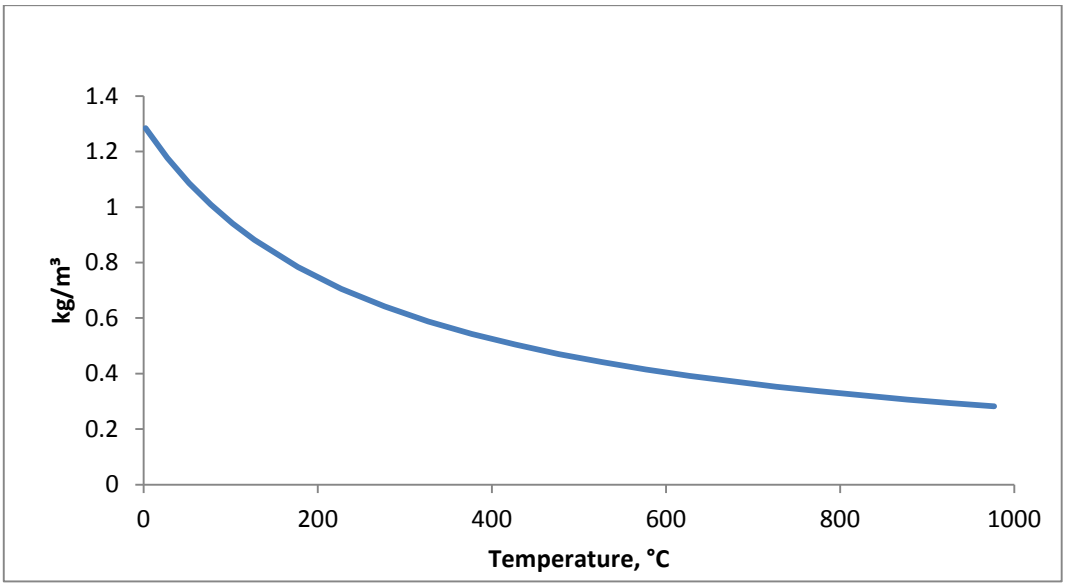

Figure 33: Density of air versus temperature

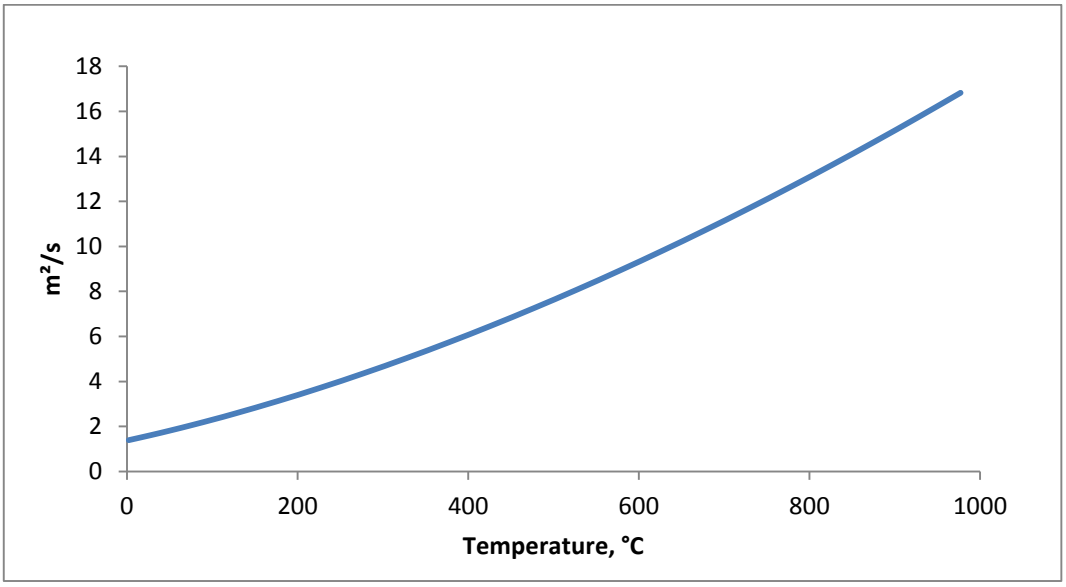

Figure 34: Kinematic viscosity versus temperature

The resulting relative flow velocity and volumetric flow rate in Figure 35 show steady declines for increasing temperature at constant pressure across small gaps where the flow regime is predominantly laminar approaching transition but not turbulent.

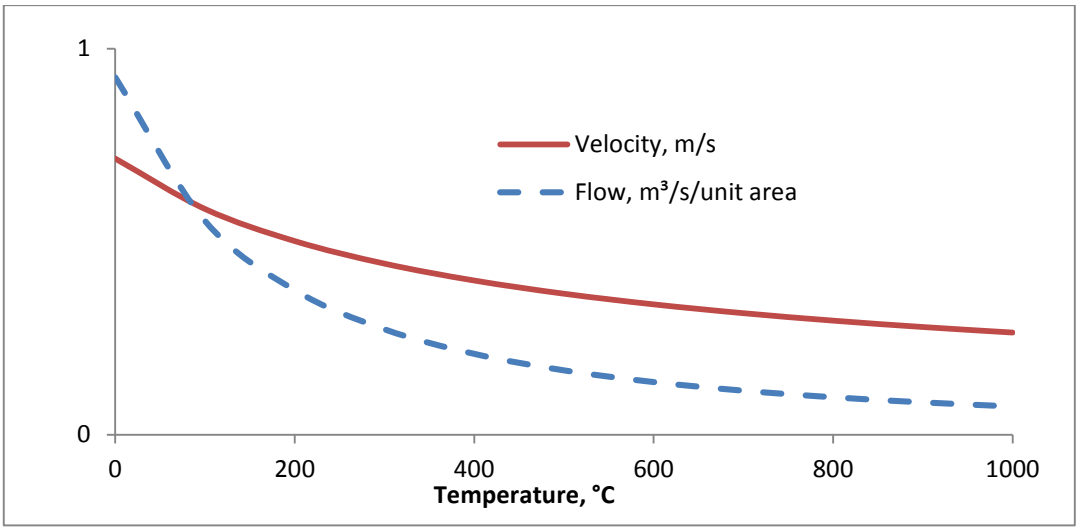

Figure 35: Relative flow through gaps for laminar flow

Including the reducing density in the volumetric flow rate gives the relative mass flow rate (kg/s) in Figure 36 and results in a dramatic reduction in the mass flow.

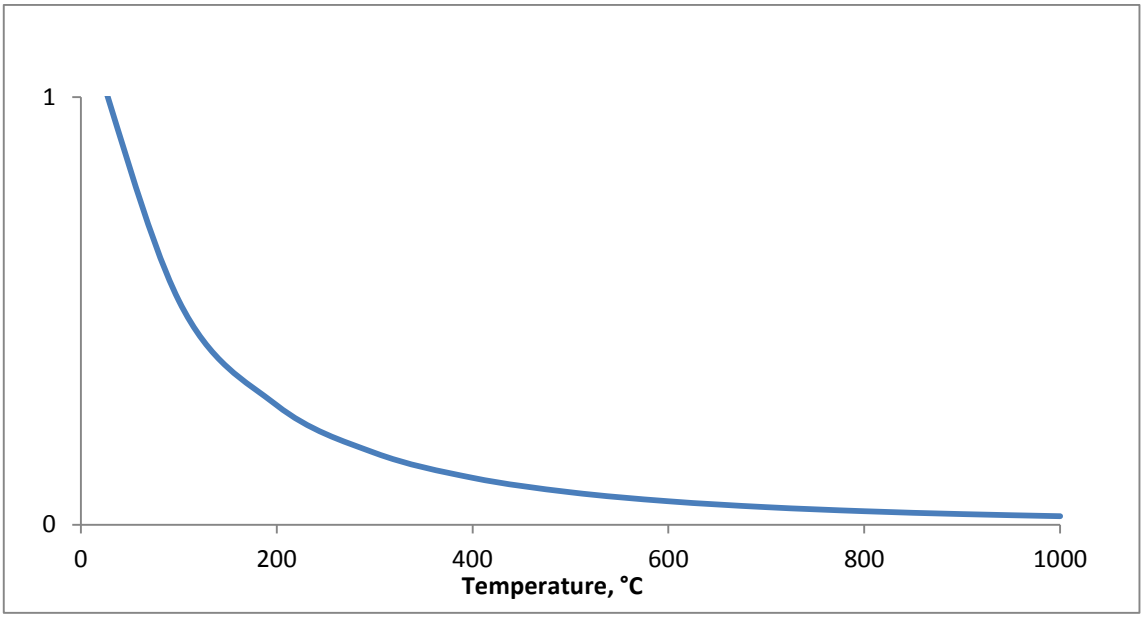

Figure 36: Relative mass flow, kg/s

Combing the mass flow with the temperature difference between the hot gases and ambient the relative heat flow or heat carrying capacity in Figure 37 reaches a maximum at about 100°C, shows a gentle decline to 200°C and a more rapid decline to about 50% of the maximum at 1000°C.

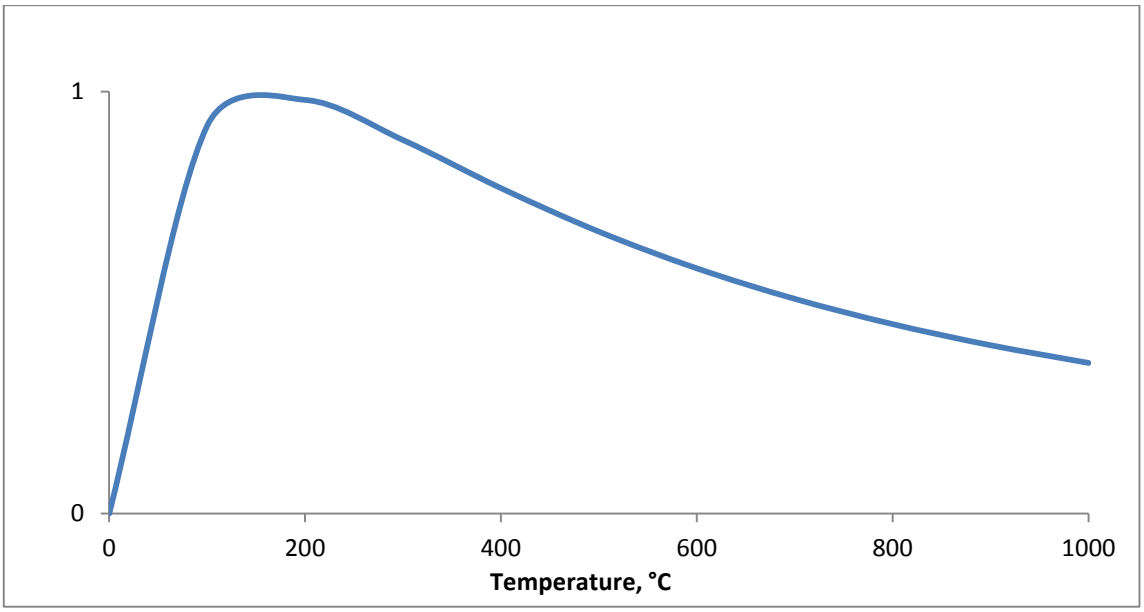

Figure 37: Relative heat flow

The relative heat flow above does not take the heat transfer properties into account, such as convection or radiation, which will depend on a number of other factors. But given the limited heat carrying capacity of the gas due to the low density and restricted flow there is likely to be a limited quantity of heat to transfer and the temperature of the gas will rapidly reduce.

From the author's observations of many fire resistance tests where hot gases have leaked outward from small gaps and fissures, the theory presented above from a qualitative viewpoint explains why there appeared to be some unseen resistance to the flow and is quite plausible. Conversely, when the pressure reverses (oscillating) and draws cool air into the furnace often entraining smoke with it, the velocity appears to be much greater.

5.2 Opposed-flow flame spread

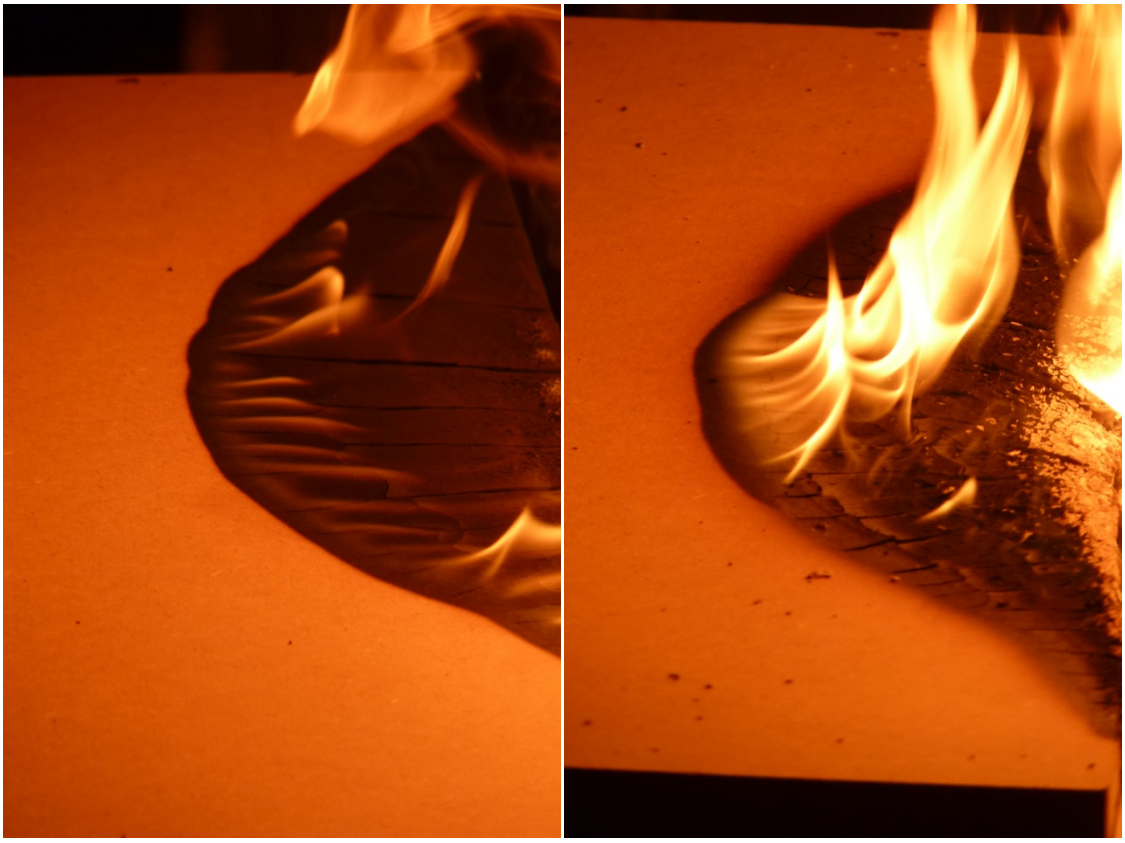

Figure 38: Opposed-flow flame spread on horizontal surface

An example of opposed-flow flame spread is shown in Figure 38. The horizontal surface is the top of a 600 x 600 x 600 mm cube constructed from sheets of 18 mm thick MDF. The right hand vertical surface of the cube was exposed to a 100 kW (170 x 170 mm) gas burner, the plume of which generated the entrained air flow in a left to right direction across the surface. In the left picture the flames on the surface are blown almost horizontal by the air flow (at a moderate velocity) in the left to right direction while the charred boundary (flame front) moves much more slowly in the right to left direction against the air flow. In the right hand picture (taken at a later time) the MDF fuel had undergone more heating and was pyrolysing at a greater rate thus providing more fuel to the flames but without a corresponding increase in air flow to support the combustion. This is evident by the reduced tendency for the flames to lean over and counter the additional heat rising upward from the combustion, hence the more luminous flame and possibly greater radiation being emitted from it back to the MDF and so on.

The theory on (Hasemi 2008) opposed-flow flame spread uses the Damkohler number (Da) to characterise the effects in Equation 3 and Figure 38.

$$Da = \frac{t_{flow}}{t_{chemical}} \propto \frac{1}{V_g^2} \quad \text{.....Equation 3}$$

Where: V_g = flow velocity

t_{flow} = transport time

$t_{chemical}$ = chemical time

In Figure 39, increasing the Damkohler number (reducing flow velocity) indicates more rapid burning and flame spread, and conversely reducing Damkohler numbers (increasing the flow velocity) results in the extinction of the flame.

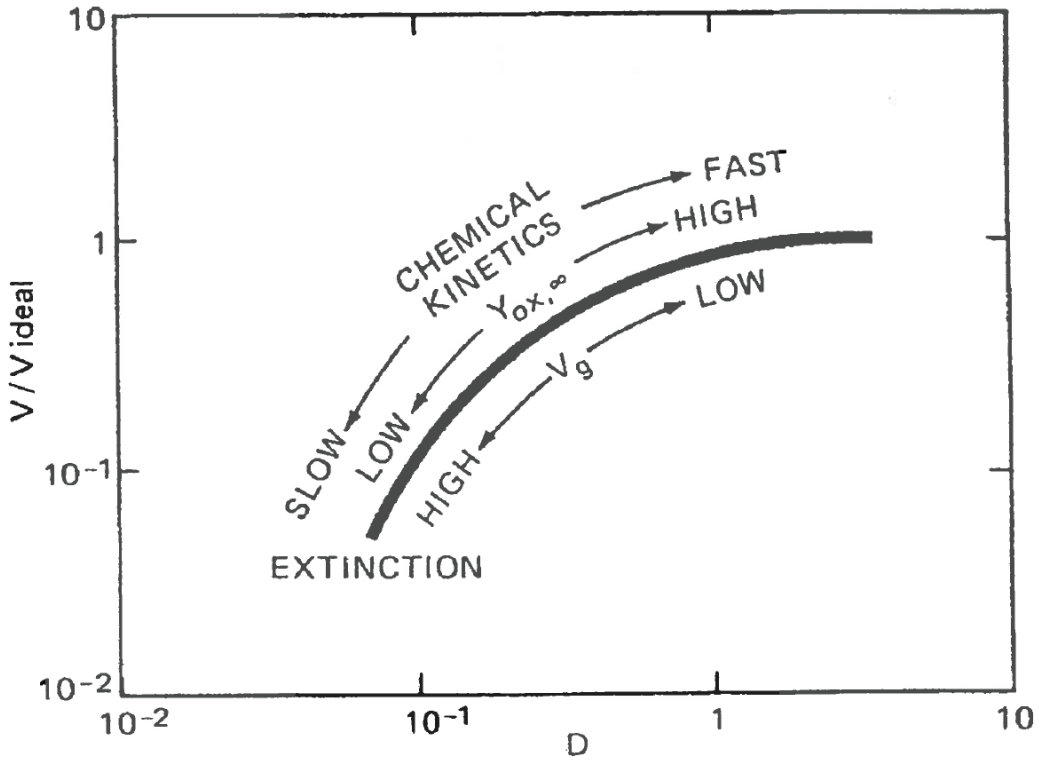

Figure 39: Opposed-flow flame spread versus Damkohler number

Drysdale (1998) describes counter-current spread as occurring naturally by entrainment if a flame is spreading horizontally or downwards. An imposed counter-current flow will have two effects:

1. Promoting mixing and combustion at the leading edge of the flame tending to increase the spread rate and
2. Cooling the fuel ahead of the flame front tending to decrease the rate.

The latter will become increasingly important as the air velocity is increased. The two effects described are illustrated in Figure 40 showing a family of curves where the composition of the counter-current flow is 100%, 62% and 46% O_2/N_2 for the curves top to bottom respectively. The enriched O_2 accounts for the increasing rate of flame spread up to a maximum after which the greater flow velocity tends to decrease the rate.

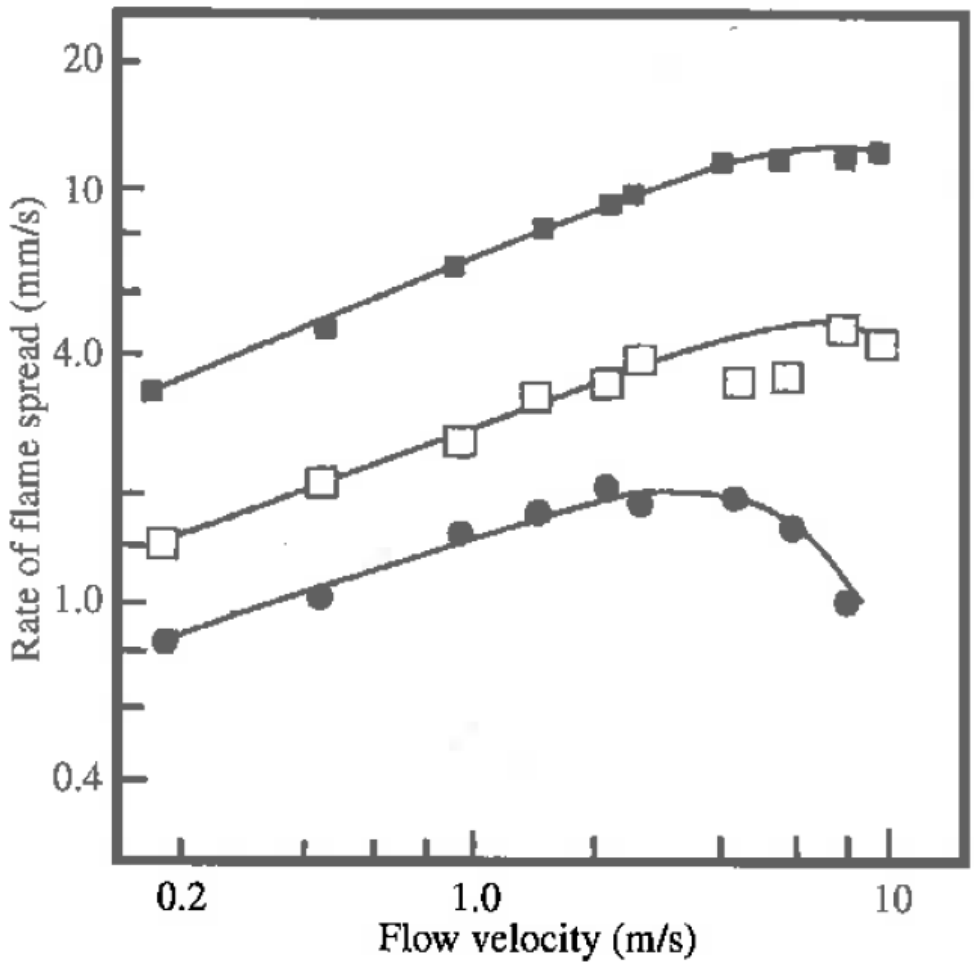

Figure 40: Variation of rate of flame spread with velocity of counter-current flow for 100%, 62% and 46% O_2 (top to bottom)

To consider the effect of opposed flow with atmospheric 21% O_2, Figure 41 shows a range from 100% down to 21% on a per weight basis (g/g), so the 0.233 curve corresponds to atmospheric O_2 content. For the lower concentrations of O_2 in the range of 33% and below, there does not appear to be the increase in flame spread rate with the opposed-flow velocity. Instead the graphed curves are relatively flat, indicating that the rate of flame spread is relatively independent of the opposed-flow velocity up to a point when the rate of flame spread reduces to a level where extinction is likely.

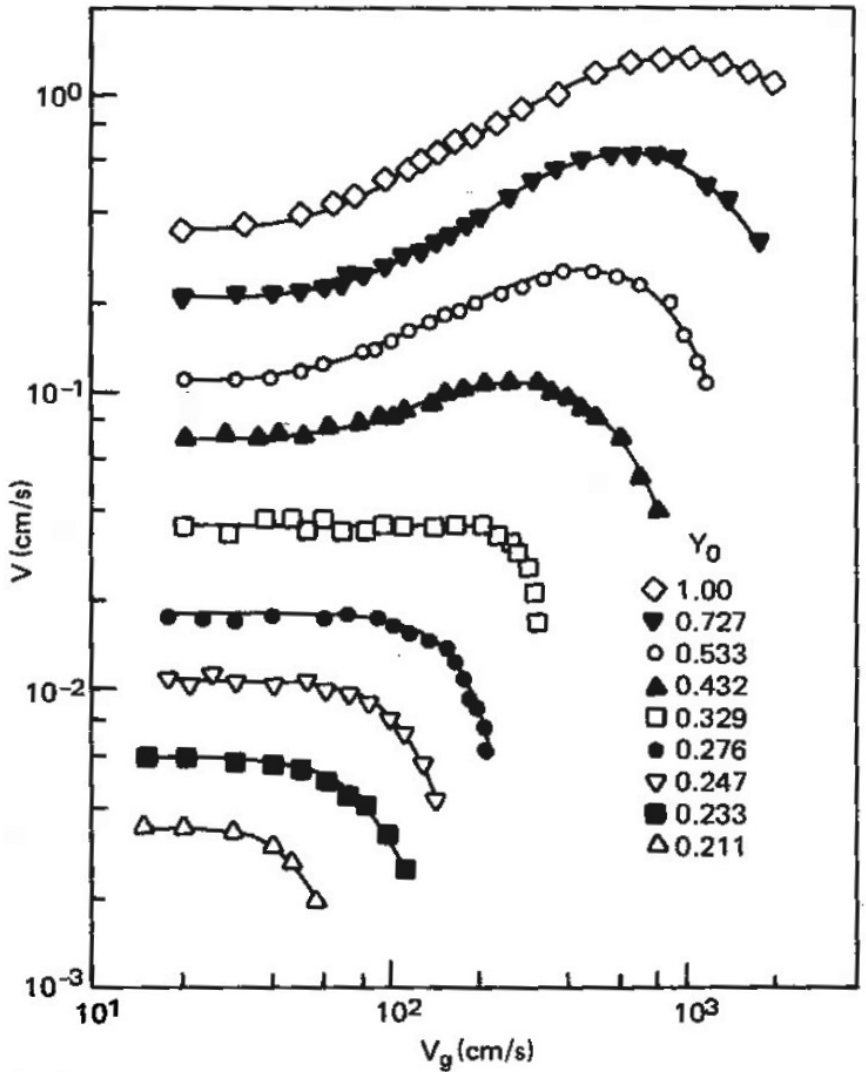

Figure 41: Effect of counter-flow velocity and O_2 concentration (from 100% to 21% O_2 by weight) on flame spread velocity

From the opposed-flow theory presented above it is reasonable to hypothesise, even if only qualitatively speaking, that similar trends of flame spread will occur:

- On two surfaces with a narrow gap between
- And when the flow in such a gap varies due to pressure fluctuations.

In the instance of a variable flow the flame spread rate may settle to an average value in accordance with Figure 41. However, if the pressure fluctuations actually oscillate to the extent that the pressure reverses then it is possible the surfaces will be alternately heated with hot gases and then cooled with O_2 (21%) air. Such a process may increase the flame spread rate by keeping the flame front hot and then supplying it with air for combustion.

The following experimental programme was designed to trial this possible mechanism as an explanation of how and why some Integrity failures occur.

6. EXPERIMENTAL

The experimental trials or fire tests conducted in accordance with test standard AS1530.4 (SAA, 2005) were directed at replicating the types of damage to a selection of PFP systems that were identified in the building surveys. Timber-based systems with plasterboard were selected for testing rather than concrete panels or intumescent paint systems. In the case of concrete panels it could be argued that the sizes of the gaps already exceeded the gauge size of 6 x 150 mm so would have technically failed as soon as a fire test had started. Similarly the loss of intumescent paint meant no protection would have been afforded on areas where the paint was lost and it was never considered that these systems should be tested in a damaged condition. Finite element modelling of damaged systems would provide some indication of the loss of fire resistance but that was outside the scope of this project.

The focus (for testing) was on damage in the moderate to superficial range and the damage features were instrumented with thermocouples to collect temperature data that would assist in determining failure mechanisms, in particular Integrity failures. More extensive damage had been examined by fire resistance testing in an earlier project (Collier 2005, 2008) so the objective in this experimental programme was to consider more subtle damage.

6.1 Aim of fire tests

From earthquake damage surveyed, the damage types considered for investigation in the fire tests were:

- A range of circular hole sizes and elevations
- Vertical slots in timber-framed plasterboard walls
- Horizontal slots in timber-framed plasterboard walls
- Detachment of lining on timber frames
- Cracking of plasterboard lining above door frames
- Doorset leaf to frame gaps
- Some of the above were repeated at different elevations and pressures.

Three fire resistance tests with the above defects or damage features were designed and constructed.

In the context of the tests conducted, the following failures based on AS1530.4 (SAA 2005) were monitored and assessed by:

- Integrity failure – the development of cracks, fissures or other openings through which flames or hot gases can pass, also characterised by an exit temperature of 300^{o}C as measured by a fitted mineral insulated metal sheath (MIMS) thermocouple being exceeded
- Insulation failure – the temperature of any of the relevant thermocouples attached to the unexposed face of the test specimen rises by more than 180K above the initial temperature.

6.2 Instrumentation on tests

The test instrumentation was based on 1.6 mm ISO type MIMS and disc thermocouples of type K.

The MIMS thermocouples were embedded in a range of opening sizes and shapes to record the rate of flame/fire spread, at different pressures and elevations, in Figure 42 and Figure 43.

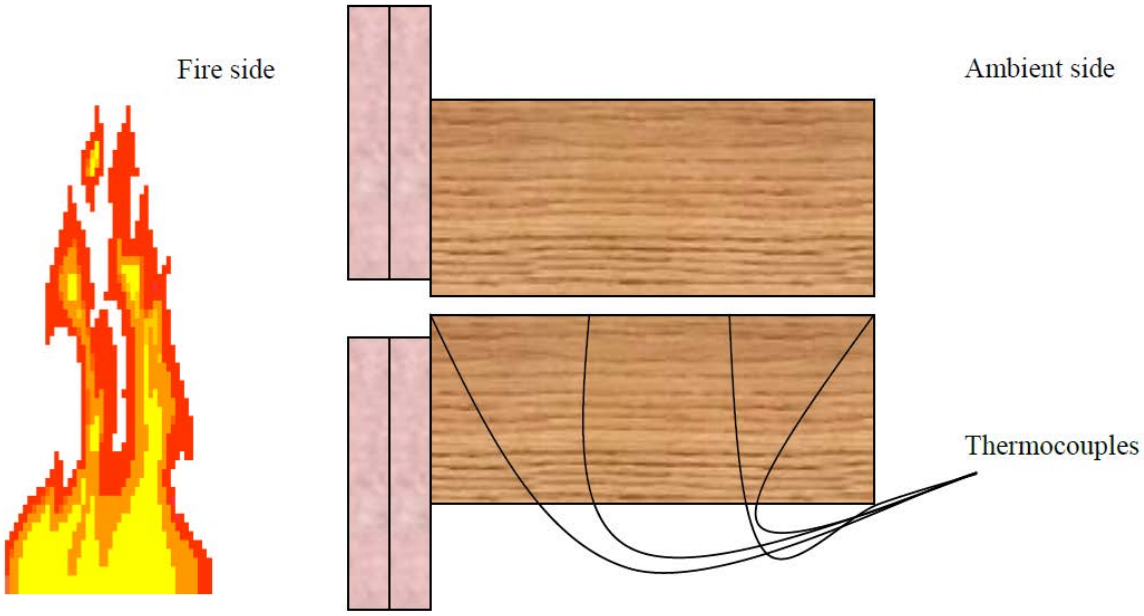

Figure 42: Instrumentation of circular holes in Test 1

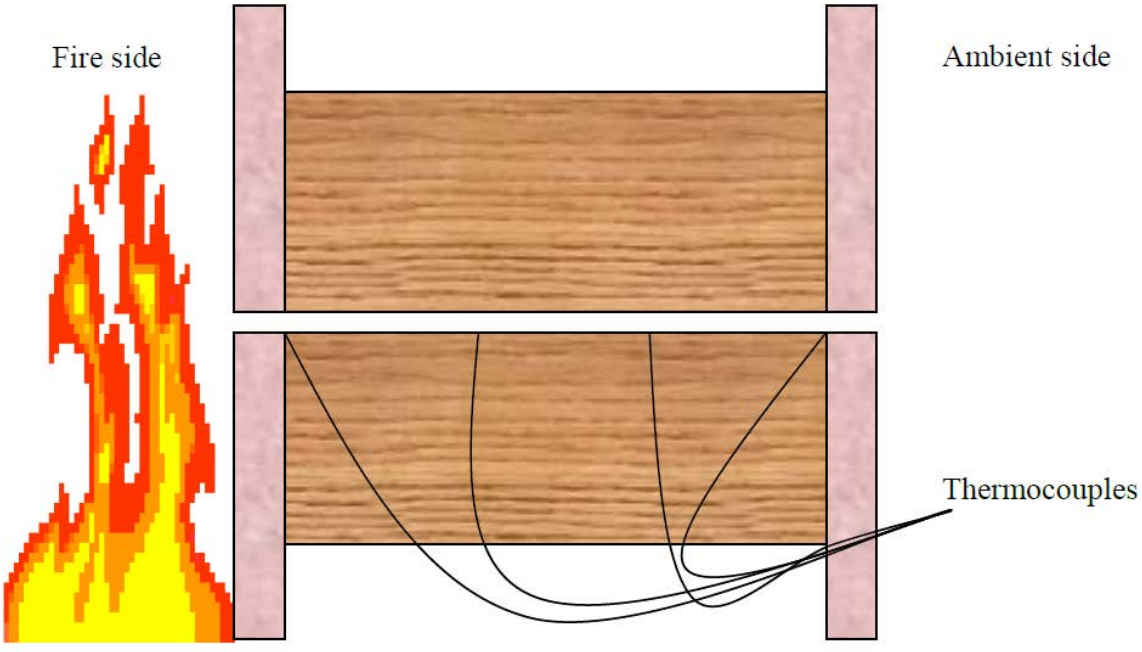

Figure 43: Instrumentation of vertical and horizontal gaps in Tests 2 and 3

The temperature of the flame/fire spread front was expected to follow a profile similar to that in Figure 44 (from Drysdale 1998) and the thermocouples were positioned to record the transition through 300°C.

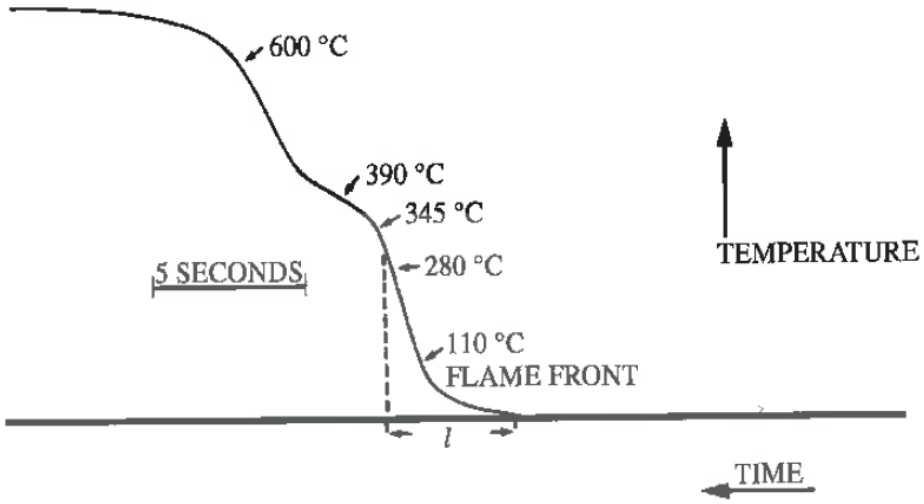

Figure 44: Temperature wave accompanying flame front in gaps

Whether flame spread through a gap is in the direction of gas flow or an opposed-flow mechanism as shown in Figure 45 (Atreya and Baum, 2003), the thermocouples at the surface will also register the commencement of charring at 300°C.

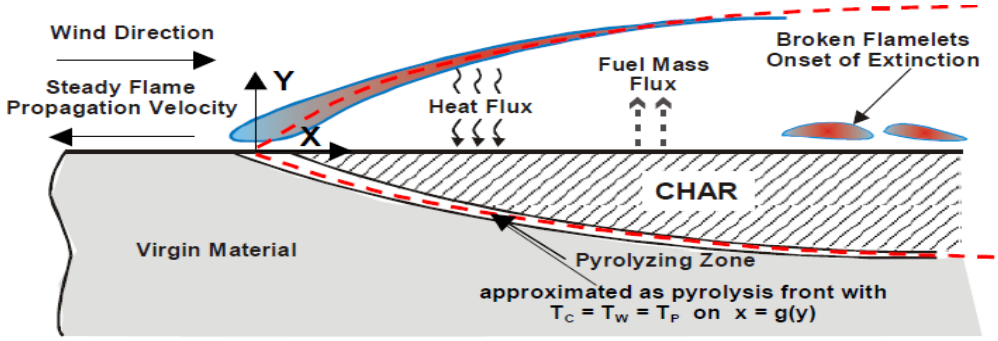

Figure 45: Mechanism of opposed-flow flame spread on a surface

Considering two symmetrically-opposed surfaces such as that shown in Figure 46, it is assumed that the mechanism may also be applied to a cavity even if there is increased feedback from the opposing surface as well as the flame, where the combustion is increasingly supported by a gentle supply of fresh 21% oxygen air.

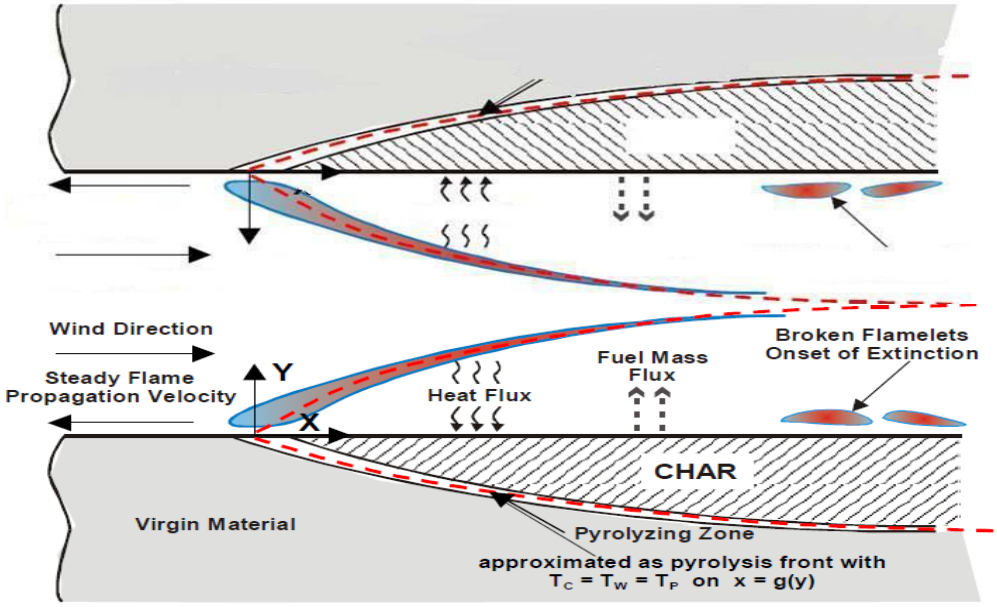

Figure 46: Mechanism of opposed-flow flame spread on a surface in a gap

The intention was that the thermocouples would provide some understanding as to what was happening. Figure 47 shows with two cross-sectioned 90 x 45 timber samples how the cone-shaped charring region has developed against an opposing air flow. One of the thermocouple holes is visible in the bottom sample.

Figure 47: Cone-shaped charring profile in opposed-flame spread

For the lining defects that included cracks and detachments in cavity walls, the samples were instrumented in accordance with Figure 48. The objective was to record the temperature rises across the linings and cavity, and compare the results to control samples with no damage.

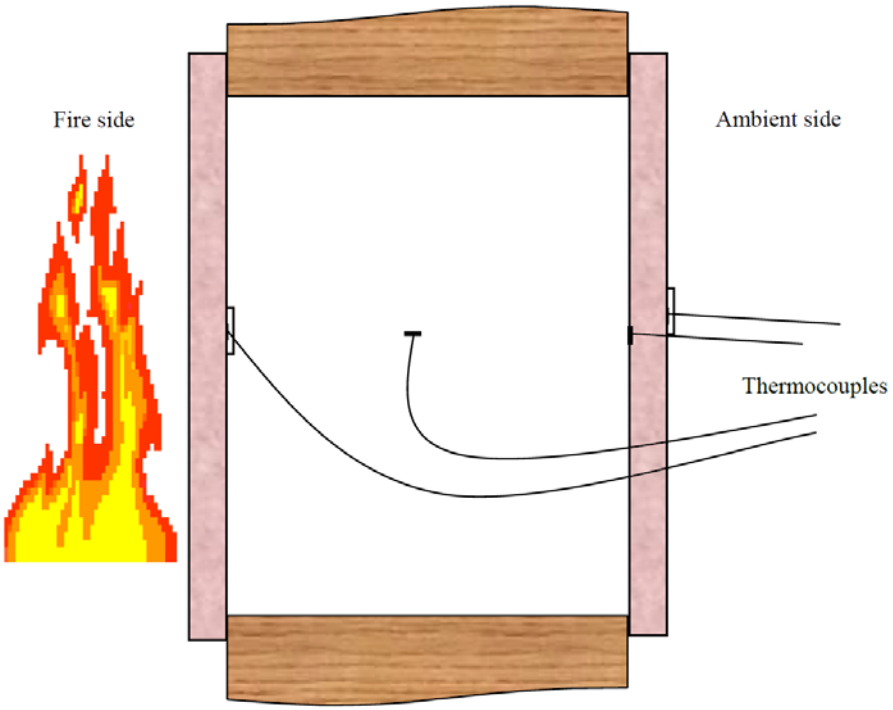

Figure 48: Instrumentation of cavity wall

6.3 Test 1

Test 1 was a small-scale pilot 2200 mm high x 1000 mm wide with 3, 6, 12 and 24 mm holes 90 mm through 90 x 45 mm timber studs at six different 400 mm elevation intervals as shown in Figure 49 and Table 2. The fire-exposed side was lined with 2 x 16 mm fire-rated plasterboards protecting the studs and the non-exposed side was unlined. Thermocouples (Figure 42) were installed in each hole at 0, 30, 60 and 90 mm intervals from the exposed side to record the progress of the fire front or charring where 300^{o}C is taken as the arrival of the front or commencement of charring.

Figure 49: Test 1 pilot scale 3, 6, 12 and 24 mm holes at different elevations and furnace pressures

Table 2: Test 1, locations and sizes of circular holes

Elevation, mm	Pressure, Pa	3 mm dia	6 mm dia	12 mm dia	24 mm dia
2100	11.64	A	B	C	D
1700	6.92	E	F	G	H
1300	2.2	I	J	K	L
900	-2.52	M	N	O	P
500	-7.24	Q	R	S	T
100	-11.96	U	V	W	X

The test results are analysed in Section 7 and additional post-test photographs are included in Appendix B.

6.4 Test 2

The second test was a full-size fire resistance test at 3000 mm x 3000 mm (h) used to trial a number of damage features found in the building surveys.

On 90 x 45 mm timber framing with studs at 600 mm centres and nogs at nominally 600 to 800 mm centres, each side was lined with 13 mm fire-rated gypsum plasterboard and the following defects were included:

- Detached lining top and bottom of wall
    - 3 mm on exposed side of cavity
    - 3 mm on non-exposed side of cavity
    - 3 mm on both sides of cavity
- Damaged lining
    - 1.5 mm diagonal crack on exposed side of cavity
    - 1.5 mm diagonal crack on non-exposed side of cavity
    - 1.5 mm diagonal cracks on both sides of cavity
    - No cracks, control specimen
- Vertical slots
    - 3 mm from 0 to 3000 mm elevation in five sections and
    - 6 mm from 0 to 3000 mm elevation in five sections
- Horizontal slots stepped
    - 3 mm increasing to 6 mm
        - At elevations of 630, 1225 and 1775 mm
    - 6 mm reducing to 3 mm
        - At elevations of 630, 1225 and 1775 mm
    - 1.5 mm increasing to 3 m
        - At elevations of 630, 1225 and 1775 mm
    - 3 mm reducing to 1.5 mm
        - At elevations of 630, 1225 and 1775 mm

- Horizontal slots tapered (left to right) instrumented at 3 and 6 mm
    - 3 mm
        - At elevations of 630, 1225 and 1775 mm
    - 6 mm
        - At elevations of 630, 1225 and 1775 mm
- Control lining no damage.

The defects in Test 2 were instrumented in accordance with Figure 43 and Figure 48 and the layout is shown in Figure 50 at the test start.

Figure 50: Test 2 at start of test

The end of test (Figure 51) at approximately 60 minutes shows where some of the Integrity failures have occurred, the gaps covered with ceramic fibre occurred well before 60 minutes and were covered over so that the test could continue and data was collected for as long as practicable.

Figure 51: Test 2 at end of test

6.5 Test 3

The third test was a full-size fire resistance test 3000 mm x 3000 mm (h) used to trial a number of damage features found in the building surveys.

On 90 x 45 mm timber framing with studs at 600 mm centres and nogs at nominally 600 to 800 mm centres, each side was lined with 13 mm fire-rated gypsum plasterboard and the following defects were included:

- Vertical slots 1.5 and 3 mm
    - 1.5 mm from 0 to 3000 mm elevation in five sections and
    - 3 mm from 0 to 3000 mm elevation in five sections
- Gaps simulating door frames side and top, both directions
    - L-shaped gap 1.5->3 mm six vertical sections 0 to 2000 mm elevation
    - L-shaped gap 3->1.5 mm six vertical sections 0 to 2000 mm elevation
    - L-shaped gap 3->1.5 mm one horizontal section at 2000 mm elevation
    - L-shaped gap 6->1.5 mm one horizontal section at 2000 mm elevation
    - L-shaped gap 1.5->3 mm one horizontal section at 2000 mm elevation
    - L-shaped gap 1.5->6 mm one horizontal section at 2000 mm elevation
- Cracked lining above door corners
    - 3 mm diagonal crack on fire-exposed side lining
    - 3 mm diagonal crack on non-fire-exposed side lining

- Control lining no damage.

The defects in Test 3 were instrumented in accordance with Figure 43 and Figure 48 and the layout is shown in Figure 52 at the test start.

Figure 52: Test 3 at start of test

The end of test (Figure 53) at approximately 60 minutes shows where some of the Integrity failures have occurred, the gaps covered with ceramic fibre occurred well before 60 minutes and were covered over so that the test could continue and data was collected for as long as practicable.

Figure 53: Test 3 at end of test

7. RESULTS AND ANALYSIS

In the experimental programme the three furnace tests were designed to gather data to demonstrate and explain how the PFP may be compromised if defects consistent with earthquake damage were exposed to a controlled fire environment.

Two essential parameters not usually monitored or scrutinised in fire tests were included in this investigation, namely the gas content in the furnace and the pressure or more importantly, the pressure fluctuations. Coupled with the theoretical flow characteristics covered in Section 5 where the temperature of the gases has a significant influence on the flow characteristics, some explanations of the variations in fire resistance measured can be advanced.

7.1 Pressure fluctuations and furnace gas content

For the fire tests two further measurements of the furnace pressure were taken in addition to the regular measurement at around the neutral plane and these were used to control the furnace pressure to meet the fire test standard, in this case AS1530.4 (SA, 2005). These two additional measurements were also included in this series of tests in order to capture fluctuations in pressure that are assumed to be responsible for oscillating flow through gaps that is often observed in fire tests and is perhaps the cause of reduced fire resistance. Figure 54 shows typical pressure fluctuations at three elevations of 100 mm, 720 mm (furnace pressure control) and approximately 100 mm below the top of the test specimen.

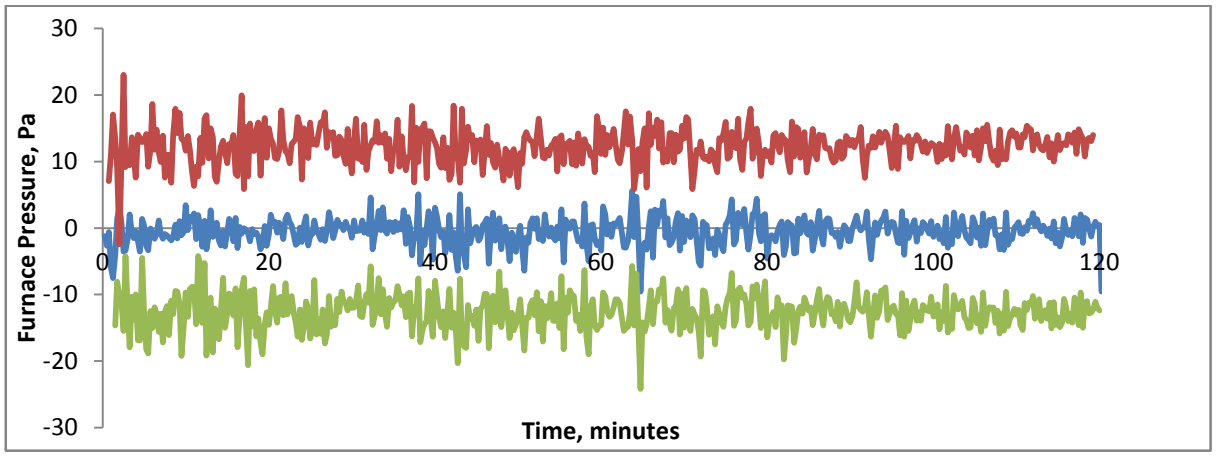

Figure 54: Typical furnace pressure stability in fire test at top, middle and bottom elevations

The graph clearly shows the pressure oscillations where readings are taken at intervals of 15 seconds and the oscillations are appearing to cycle in tens of seconds. The instrumentation measuring the furnace pressure is connected to the furnace through long tubes that have a tendency to dampen out the oscillations, so the actual amplitude may be greater than that shown in Figure 54 and since data is recorded at 15-second peaks, extreme values may not be captured but the test specimens are nevertheless subjected to those extremes.

It is noteworthy that in the middle region there apparently exists a cycle that covers both positive and negative pressures, and the implications of this are illustrated in Figure 55. Depending on how closely the neutral pressure plane is maintained there is a region in

around the mid-height of a wall specimen that is likely to be subjected to pressure reversals.

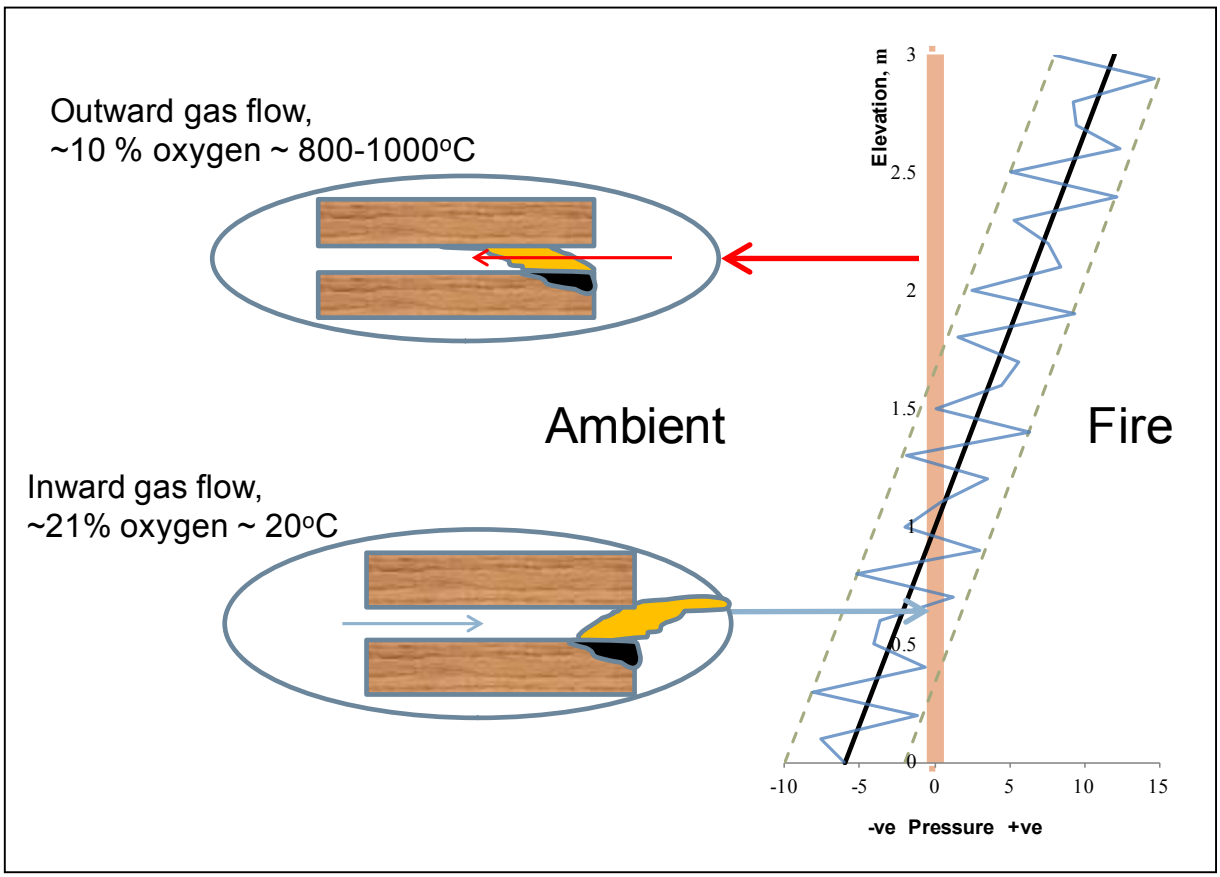

Figure 55: Pressures in fire and flow through gaps

Throughout the three tests the furnace gas was sampled for oxygen (O_2) and carbon dioxide (CO_2). Typical results for the three tests are shown in Figure 56 in combination with furnace temperature.

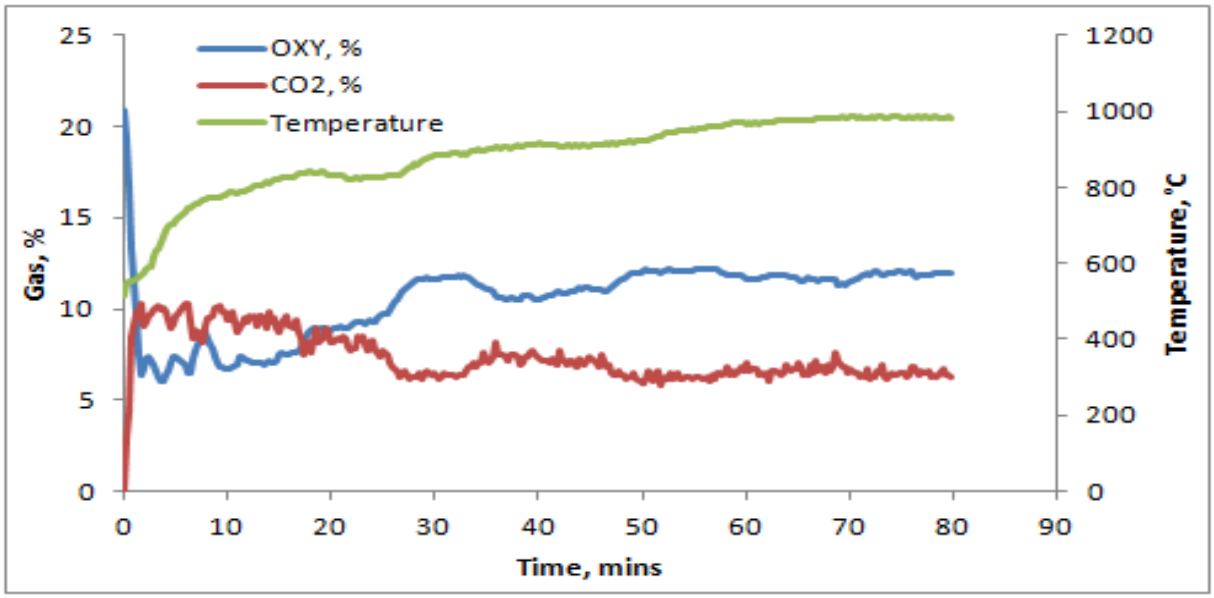

Figure 56: Typical gas composition in furnace

The clear trend is that the O_2 rapidly decreases to about 6% as the temperature quickly increases and the fuel is rapidly burnt to follow the prescribed time-temperature curve. After this initial period the O_2 increases as more steady temperature conditions are achieved and it settles in a band of 10 to 12% and then 6% CO_2 after 30 minutes. Throughout this time the O_2 and CO_2 contents appear to be mirror images of each other, which was not at all unexpected as the more O_2 that is consumed the more CO_2 that will be produced.

As introduced in the theory within Section 5, a possible mechanism for the timing of Integrity failures (flaming through gaps) as illustrated in Figure 55 is a result of pulsating and oscillating flow of gases through the gaps mostly likely in the mid-height range. For the outward flow of hot gases through gaps but with the reduced O_2 content and the presence of CO_2 – although charring may not be reduced very much – the likelihood of combustion in the gap is inhibited, especially if the flow resistance is increased due to the elevated temperature. On the other hand, inward flow of cool air may introduce 21% O_2 to the heated (timber) interface thus feeding a glowing combustion. A situation where the flow is oscillating, such as the mid-height of a wall with gaps alternately subjected to hot gases at 10% O_2 and then ambient air at 21% O_2, represents a worst-case scenario likened to a ”whipsaw effect” where it would not be unexpected for the first flaming and Integrity failures to occur at middle elevations.

7.2 Fire resistance performance of walls with small gaps

Three fire tests trialled a variety of defects comprising gaps, where the path was timber on all surfaces, such that the failure would be by Integrity when flaming or hot gases exceeding 300°C had reached the ambient side.

7.2.1 Circular holes

Timber was protected on the fire side with two layers of 16 mm (32 mm total) fire-rated plasterboard so there was a considerable delay in the commencement of charring of the studs.

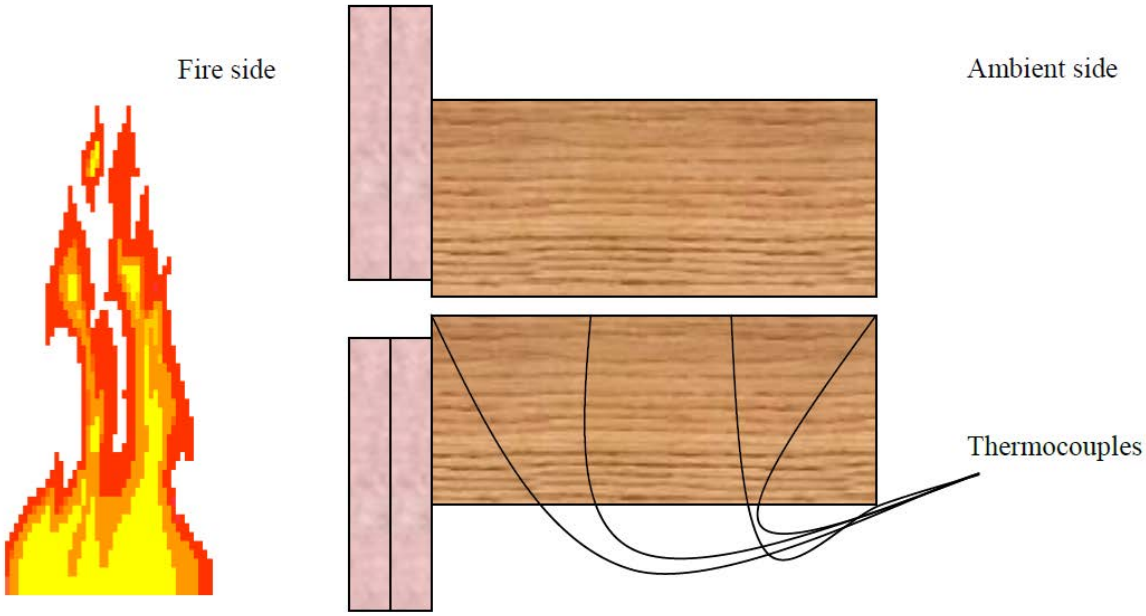

Figure 57: Instrumentation of gaps in wall to measure flame spread and progress of Integrity failures

Two examples of temperature measurements throughout the test duration are shown in Figure 58 and Figure 59 where the 0, 30, 60 and 90 mm refer to the thermocouple positions along the gap from the fire side. The significant milestones are the times at which the temperatures exceed 300ºC as an indication of the rate at which the flame front advances over the timber and 300ºC was selected on the basis of the flame front in Figure 44. The rapid increase in the rate of temperature rise beginning at ~300ºC, increasing beyond 500ºC and continuing to 700-900ºC at depths of 0, 30 and 60 mm as shown in Figure 58 and Figure 59, indicate 300ºC is on the conservative side but is an accurate indication of the time that the flame front arrives. In instances where the Integrity failure was assessed by the time that the flame front exits the holes at the 90 mm depth, 300ºC was found to be a reliable indicator even if it would have been expected the temperature of external flaming would be higher. Considering the thermal inertia of the thermocouple tips at the exit and the often oscillating nature of the flow drawing cool air back over the tips, 300ºC was the preferred benchmark to indicate and record external flaming and it generally agrees with observations of flaming.

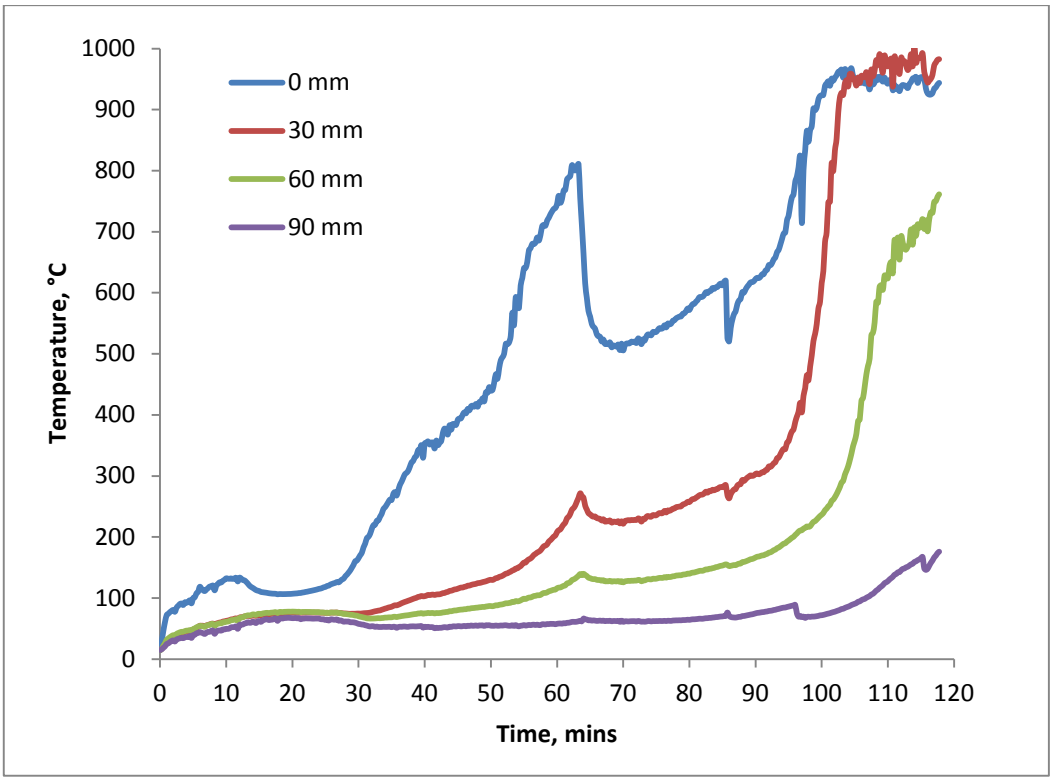

Figure 58: Temperature rises in 6 mm hole at 6.9 Pa furnace pressure

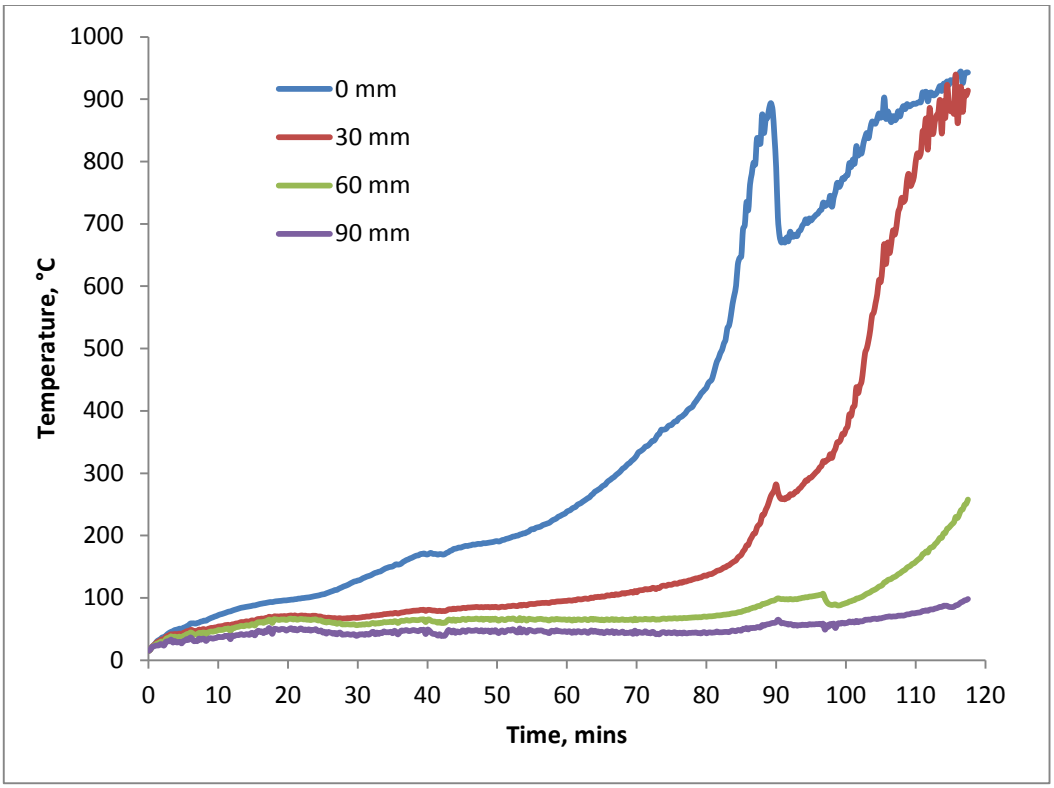

Figure 59: Temperature rises in 6 mm hole at 2.2 Pa furnace pressure

Comparisons of the actual sectioned holes are shown in Figure 60 after 118 minutes' fire exposure and it is evident that there is reasonable agreement with the final

temperature recordings in Figure 58 and Figure 59. The complete selection of photographs of sectioned holes that survived the test are included in Appendix B.

Figure 60: Extent of charring in 6 mm holes at 6.9 and 2.2 Pa furnace pressures

Further analysis of the thermocouple results measuring the flame progression through the circular holes where 300°C was considered the arrival of flaming, are summarised in Figure 61 for comparison with the trends of the predicted flow velocities in Figure 30.

The most significant trend for the 3, 6 and 12 mm holes is the relatively constant flame spread velocity in the furnace pressure range -7 Pa to +11 Pa and for the 24 mm hole, the flame spread rate, although of significantly greater magnitude, actually shows a small reduction at the upper and lower limits of the range. Drawing too many conclusions from the first test is not warranted, as other parameters such as the delay time (in Figure 62) until the flame spread commences need to also be accounted for in order to make predictions regarding Integrity failures.

The progression of the charring and hence fire spread along the holes as recorded by the temperatures and confirmed by physical measurements of the sectioned samples in Appendix B at the end of the test are recorded in Table 3, with “90+” indicating an Integrity failure occurred and there was no sample left to measure. In these cases the times at which 90 mm of fire spread was exceeded are listed in Table 4.

Table 3: Progression of fire spread or charring in holes at end of Test 1, in mm

Elevation, mm	Pressure, Pa	3 mm dia	6 mm dia	12 mm dia	24 mm dia
2100	11.64	74	79	90+	90+
1700	6.92	54	84	90+	90+
1300	2.2	22	58	90+	90+
900	-2.52	19	37	69	90+
500	-7.24	29	30	20	90+
100	-11.96	20	23	0	46

Table 4: Times for fire spread or charring in holes to reach 90 mm, minutes

Elevation, mm	Pressure, Pa	3 mm dia	6 mm dia	12 mm dia	24 mm dia
2100	11.64	-	-	48	22
1700	6.92	-	-	70	25
1300	2.2	-	-	85	32
900	-2.52	-	-	-	64
500	-7.24	-	-	-	76
100	-11.96	-	-	-	-

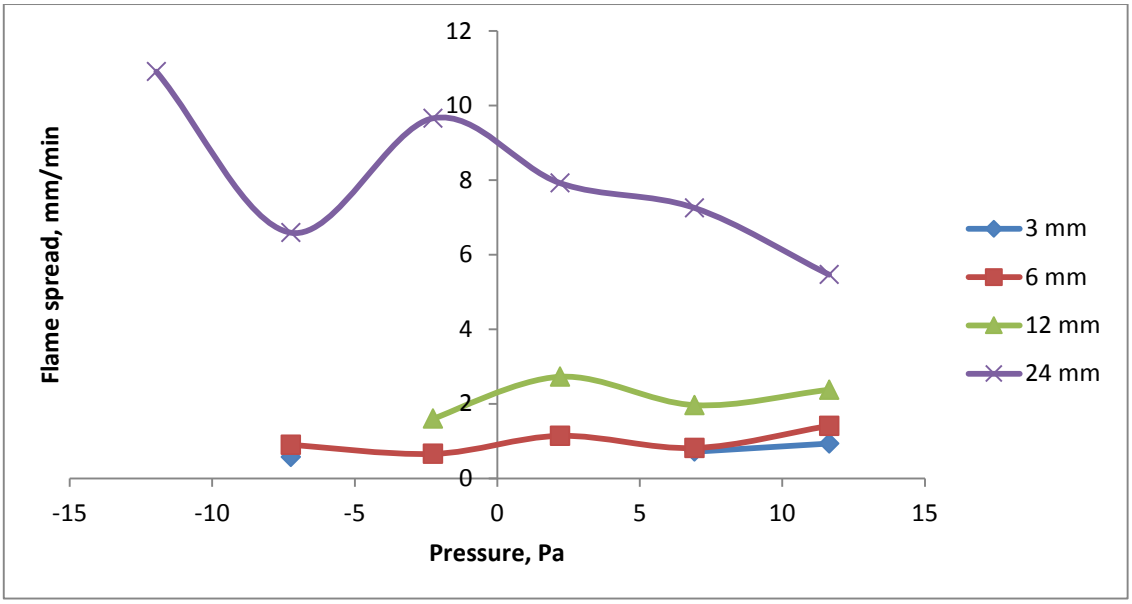

Figure 61: Flame spread rate through circular gaps

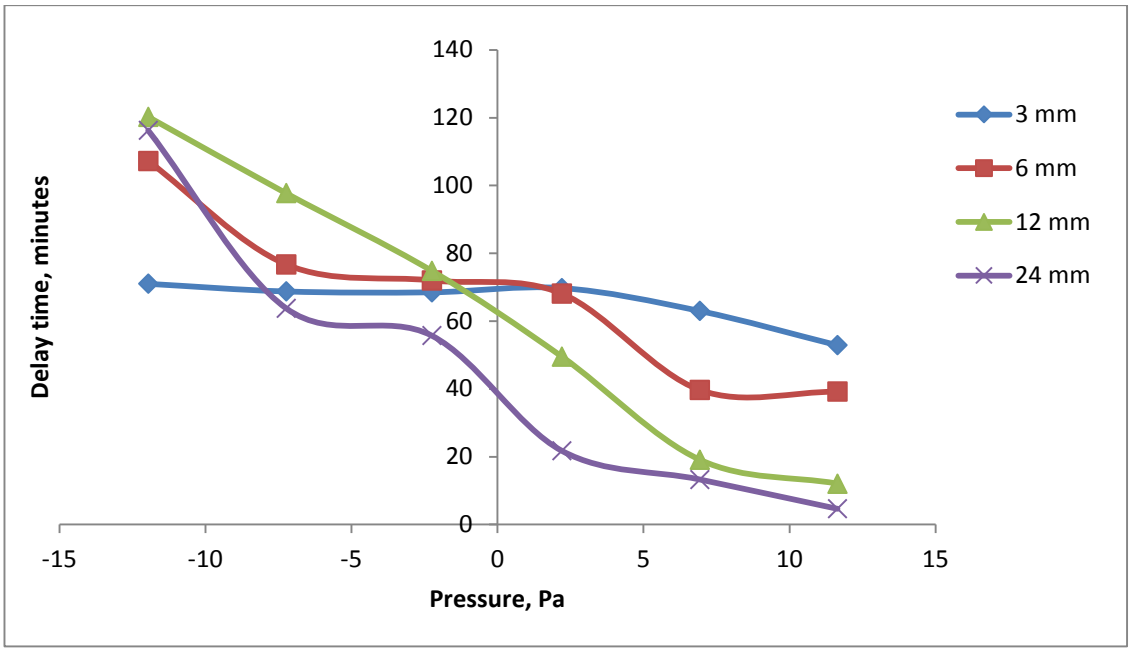

Figure 62: Delay time until the flame front arrives

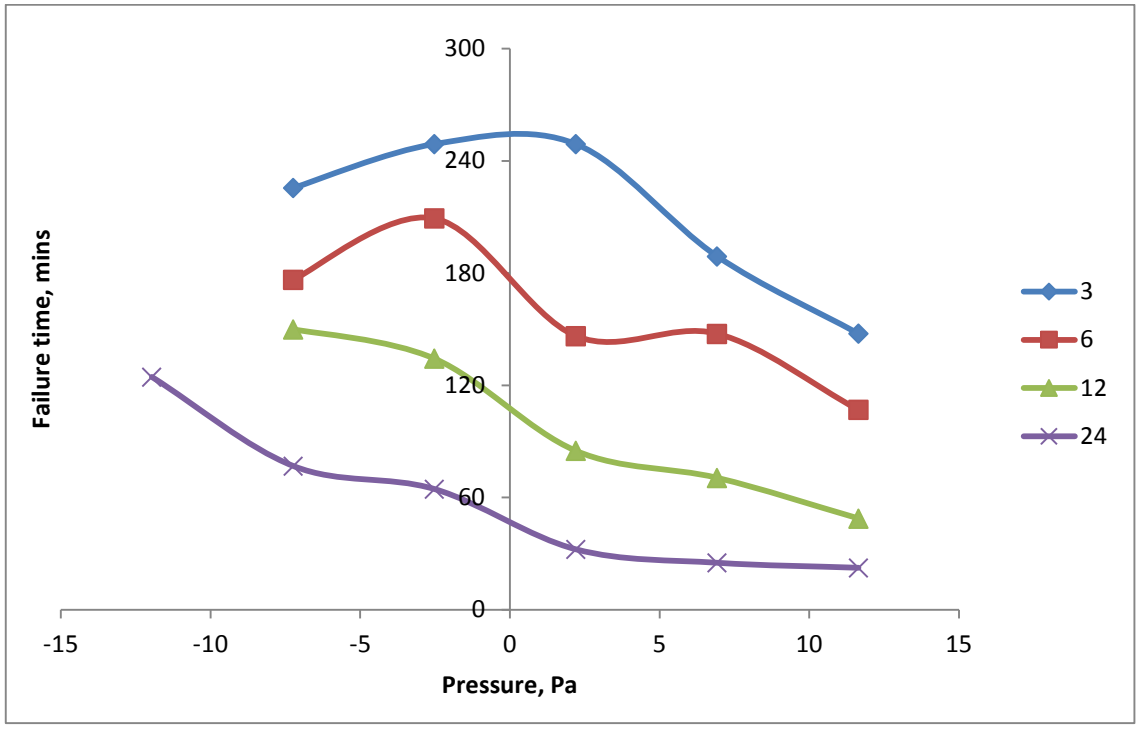

Figure 63: Integrity failures of circular holes

Integrity failures are shown in Figure 63. Although the test was stopped at 118 minutes without Integrity failures in some locations, the data at that time has been projected forward to a likely failure time. In a proportion of cases, an actual fire resistance wall will have failed by a mode other than Integrity, so the Integrity result predicted may not be relevant.

To summarise, the results from Test 1 show the trends in relation to the hole size and furnace pressure, with a just perceptible increase in flame spread rate or reduction in

flame-through time (Integrity failure) around the point where the pressure is close to 0 Pa, offering evidence that pulsating or indeed oscillating flow in a gap has a detrimental effect. Alternatively it can be suggested that higher pressures are not proportionately detrimental to the fire resistance.

7.2.2 Vertical gaps

The temperature data recorded in the gaps as illustrated in Figure 43 was analysed on the basis that the flame front is approximately 300°C in accordance with the theory presented in Section 5 and Figure 44.

As an example, the four temperature recordings at 0, 30, 60 and 90 mm through a 2.6 mm wide vertical gap (approx 600 mm long vertically) subjected to a furnace pressure of approximately 4.9 Pa at a height of 1500 mm are graphed in Figure 64. The flame front progression is indicated by the times at which the temperature exceeds 300°C. Eventually, the temperature at the 90 mm thermocouple exceeds 300°C indicating flame-through and Integrity failure at approximately 38 minutes, also visually confirmed by flaming.

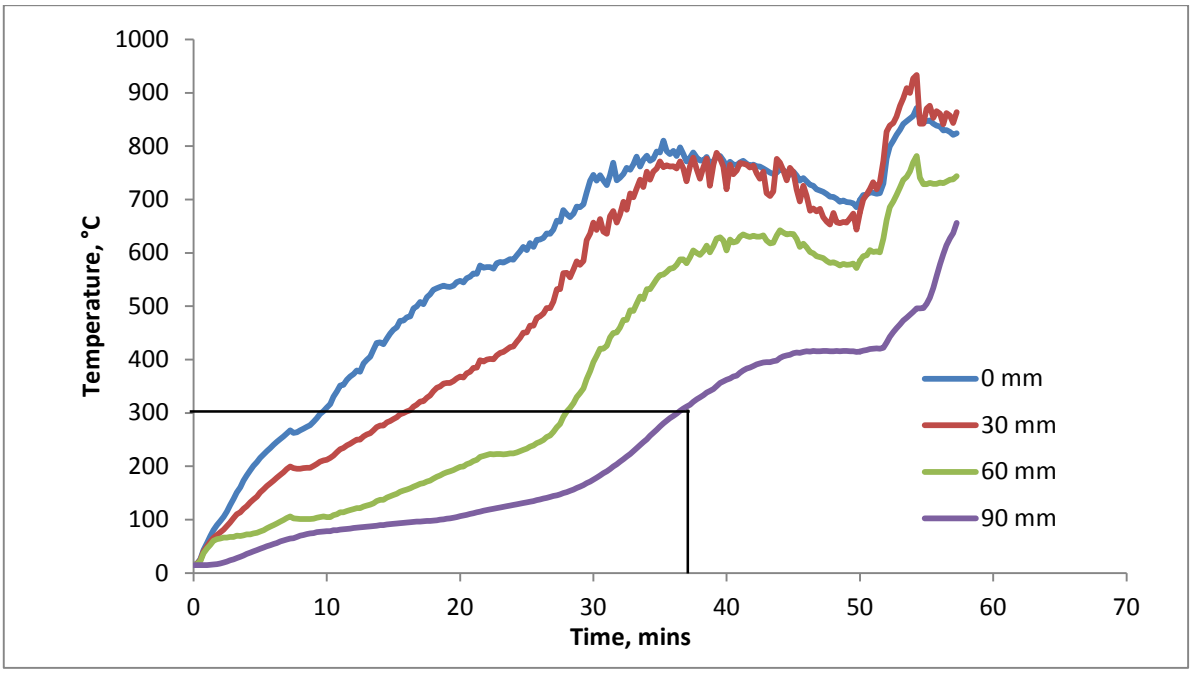

Figure 64: Typical results from thermocouples for 2.6 mm vertical gap at an average furnace pressure of 4.9 Pa

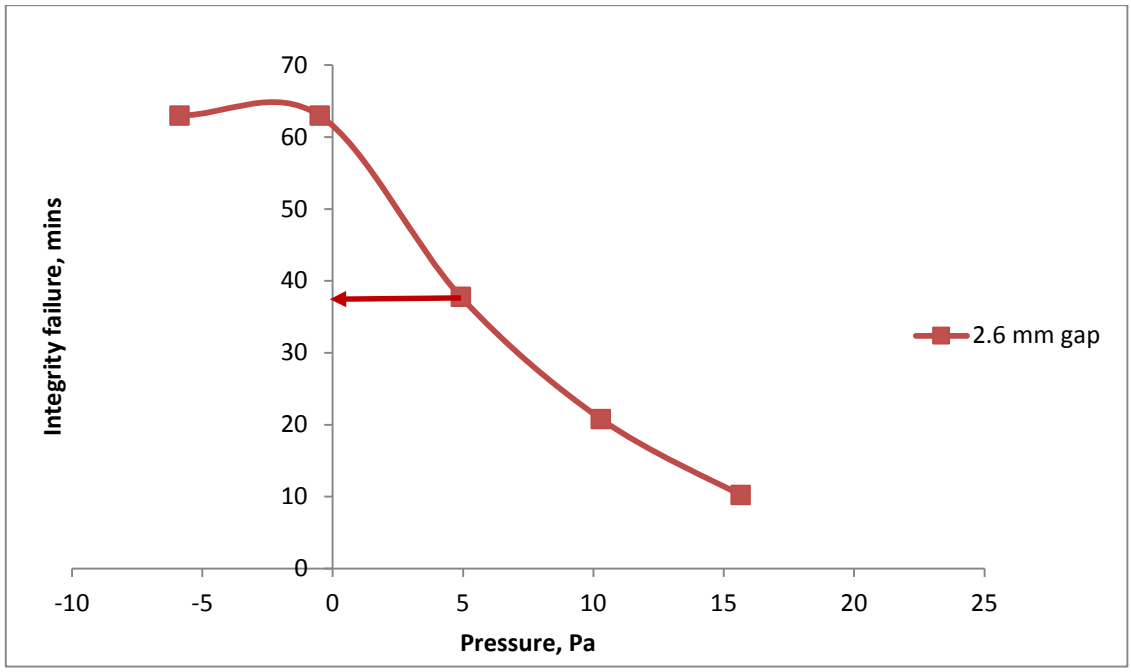

Figure 65: Typical reduction in Integrity FR with increasing pressure and elevation

In Figure 65 the Integrity fire resistance (FR) failure times from other elevations and pressures are determined from the temperature data in the same manner as that in Figure 64 to create a trend with increasing pressure. The results from a range of vertical gap sizes are added to the result in Figure 65 to produce Figure 66.

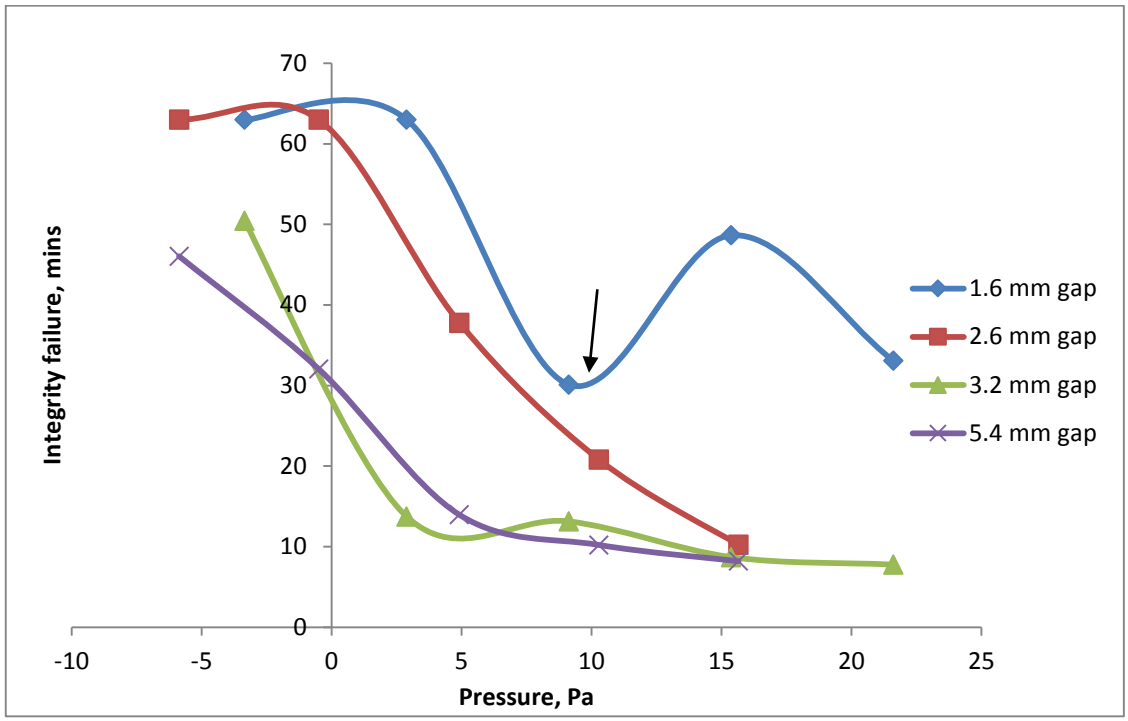

Figure 66: Reduction in Integrity FR with increasing pressure and elevation for a range of vertical gaps

For the vertical gaps in Figure 66, the reduction in Integrity to ten minutes occurs markedly with increasing furnace pressure. In the case of the wider gaps of 5.4 and 3.2 mm, the reduction occurs around the neutral pressure (0 Pa), whereas for the 2.6 mm gap, the Integrity reduction only occurs once a positive pressure is present but reduces to the same ten-minute fire resistance at 15 Pa. The wide difference in failure times between the small increase in gap from 2.6 mm to 3.2 mm in the range 0 to 10 Pa pressure possibly indicates some sensitivity due to gas flow changes over that narrow gap range.

With the narrow 1.6 mm gap, the Integrity trends similarly with the 2.6 mm gap result to a minimum at 10 Pa and then increases again. The local minimum at 10 Pa (marked by the arrow) is possibly an outlier – flaming at that location was confirmed by visual observations, the gap was covered with ceramic fibre and the test continued. Closer examination of the delay time (to reach 300^{o}C) in Figure 67 shows a reduction from about 15 minutes to eight minutes for the initiation of the flame front at 0 mm and a corresponding increase in the rate of flame spread from 1 to 4 mm/min, the combination of which explains the reduction in failure time to 30 minutes. A possible explanation can be hypothesised that the gap (at an elevation of 10 Pa) was subject to a pulsating/oscillating flow, whereby the hot gases gently heating the gap are periodically replaced with cool 21% O_2 air that supports a glowing combustion on the timber surfaces, with increased heat input accelerating the failure. This is evidence of the earlier suggested whipsaw effect in Sections 5.1 and 7.2.

On further analysis, the increased Integrity failure time for the 1.6 mm gap at 15 Pa was found to be due to an increased delay time in establishment of the flame front in the gap at a pressure of 15 Pa as shown in Figure 67 and a reduced rate of flame spread. For pressure of 22 Pa the increased rate of flame spread is mainly responsible for the reduction in failure time.

Similar analysis is presented in Figure 68, Figure 69 and Figure 70 for the 2.6, 3.2 and 5.4 mm vertical gaps. What is notable is how the flame spread rate dictates the overall failure time along with the delay time in the establishment of the flame front in the gap. Other factors are the presence of oscillating furnace pressure and the high gas temperature causing greater resistance to flow as indicated in Figure 30, all of which play a part in the overall fire resistance.

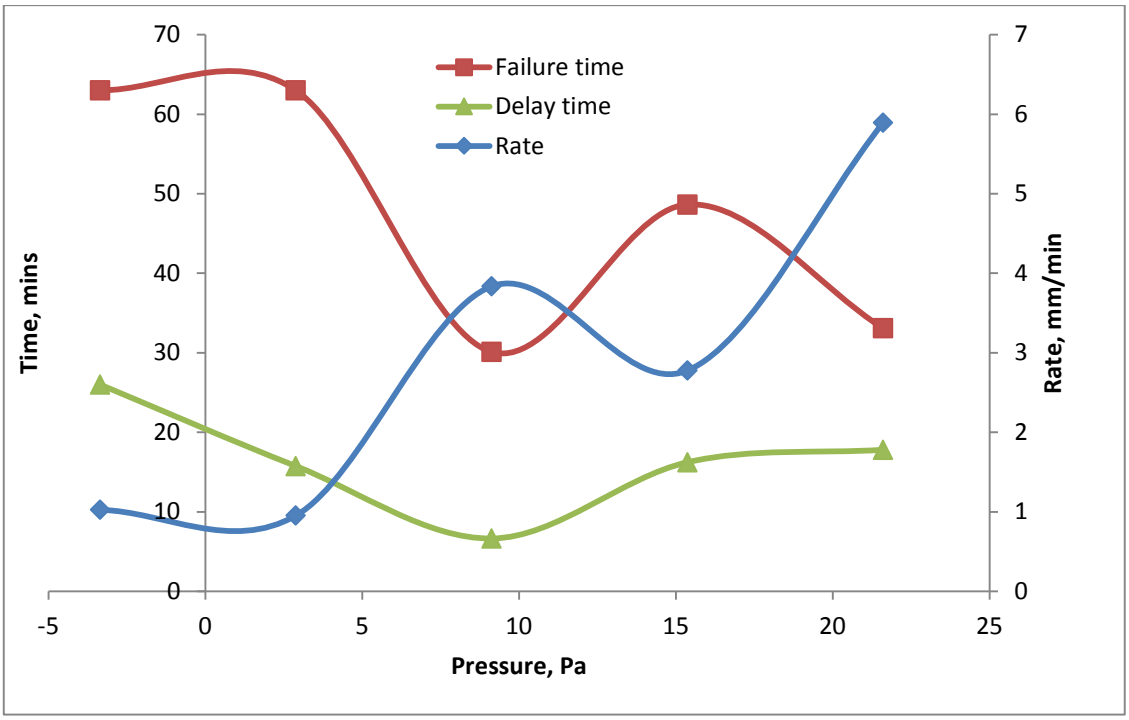

Figure 67: Failure time compared with delay time and flame spread rate for the 1.6 mm vertical gap

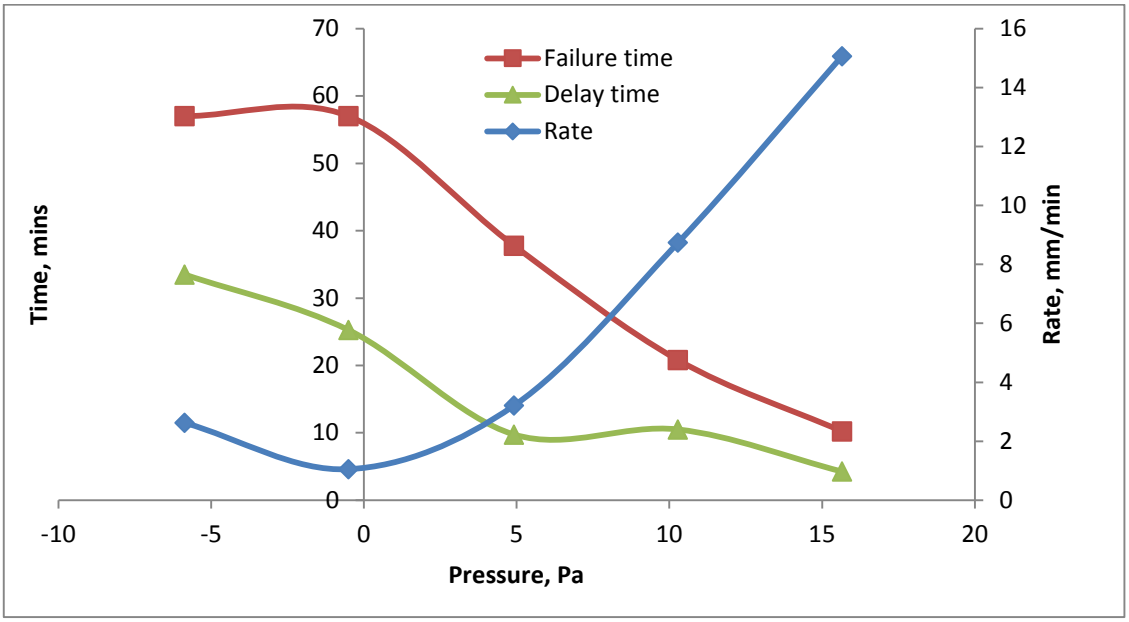

Figure 68: Failure time compared with delay time and flame spread rate for the 2.6 mm vertical gap

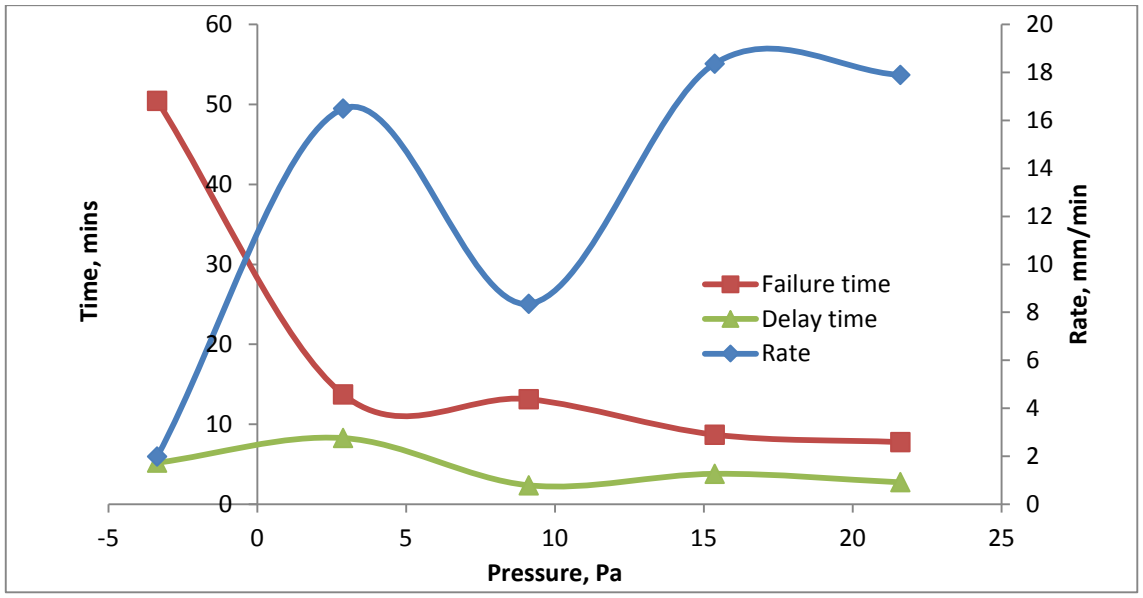

Figure 69: Failure time compared with delay time and flame spread rate for the 3.2 mm vertical gap

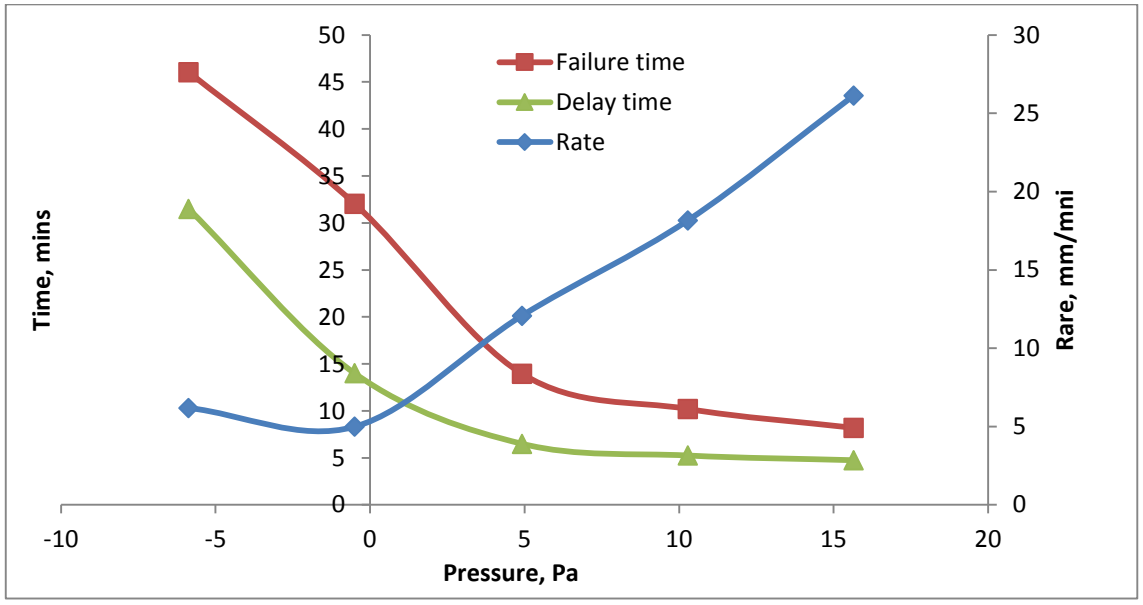

Figure 70: Failure time compared with delay time and flame spread rate for the 5.4 mm vertical gap

7.2.3 Horizontal gaps

Horizontal gaps at three different elevations and a variety of gap profiles were included in the test walls, the trend is the same at the vertical gaps, as shown over a narrower pressure range in Figure 71.

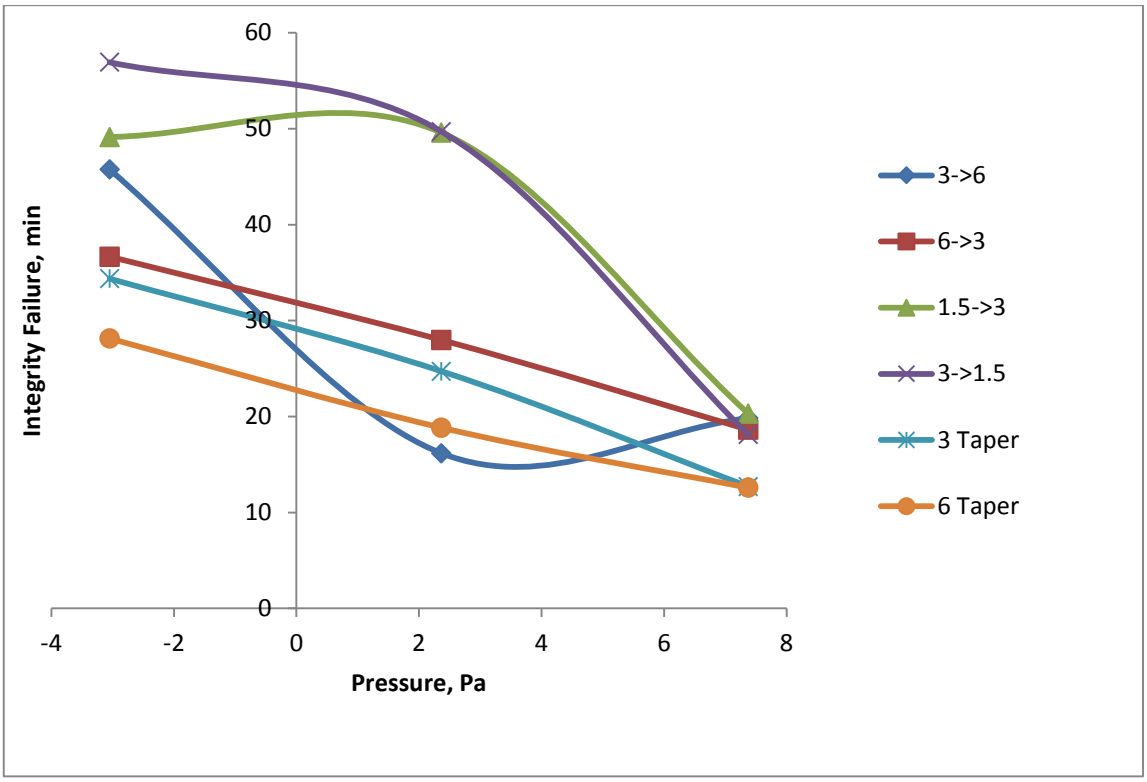

Figure 71: Integrity failure of horizontal gaps

The parameters in the legend refer to the gap size in the direction of the fire to ambient sides, such that "3→6" means a 3 mm gap stepping to 6 mm gap at the midway point of the 90 mm depth. The legend "3 and 6 Taper" means a 600 mm wide tapered horizontal gap between timber nogs, that has 0 mm height at one end increasing to 6 mm height at the other and is instrumented with thermocouples at 3 and 6 mm gaps to measure flame spread through the 90 mm passage. At lower elevations and furnace pressure, the flow resistance makes a difference to the fire resistance but as the elevation and pressure increases, the Integrity fire resistance decreases to about the same level.

A separation of the components of delay time to the arrival of the flame front and rate of fire spread are shown in Figure 72. Comparisons with the vertical gap data is limited as the range of pressures is narrower because the gaps were only installed in the mid-height range of 600, 1200 and 1800 mm elevations instead of from 300 mm to 2700 mm. However, there is still some evidence of minimums for both the delay time and the flame front travel rate occurring at low positive pressures.

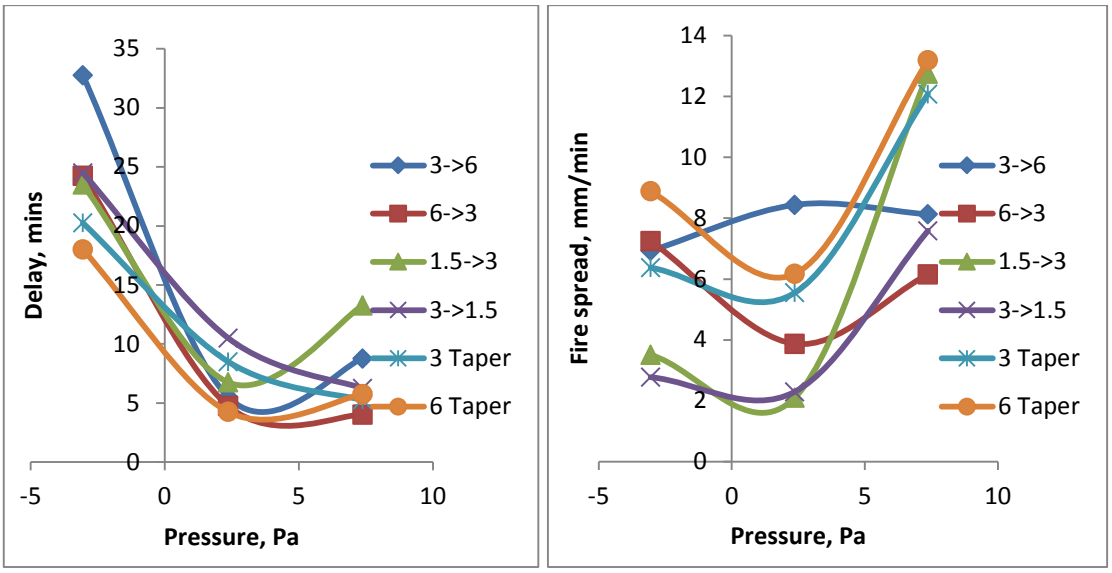

Figure 72: Delay time for arrival of flame front and rate of fire spread for horizontal gaps

7.2.4 Simulated door frames

The relative Integrity fire resistance of simulated door leaf and frame assemblies (Figure 73) is shown in Figure 74. Similar trends are evident if compared with the trends above. In practice, a fire door would include intumescent seals in the frame designed to expand on heating and restrict the flow of hot gases for a sufficient period to permit the required fire resistance to be achieved. What the above trends have shown is the sensitivity of the Integrity fire resistance to small changes in gaps and flow direction. It follows that a fire door designed with specific clearances between the leaf and the frame that relies on intumescent seals to close the gaps has the potential to have its fire resistance compromised in the event of earthquake-induced deflections, and it may be very sensitive to even small changes given the indicated trends above.

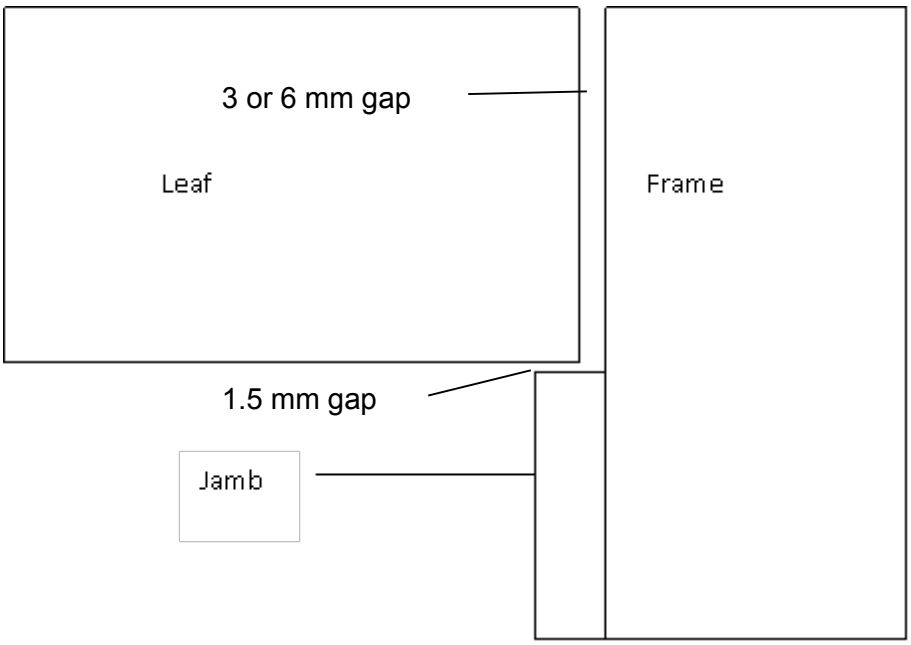

Figure 73: Simulated door frame

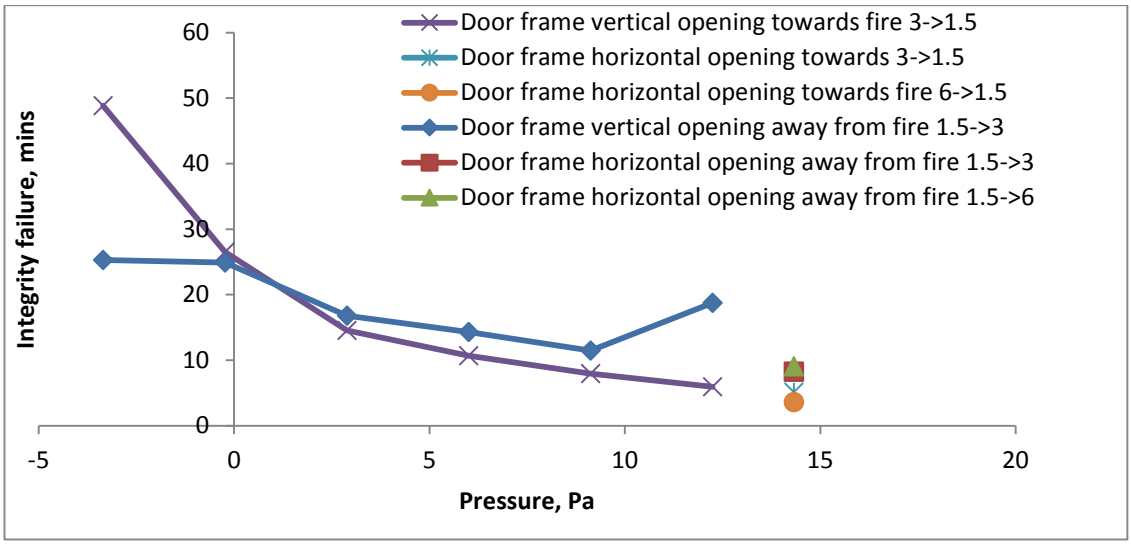

Figure 74: Integrity failures through door frame

7.2.5 Summary of failures due to gaps

When all of the vertical and horizontal data is combined in one graph, as is shown in Figure 75, there is a clear trend showing a reduction in the Integrity failure time as the furnace pressure increases with elevation. What is less certain is what gap size and shape will occur as a result of earthquake damage, but it is clear that for anything but the narrowest of gaps (less than 1.5 mm), the reduction in fire resistance is quite significant. Therefore if gap sizes resulting from earthquake movements could be kept to a minimum, this represents a possible solution to preserving the fire resistance as much as possible.

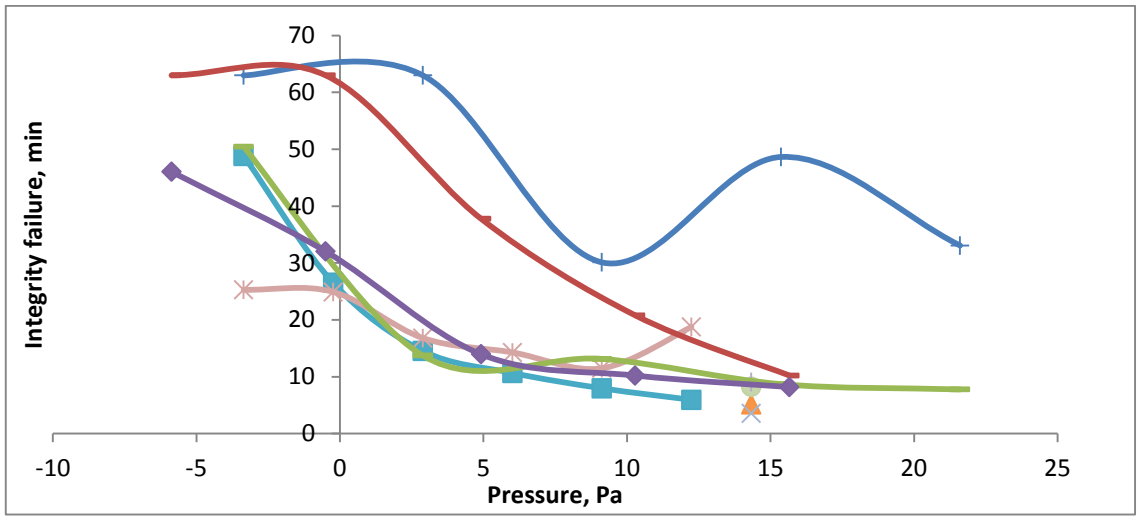

Figure 75: Integrity failure for all gaps and shapes

If the data in Figure 66 is replotted against gap size the results are shown in Figure 76. There is a marked reduction in Integrity failure times when the gap size increases from 1.5 mm to 3 mm for all pressures except -5 Pa. The shaded area represents the most

probable reductions in FRR whereby, for conservatism, the lower bound edge could be the preferred reduction acknowledged in a worst-case scenario.

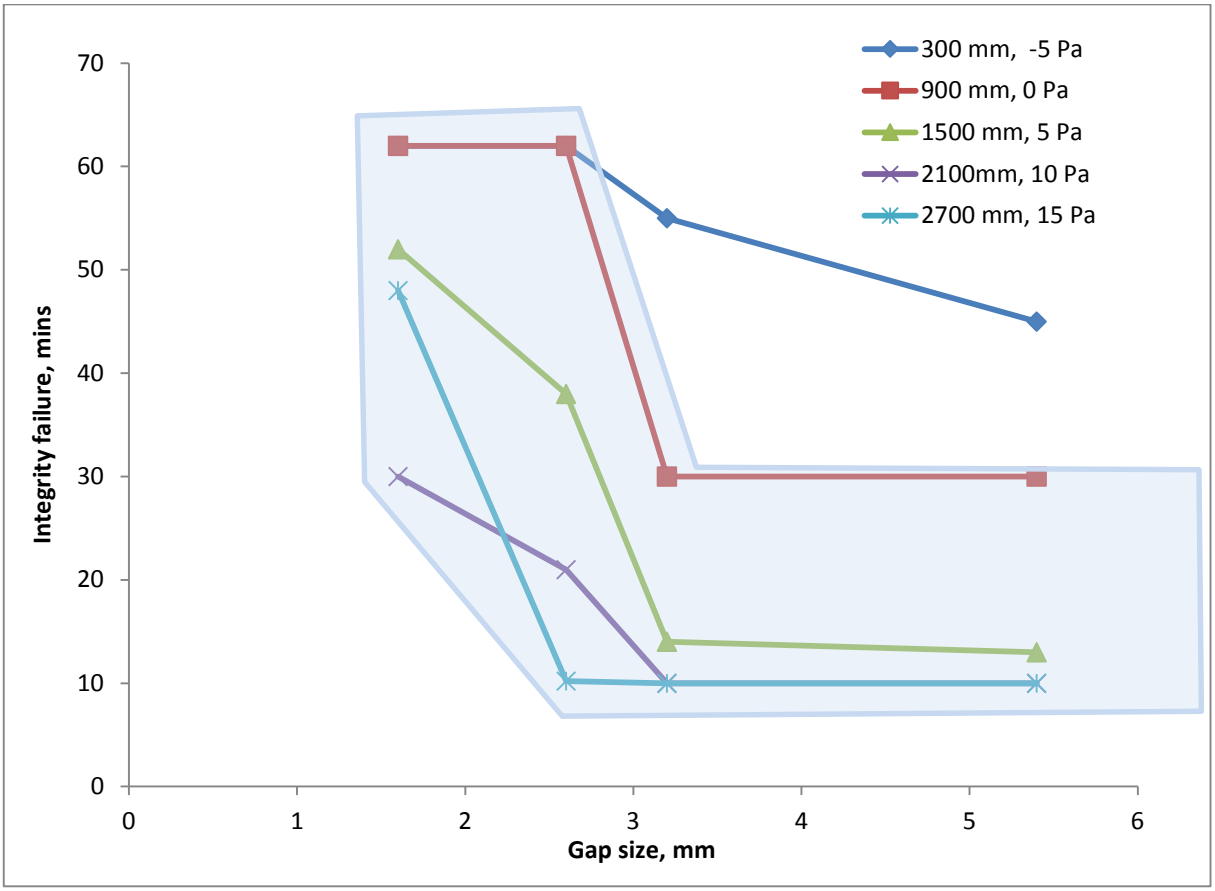

Figure 76: Downward trend of Integrity failure for increasing gap sizes at various furnace heights and pressures

This trend supports the promotion of design methods to limit earthquake damage by isolation of PFP systems from the structure as a whole, with the additional benefit being that potential reduction in damage to PFP systems is also reduced.

7.3 Fire resistance performance of walls with lining damage

Several defects consistent with the observed earthquake damage were replicated in cavity walls and subjected to the standard fire resistance test AS1530.4 (SAA 2005). The failure criterion of interest was Insulation defined by a temperature rise of 140K from ambient of the average of five thermocouples or a single thermocouple exceeding a 180K rise. Since only one thermocouple was used on each section under scrutiny, a temperature rise of 180K was taken as the milestone for failure. While Insulation failures were the focus in a large proportion of the cases trialled, it was an Integrity failure that occurred first.

The lining defects tested, shown in Table 5, demonstrated the performance of some minor defects characteristic of the low end of the damage spectrum observed. Closer analyses of the thermocouple temperatures within the cavity give some clues as to the reasons for the variations in fire resistance.

Table 5: Lining defects in cavities in a 60-minute fire-rated wall

Defect	Location
None – control	Three locations
Loose, 3 mm gap bottom edge	Fire-exposed side
Loose, 3 mm gap bottom edge	Ambient side
Loose, 3 mm gap bottom edge	Both sides
Loose, 3 mm gap top edge	Fire-exposed side
Loose, 3 mm gap top edge	Ambient side
Loose, 3 mm gap top edge	Both sides
1.5 mm diagonal crack	Fire-exposed side
1.5 mm diagonal crack	Ambient side
3 mm diagonal crack	Fire-exposed side
3 mm diagonal crack	Ambient side

The instrumentation of the damaged cavities and control sample are shown in Figure 77, with the disc-type thermocouples placed from left to right recording the:

- Non-exposed surface of the fire-exposed plasterboard lining temperature (Exp)
- Gas temperature in the centre of the cavity (Cavity)
- Cavity side surface of the non-fire-exposed plasterboard lining temperature (Non-exp)
- Ambient side of the surface of the fire-exposed plasterboard lining temperature for Insulation failure (Ins).

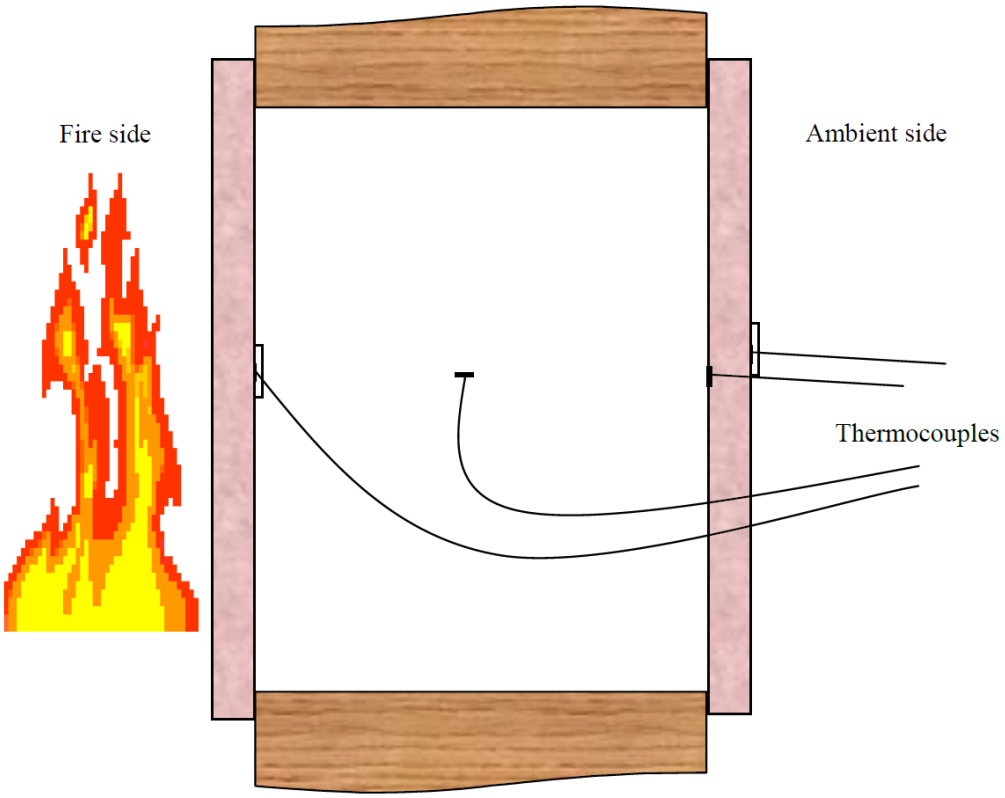

Figure 77: Instrumentation of cavity walls

7.3.1 Detached lining at bottom of wall

To simulate delaminated linings on a 90 x 45 mm timber stud wall, three 600 x 800 mm (h) cavities between the studs and nogs were lined with the bottom edge of the lining to bottom plate attachment, with a 3 mm gap on the fire-exposed, ambient and both sides. The temperature results measured in accordance with the thermocouples are shown in Figure 77, Figure 78, Figure 79 and Figure 80 and a control sample without defects is included in Figure 80.

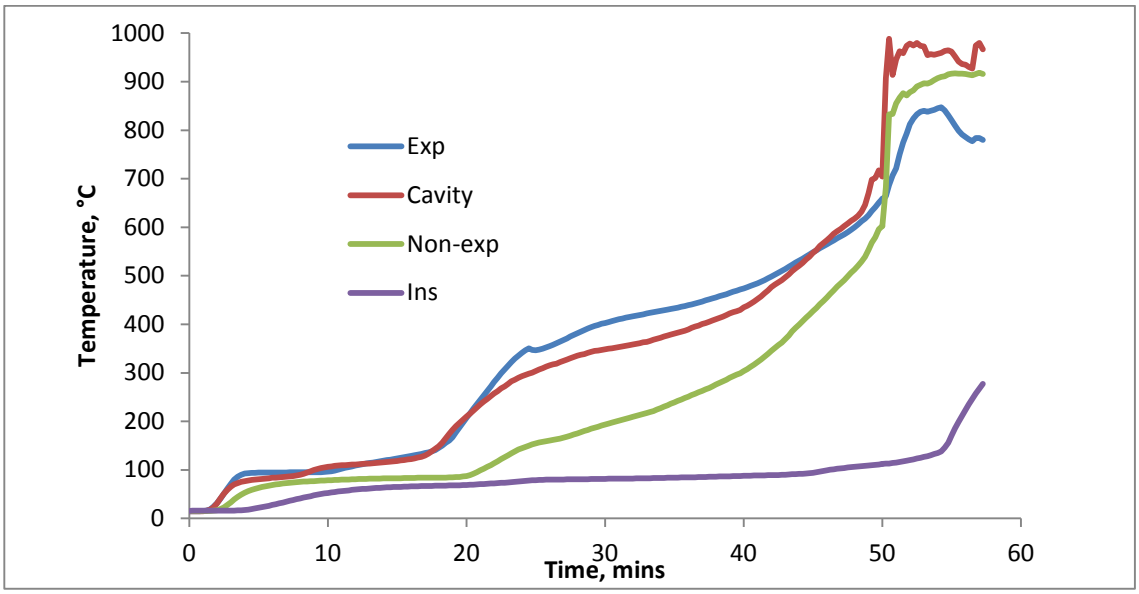

Figure 78: Loose lining with 3 mm gap bottom edge on fire-exposed side

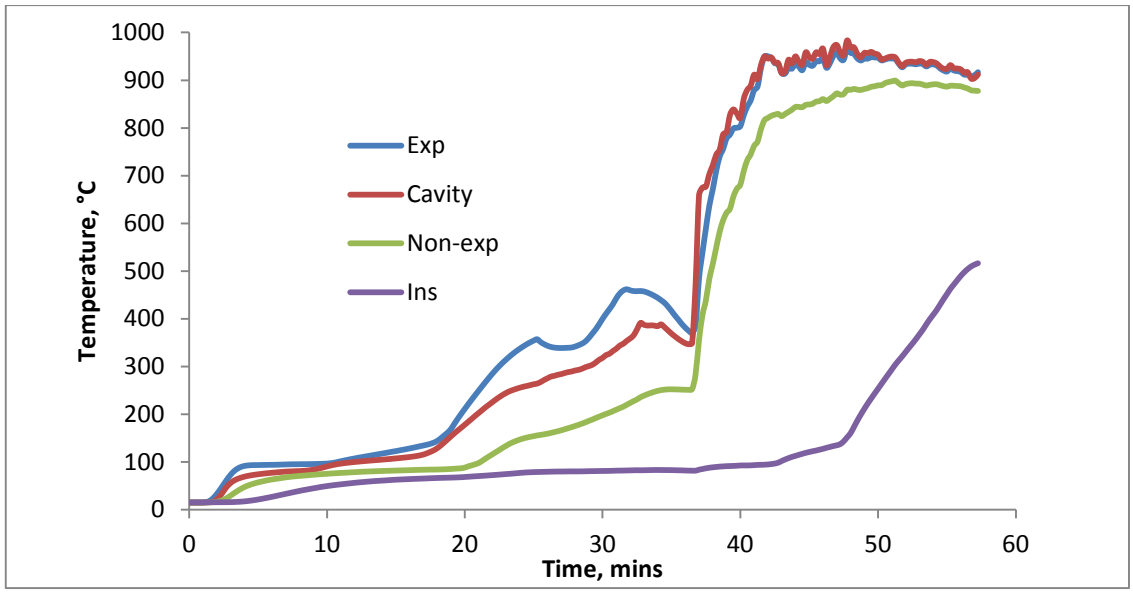

Figure 79: Loose lining with 3 mm gap bottom edge on ambient side

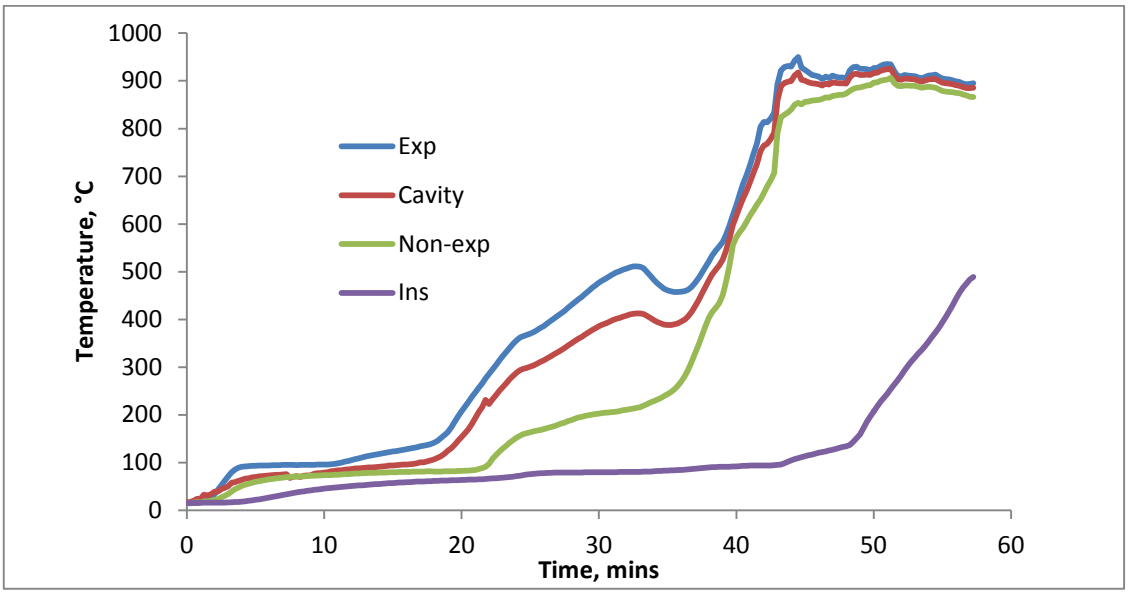

Figure 80: Loose lining with 3 mm gap bottom edge on both sides

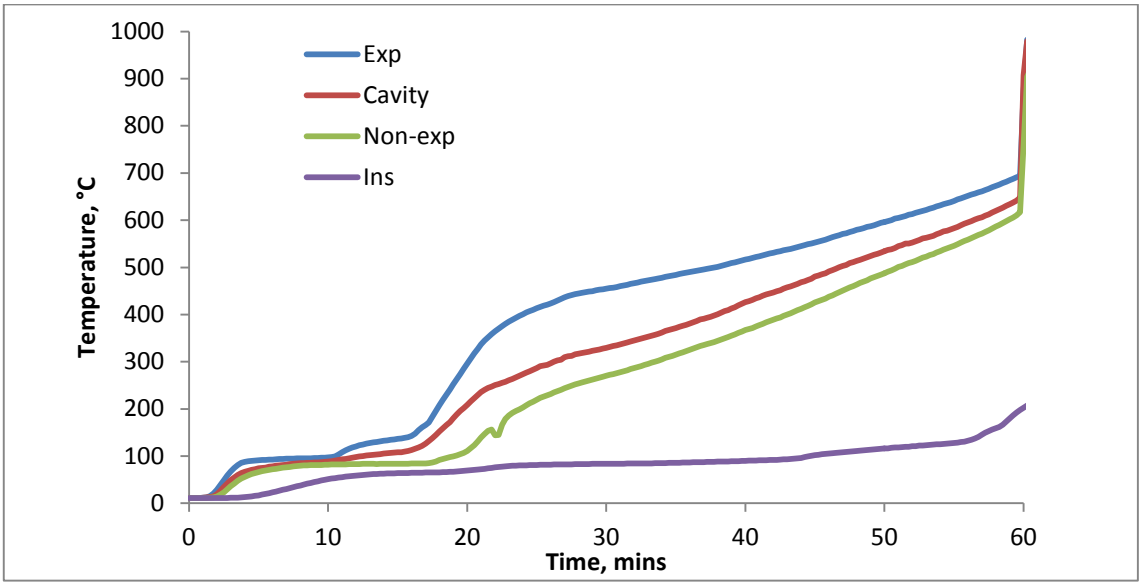

Figure 81: Control sample no damage

Some variations are evident and for closer examination the temperatures recorded at the four thermocouple locations in Figure 77 are combined in Figure 82, Figure 83, Figure 84 and Figure 85.

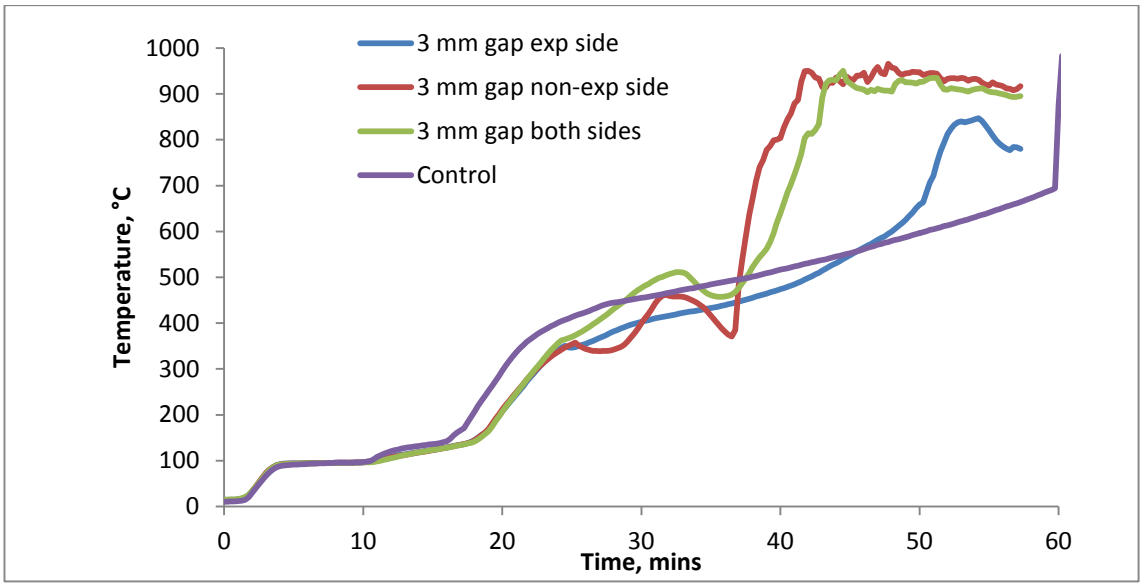

Figure 82: Comparing temperature of fire-exposed lining with gaps on bottom edge

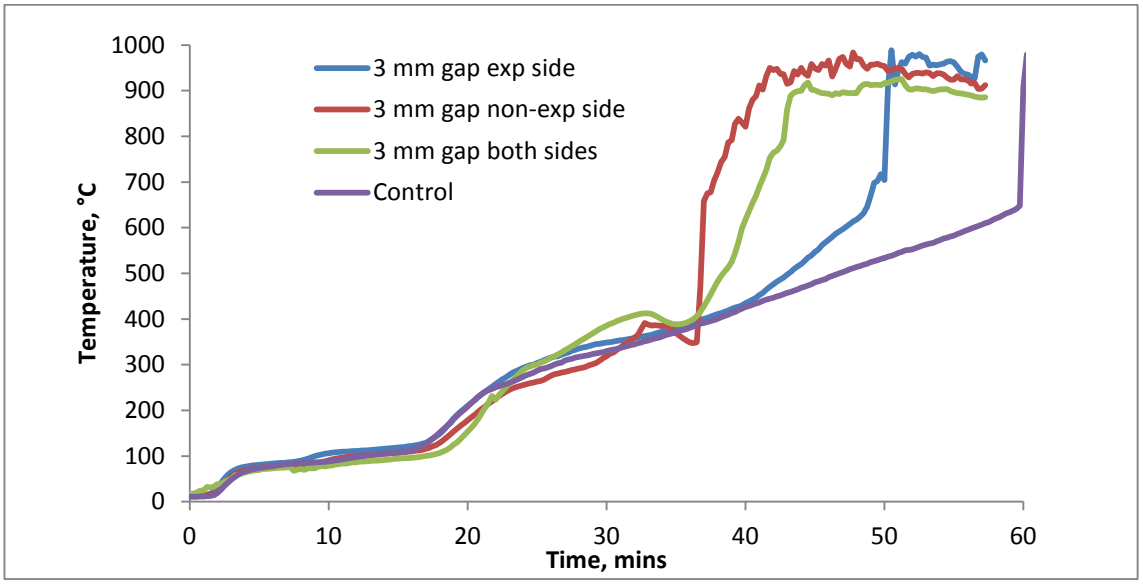

Figure 83: Comparing temperature of cavity

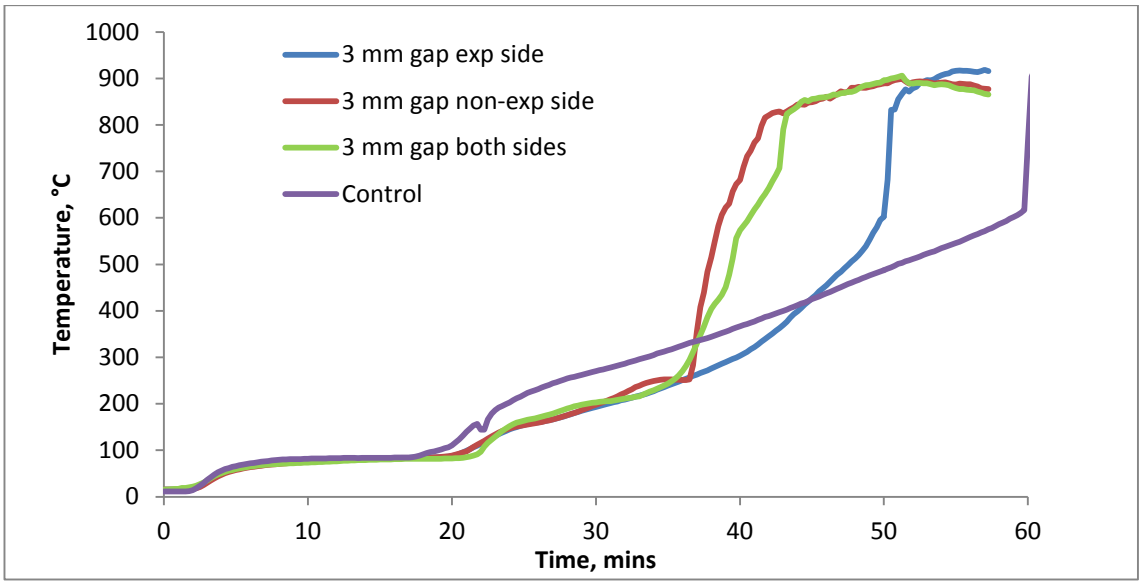

Figure 84: Comparing temperature of non-fire-exposed lining on cavity side

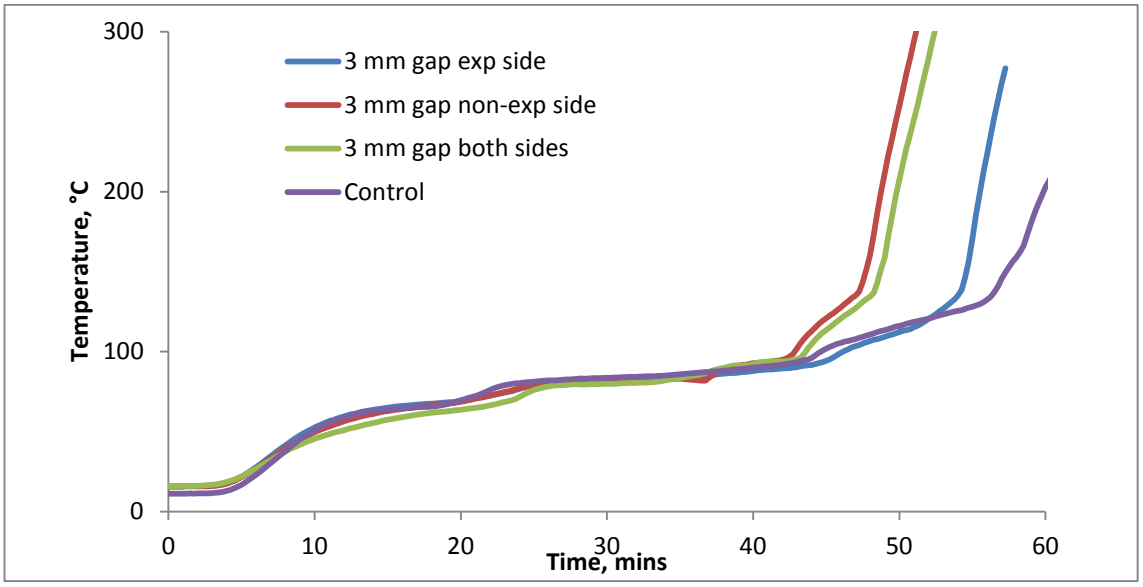

Figure 85: Comparing temperatures on ambient side

In all four locations the temperatures of the defect with the lining detached on the non-fire side rises first or performs the worst closely followed by the sample with the detachment on both sides. Unexpectedly, there is a considerable lag (~ten minutes) before the temperatures of the sample with the detached lining on the fire-exposed side similarly rises and for the control sample there is a further lag.

This result shows that lining defects on the fire side are not as detrimental to the fire resistance as on the non-fire side, but are still worse than no damage at all. Over this period no Integrity failures were recorded.

7.3.2 Detached lining at top of wall

The same (3 mm) detached lining scenario was repeated at the top of the wall. The temperature results measured in accordance with the thermocouples are shown in

Figure 86, Figure 87, Figure 88 and a control sample without defects for comparison is included in Figure 81 above.

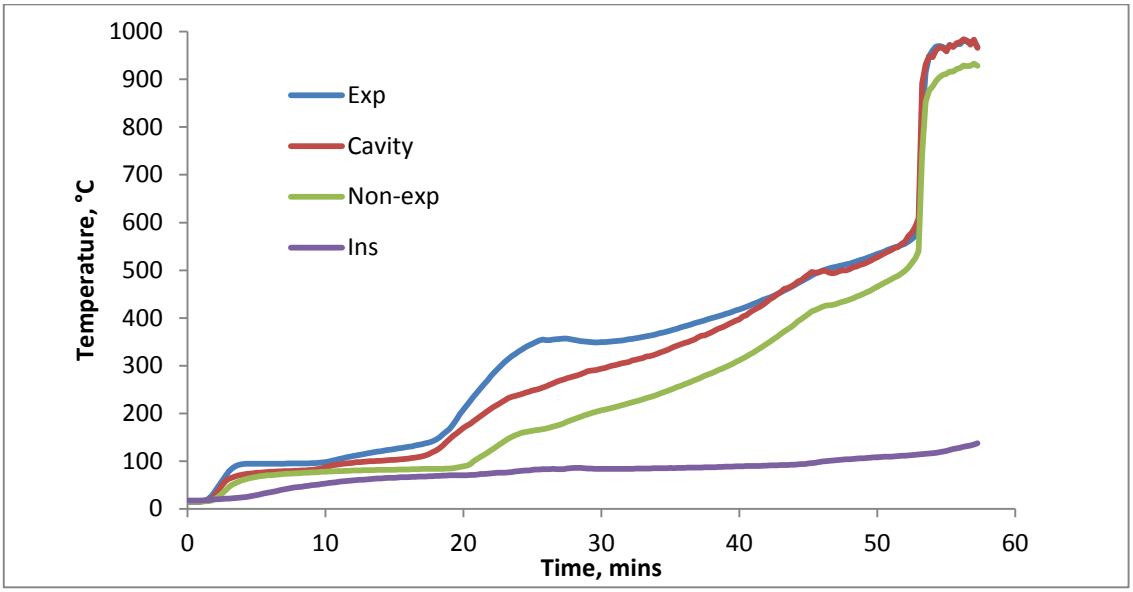

Figure 86: Loose lining with 3 mm gap top edge on fire-exposed side

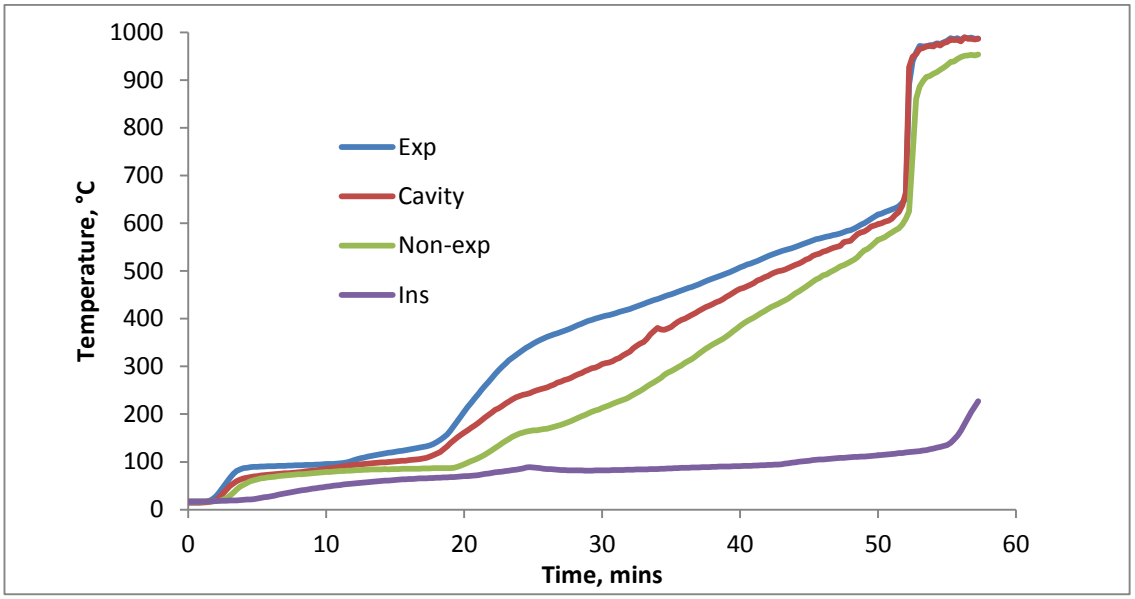

Figure 87: Loose lining with 3 mm gap top edge on ambient side

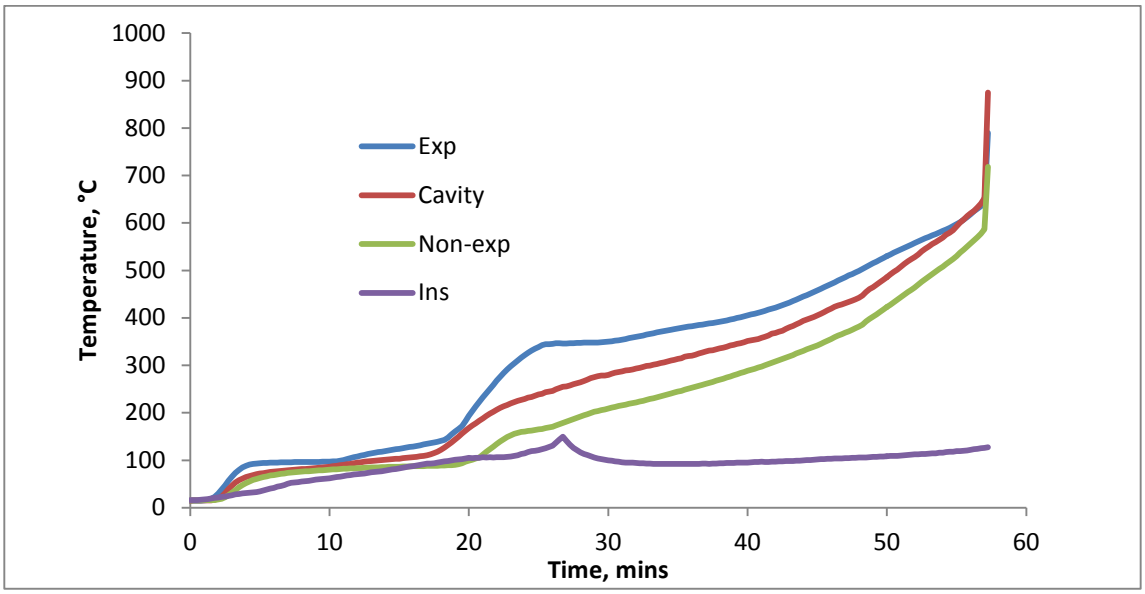

Figure 88: Loose lining with 3 mm gap top edge on both sides

A noticeable difference when comparing Figure 86, Figure 87 and Figure 88 is the relatively earlier stage that the exposed lining and cavity temperatures equalise after 40 minutes for the sample with the exposed lining attached (Figure 86), contrasted with the two later samples indicating an exchange of hot furnace gas with cavity gas instead of convective heat transfer between the exposed lining and the cavity gas. This equalisation of temperature is not evident if there is a detachment of the lining on the ambient side whereby the exchange of cooler air (perhaps due to pulsating pressure at the top level) keeps the cavity temperature marginally lower (Figure 87 and Figure 88) or so it would be expected, except that the temperature of the cavity and non-fire-exposed lining is highest (Figure 90 and Figure 91) with just a gap on the ambient side of the wall. Comparing the fire-exposed lining in Figure 89, the wall with a gap on the ambient side also has a higher temperature as does the control sample, but less reliance should be placed on these measurements as they are relatively early on in the heat transfer path.

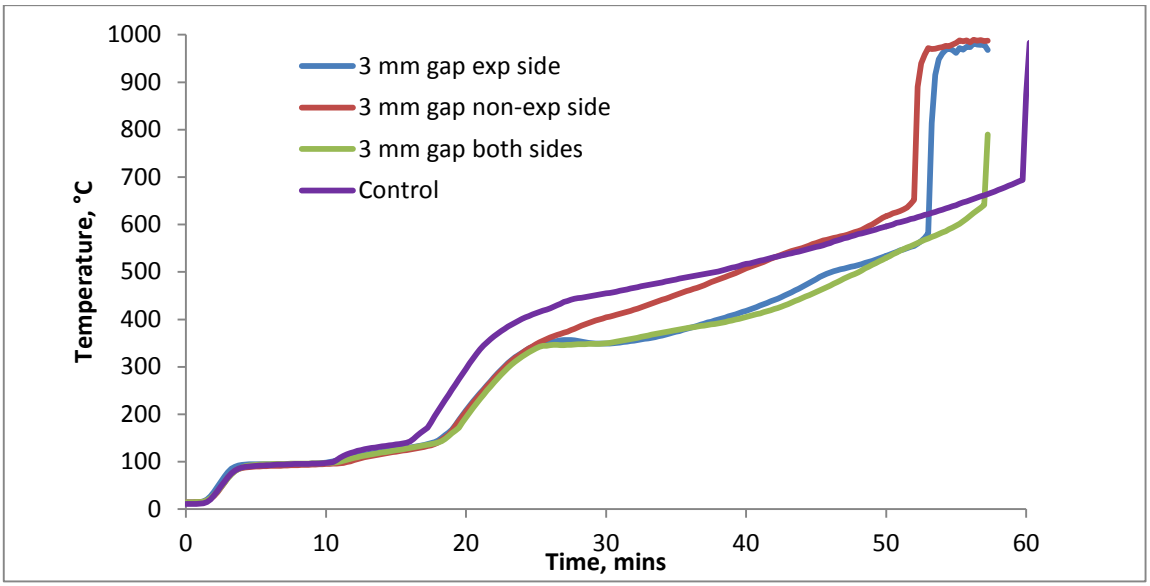

Figure 89: Comparing temperature of the fire-exposed lining with gaps on top edge

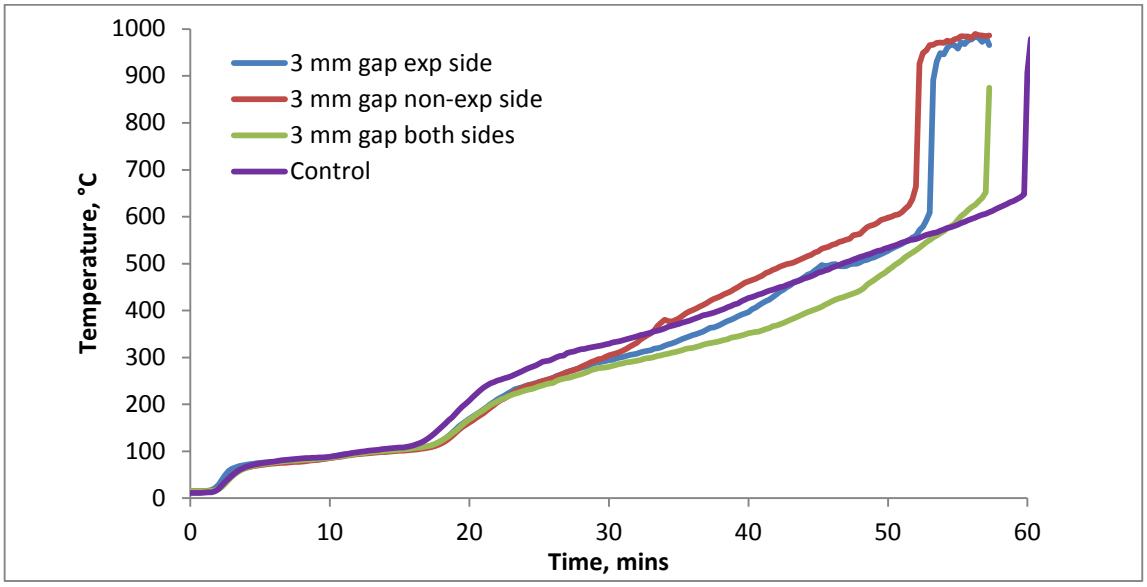

Figure 90: Comparing temperature of cavity with gaps on top edge

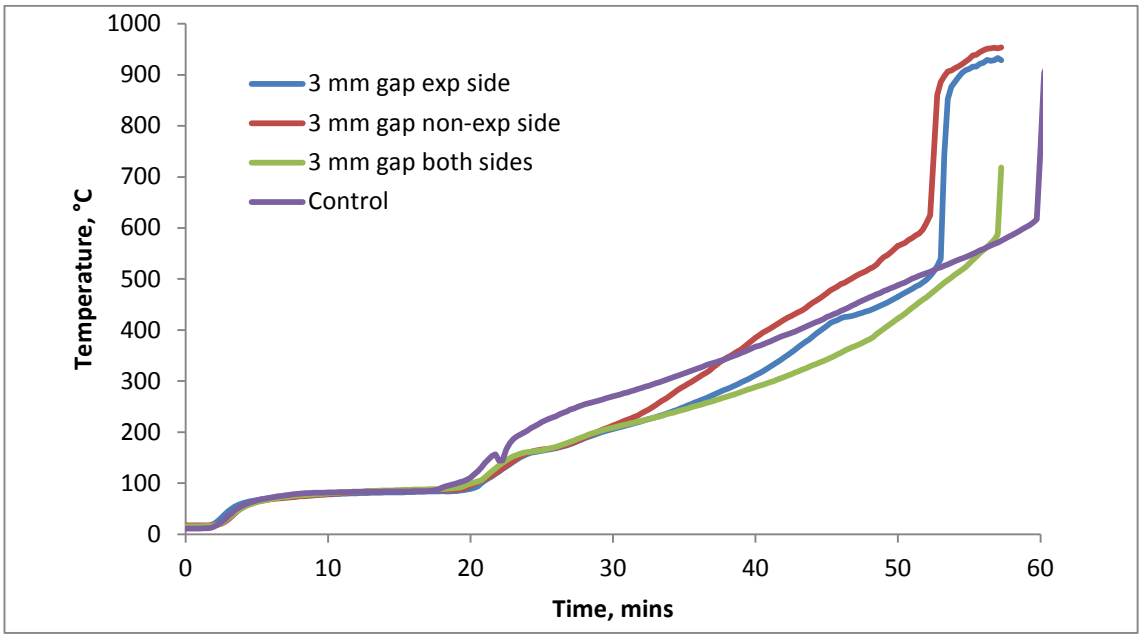

Figure 91: Comparing temperature of non-fire-exposed lining with gaps on top edge

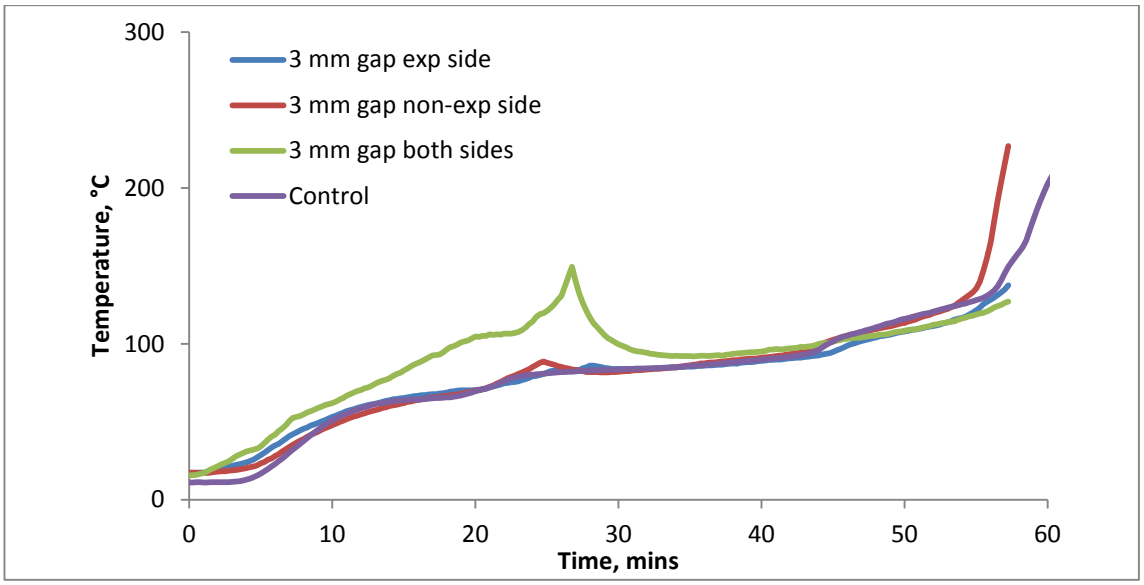

Figure 92: Comparing temperature of ambient side of non-fire-exposed lining with gaps on top edge

In Figure 92 the increase in temperature to a spike of the “3mm gap both sides” sample at about 28 minutes was caused by hot gases and flaming from a horizontal slot below heating the thermocouple measuring the temperature used for assessment of Insulation failure. The slot was covered with ceramic fibre at 28 minutes and the temperature then reduced to the same level as the other samples.

Once the ambient side temperatures settled beyond 40 minutes it is clearly evident that a 3 mm gap on the non-fire side is responsible for the first Insulation failure (140K rise) at 57 minutes with the control sample next to fail. However, this is academic only

because Integrity failure had occurred earlier at 49, 54 and 49 minutes respectively for the three damage conditions and the control sample exceeded 60 minutes.

7.3.3 Summary of lining detachment and the influence on fire resistance

Comparing the bottom and top lining detachment results in Table 6, the most significant difference between the two is the timing of the rapid temperature rises for the cavity locations at around 35 minutes (only for the detachment on the ambient or both sides) compared with just after 50 minutes for the bottom and top detachments respectively. Such rapid temperature rises are normally associated with an excellent indication the exposed lining has ablated away or simply crumbled off, usually the latter. For the rapid rise in the sample where the top edge has the defect, the temperature increases vertically indicating the lining has fallen off at 50 to 55 minutes.

The difference with Figure 79 and Figure 80 compared to Figure 87 and Figure 88 and further refined graphs that follow is the gentler rise at about 35 minutes that is also preceded by a dip just beforehand. This is not characteristic of lining falling off, as apart from being too soon, the slower temperature rise in the cavity and the closeness or closing of the temperatures within the cavity indicates a secondary heat source within the cavity rather than heat transfer across it (Figure 79 and Figure 80). Fuel sources such as the paper face of the plasterboard and the timber studs within the cavity and the heat source ensuring adequate dryness would not normally combust due to limited supply of oxygen. Comparing the furnace environment of ~10% O_2 (Figure 56) and the outside air at 21% O_2 it is feasible that air drawn into cavities provides the third component of the fire triangle to initiate and sustain combustion. Air is most likely to be drawn into a cavity at lower elevation where the furnace pressure is negative and especially if the ambient side lining is not firmly attached to the bottom plate as is the case shown above. If it is only the fire side lining that is detached then the gas available for exchange within the cavity is already O_2-depleted furnace gas and in-cavity combustion is unlikely.

The phenomenon of in-cavity combustion was observed in two furnace fire tests conducted at BRANZ (Collier 1996) intended to simulate real fire scenarios with a decay phase. During the decay phase the wall temperatures increased again and went through several oscillations due to cooling air being introduced to reduce the temperature which also supported continuing combustion of the timber studs.

Table 6: Summary of fire resistance degradation with detached lining

Defect	Location	Integrity	Insulation
None – control	Three locations	60 NF	60
Loose, 3 mm gap bottom edge	Fire-exposed side	60 NF	55
Loose, 3 mm gap bottom edge	Ambient side	60 NF	48
Loose, 3 mm gap bottom edge	Both sides	60 NF	49
Loose, 3 mm gap top edge	Fire-exposed side	49	57 NF
Loose, 3 mm gap top edge	Ambient side	54	55
Loose, 3 mm gap top edge	Both sides	49	57 NF

7.3.4 Cracks in lining, 1.5 mm diagonal crack

Based on the building surveys, a predominance of ~45^o diagonal cracks in plasterboard from the top corners of door frames was recorded. In general a diagonal crack would only appear on one side and on the other the damage was a vertical crack in the stopping

where two plasterboard sheets were joined, most frequently in line with a vertical side of the door frame and most frequently between double studs, which is a common construction practice above door frames.

To simulate this damage in fire tests, crack widths of 1.5 mm and 3 mm were selected to examine the reduction in fire resistance. Wider cracks were avoided as it was expected there would be an obvious reduction where for smaller gaps the reduction would be more subtle and mostly likely in the range where questions would be asked as to how much the reduction in fire resistance is likely to be.

The cracks in the plasterboard were created by scoring lines in the paper face and breaking. The plasterboard pieces were then assembled on the frame with gauges of 1.5 mm and 3 mm in the gaps (removed prior to fire testing) as shown in Figure 93, Figure 94 and Figure 95.

Figure 93: Left to right 1.5 mm crack on exposed lining and intact exposed lining

Figure 94: Left to right intact non-exposed lining and 1.5 mm crack in non-exposed lining

Figure 95: 1.5 mm crack on exposed side

The temperature results are presented in Figure 96 to Figure 101. The wall temperatures with the 1.5 mm crack on the exposed side lining in Figure 96 show a rapid increase to a maximum and a plateau at about 550°C for the back of the exposed lining. Unfortunately the thermocouple measuring this temperature was placed over the crack as shown in Figure 91 which gives an unrealistic result and is ignored, but the remaining temperatures across the wall section are reliable. Comparing Figure 96 and Figure 97 there is not a great deal of apparent difference irrespective of which side of the wall contains the crack.

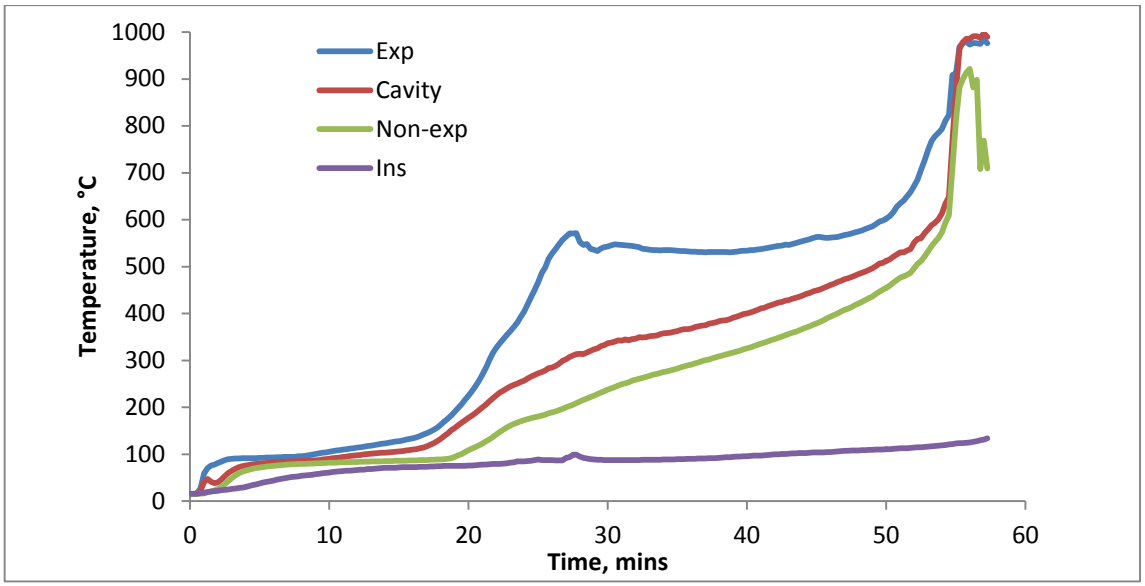

Figure 96: Temperatures in wall with 1.5 mm diagonal crack on exposed lining

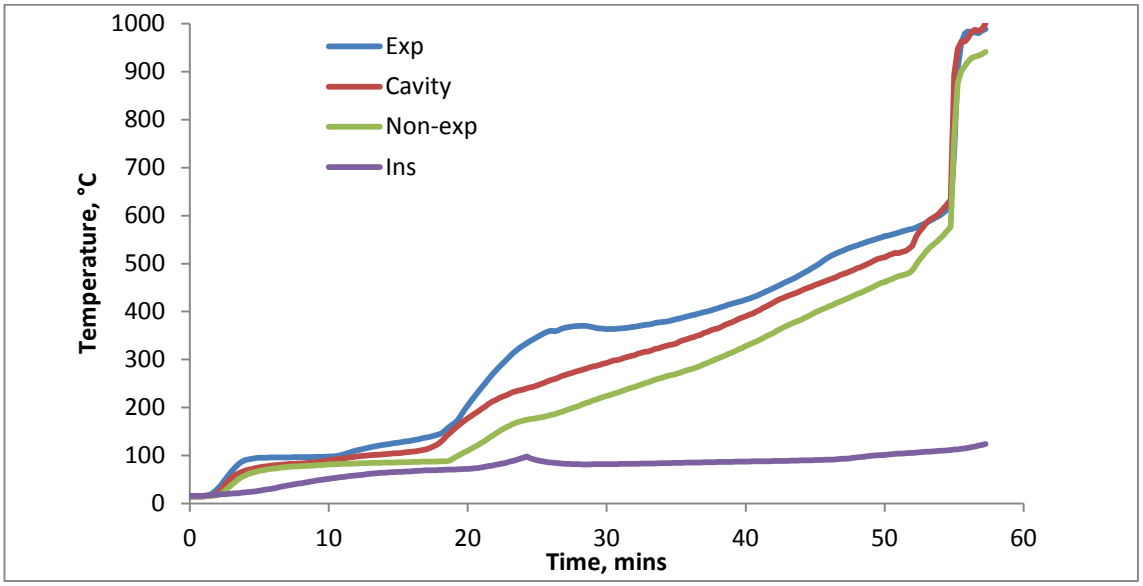

Figure 97: Temperatures in wall with 1.5 mm diagonal crack on non-exposed lining

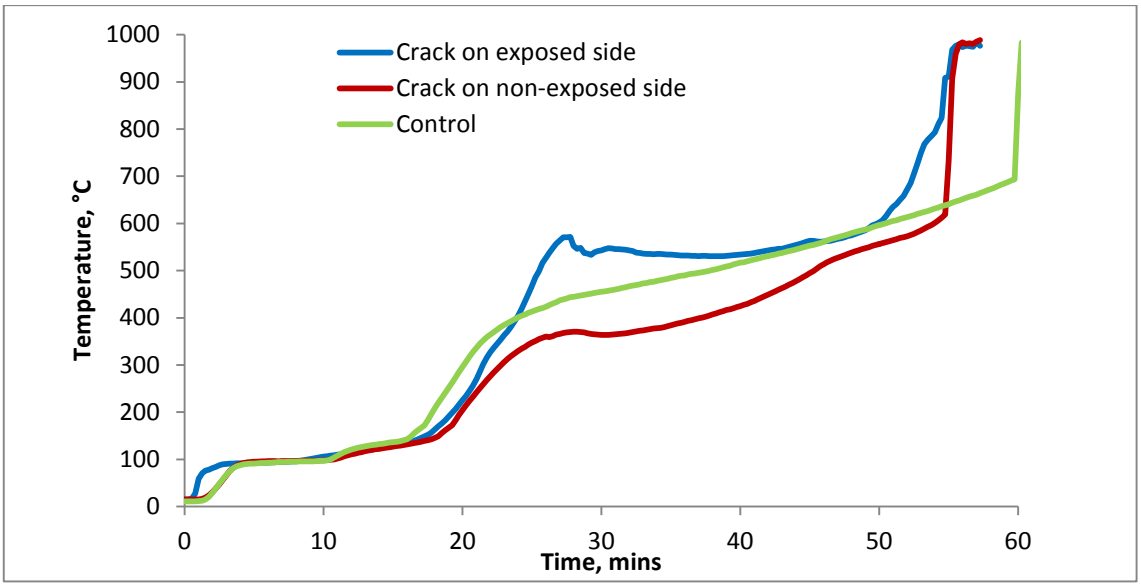

Figure 98: Comparing temperatures of exposed lining of wall with 1.5 mm diagonal cracks and control sample

The temperature comparisons in Figure 98 are of limited value given the artificially-higher reading due to the thermocouple being over the crack.

The subsequent comparisons for the cavity and both sides of the non-exposed lining in Figure 99, Figure 100 and Figure 101 indicate only minor differences due to the cracks compared with the control sample. The differences are so small that drawing conclusions about the deleterious effect of 1.5 mm cracks is probably not warranted, except to say that based on the Insulation criterion results in Figure 99, there does not appear to be any detrimental effect and perhaps a slight improvement in the fire resistance time would be realised due to the lower temperatures on the ambient side on the walls with a crack.

Incidentally the two spikes were due to flaming and hot gases from the horizontal gaps below which were covered with ceramic fibre prior to 30 minutes and the test continued with the two temperatures returning to the same rate of increase they would have had without being externally heated.

An Integrity failure at 55 minutes due to flaming from the 1.5 mm crack on the non-exposed (ambient) side was recorded and is the first failure mode for that sample.

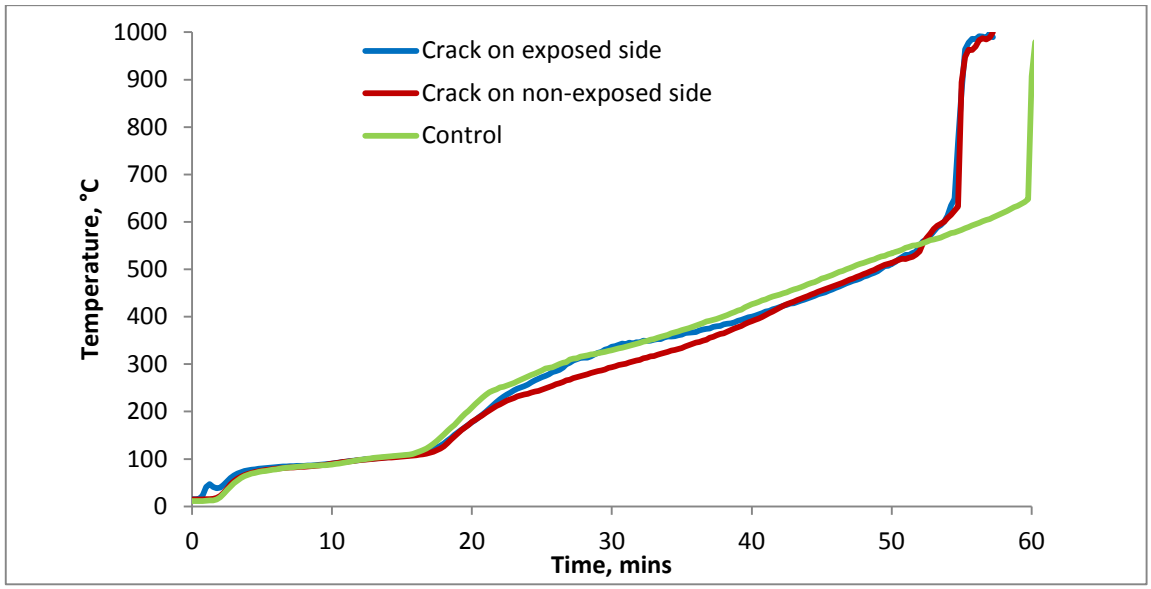

Figure 99: Comparing temperatures in the cavity of wall with 1.5 mm diagonal cracks and control sample

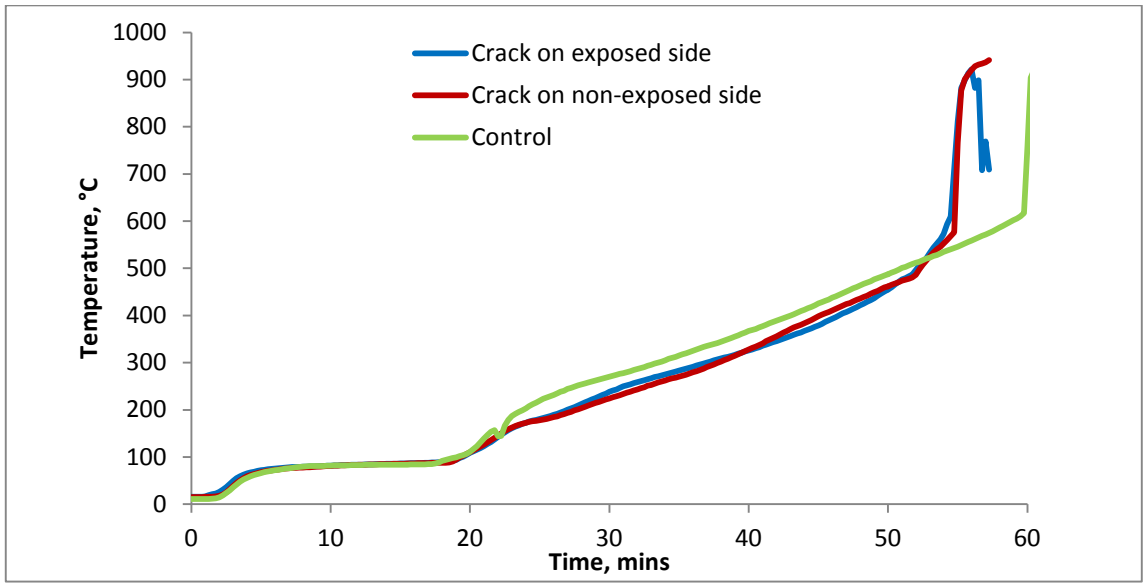

Figure 100: Comparing temperatures of the cavity side of the non-exposed lining of a wall with 1.5 mm diagonal cracks and control sample

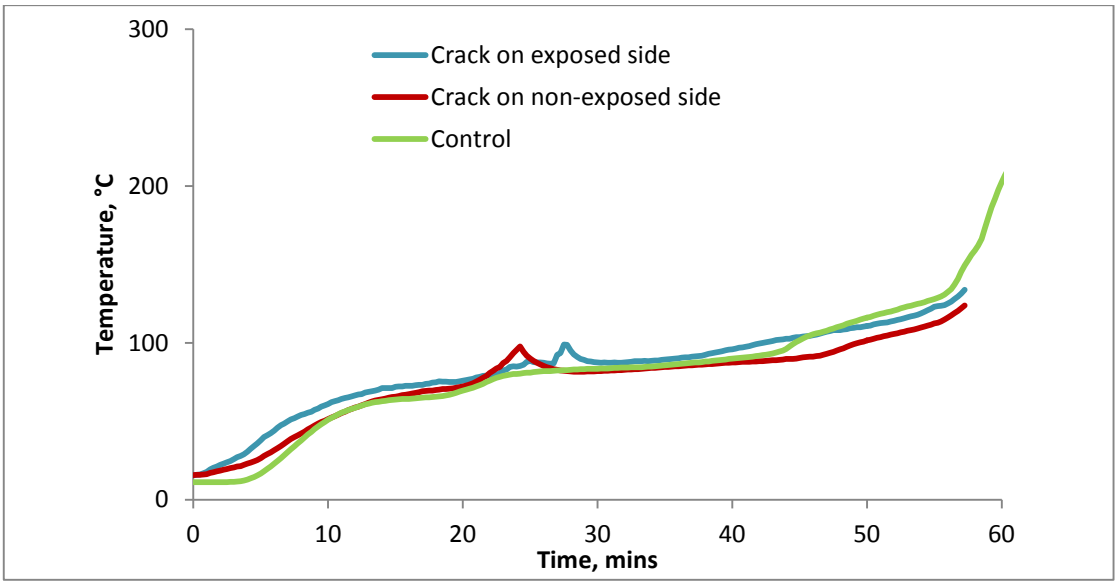

Figure 101: Comparing temperatures of the ambient side of the non-exposed lining of a wall with 1.5 mm diagonal cracks and control sample

7.3.5 Cracks in lining, 3 mm diagonal crack

The same set scenarios as for the 1.5 mm diagonal crack above was repeated for a large 3 mm diagonal crack in the lining as shown in Figure 102.

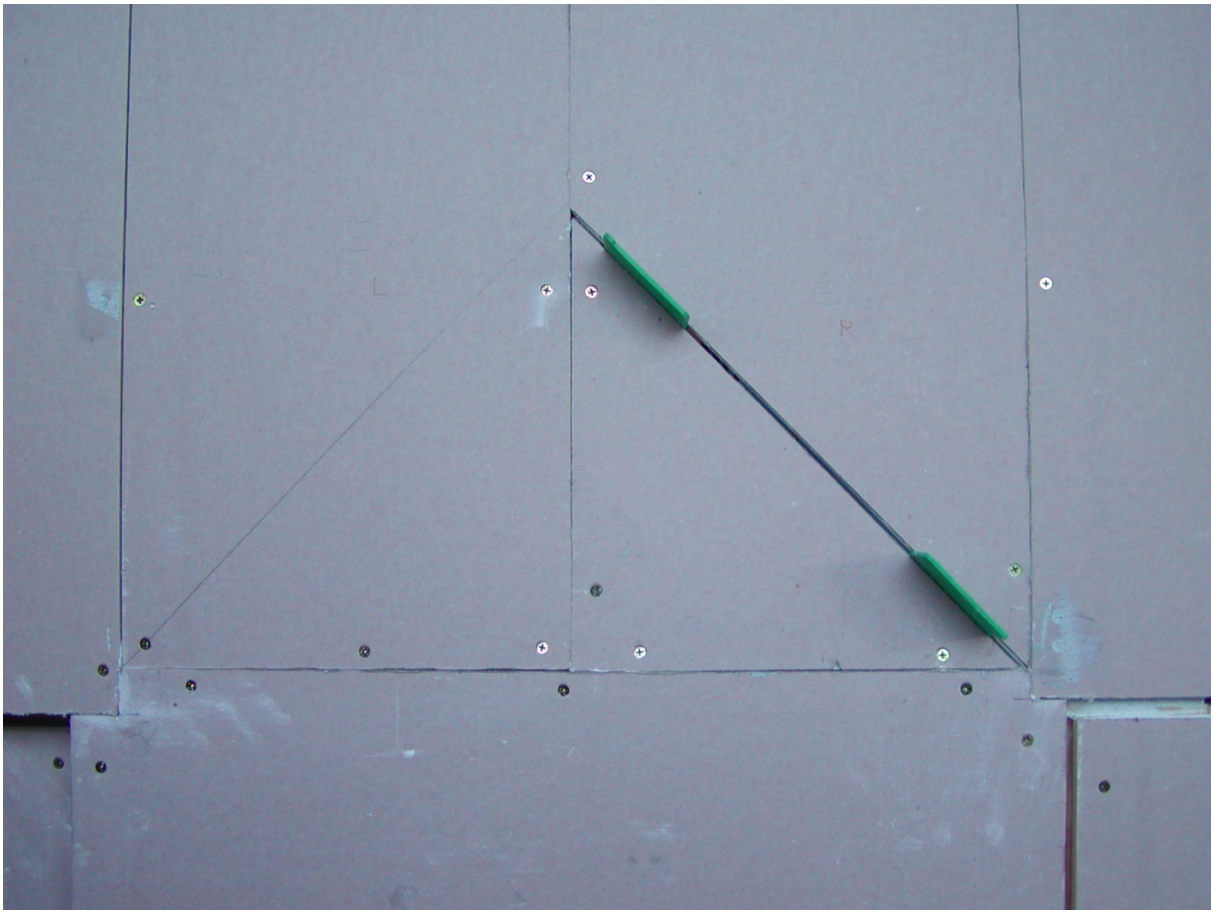

Figure 102: Diagonal cracks 3 mm wide, one each side

The temperature results are presented in Figure 103 to Figure 108. Comparing Figure 103 and Figure 104 there is not a great deal of difference that is apparent irrespective of which side of the wall the crack is.

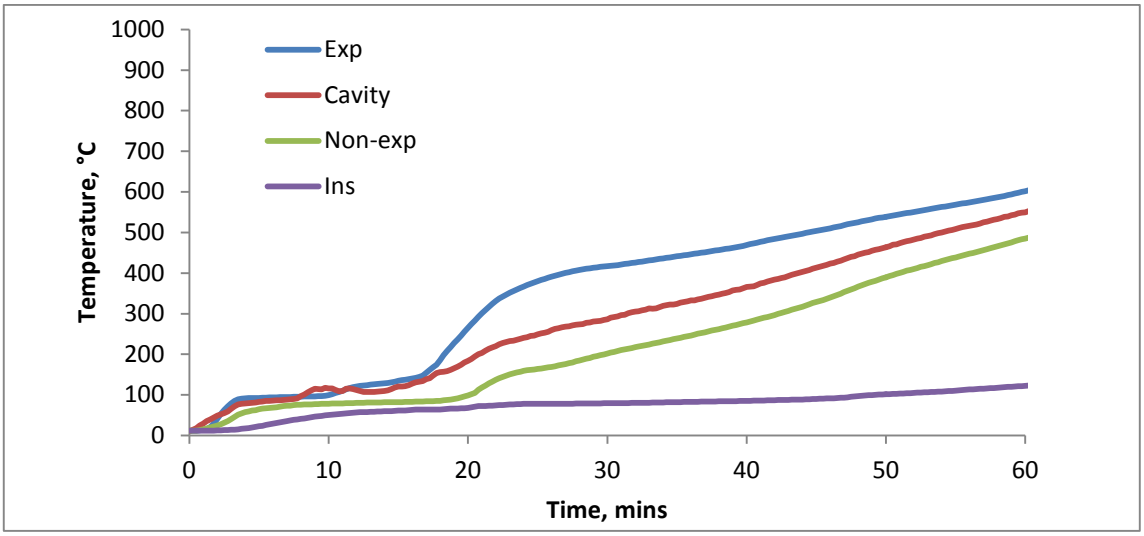

Figure 103: Temperatures in wall with 3 mm diagonal crack on exposed lining

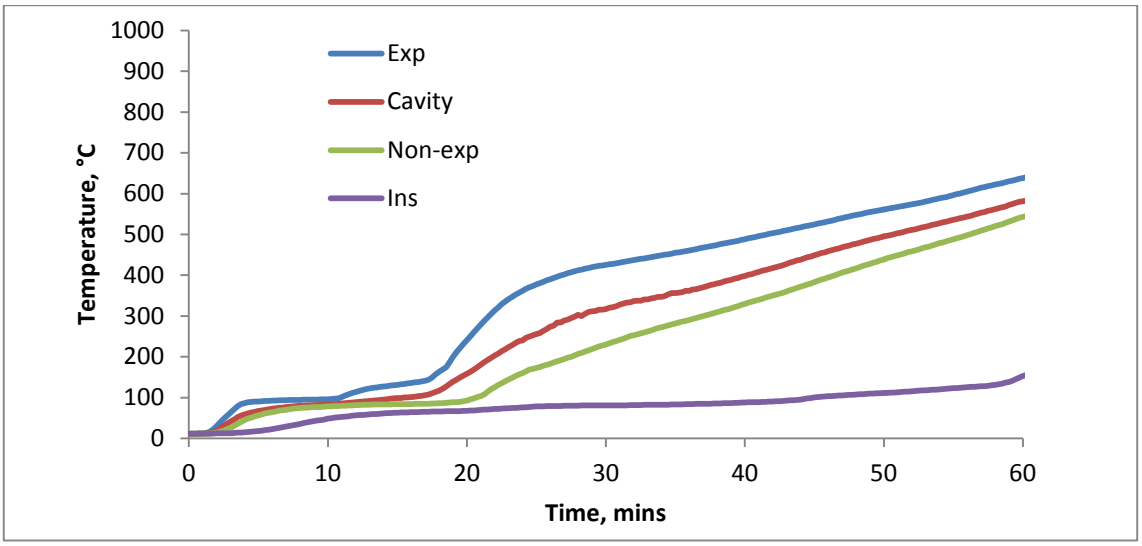

Figure 104: Temperatures in wall with 3 mm diagonal crack on non-exposed lining

The subsequent comparisons for the cavity and both sides of the non-exposed lining in Figure 105, Figure 106, Figure 107 and Figure 108 indicate only minor differences due to the cracks compared with the control sample. The differences are marginally larger compared with the 1.5 mm cracks above and for all four thermocouple locations. In every case the temperature of the sample with the 3 mm crack on the non-exposed side lining is greater than those with the cracks on the fire-exposed side. Also, in every case the temperatures for the control sample with no damage were greater, leading to the conclusion that a 3 mm crack on either side does not appear to be detrimental to the Insulation fire resistance. However, an Integrity failure was recorded for the sample with the 3 mm crack on the non-exposed side with flaming from the crack at 57 minutes.

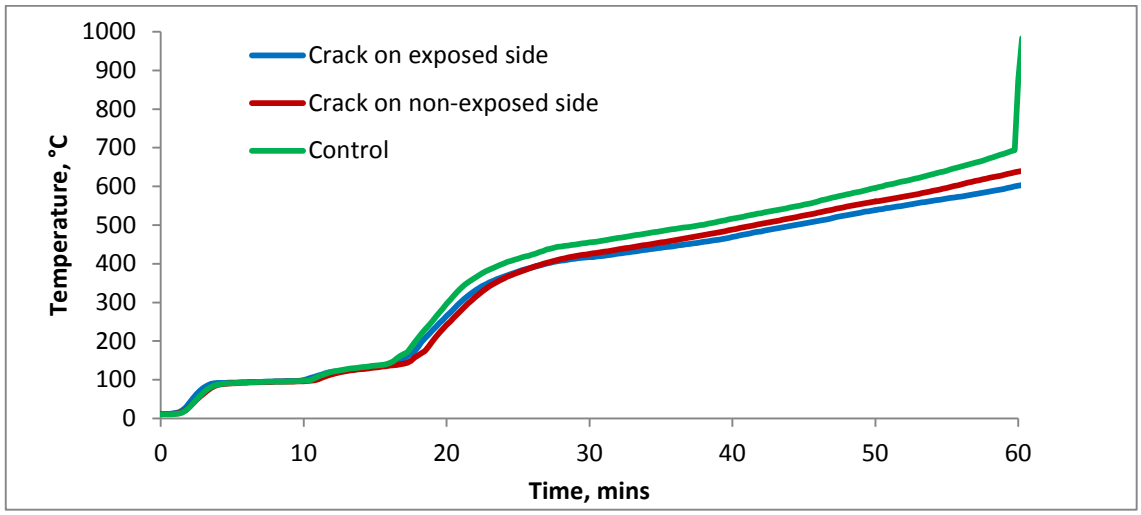

Figure 105: Comparing temperature of fire-exposed lining with 3 mm diagonal cracks

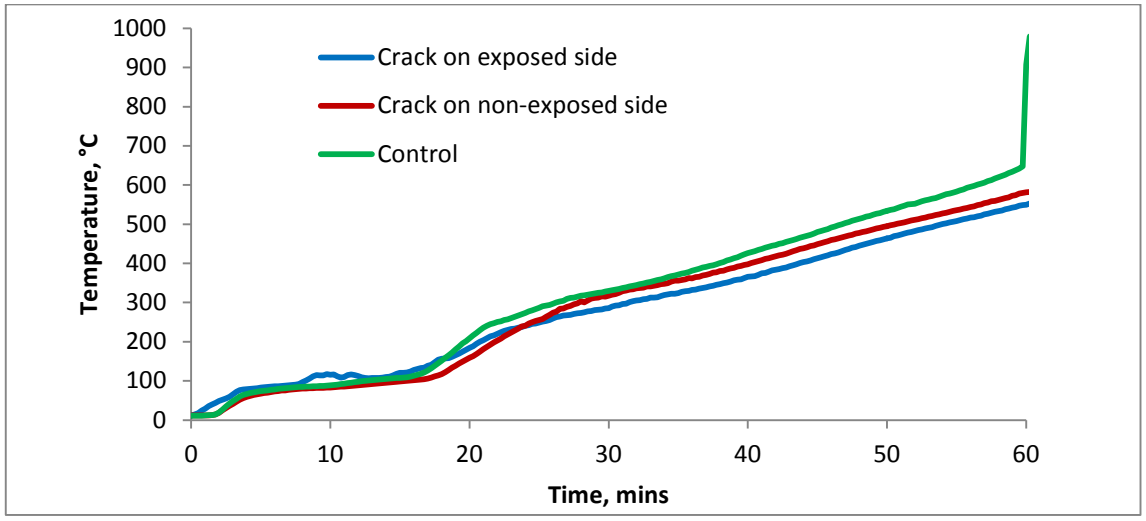

Figure 106: Comparing temperatures in cavity of wall with 3 mm diagonal cracks

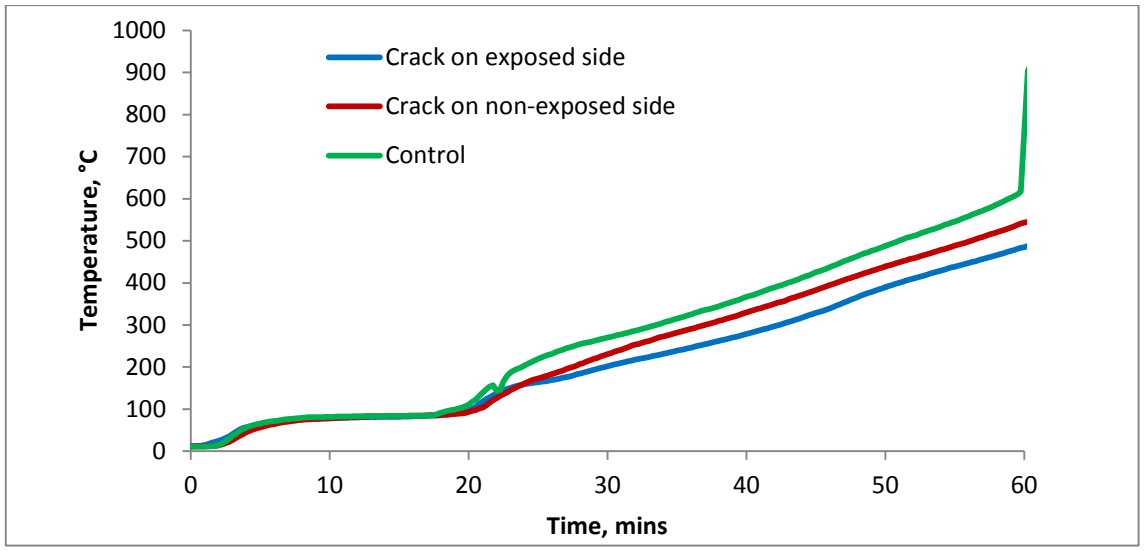

Figure 107: Comparing temperatures on cavity side of non-exposed lining in wall with 3 mm diagonal cracks

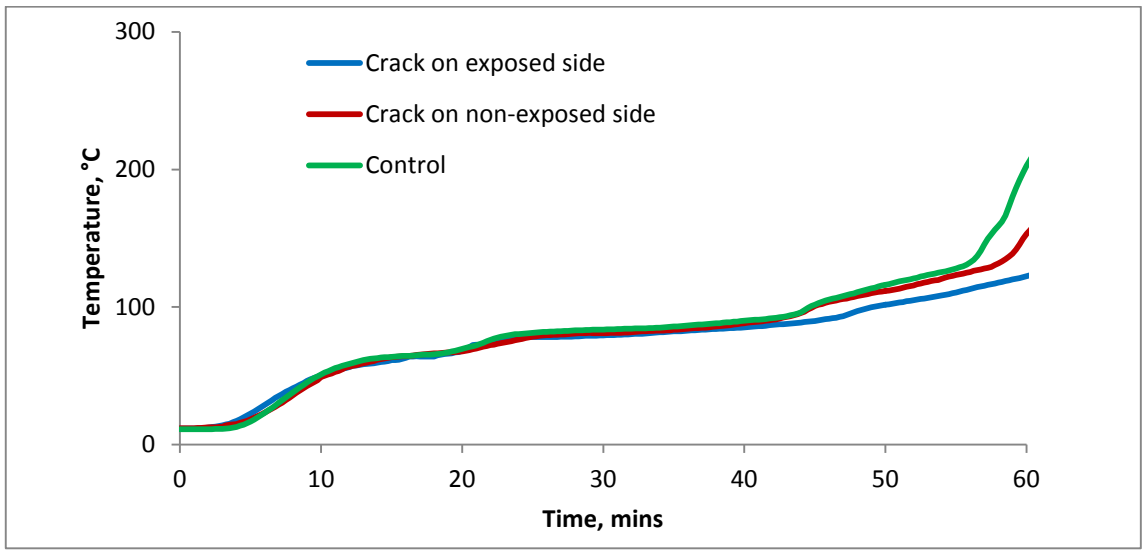

Figure 108: Comparing temperatures on ambient side of wall with 3 mm diagonal cracks

The test results for the trials with cracks in linings are summarised in Table 7. For the small cracks tested of 1.5 and 3 mm it was not apparent that there was a negative influence on the Insulation criterion performance. But the Integrity was reduced by flaming from the gaps on the ambient side through a combination of the admission of 21% O_2 air into the cavity that supports combustion within and a possibly lesser moderating effect that the cooler air serves to reduce the temperature in the cavity slightly. Another factor is the availability of fuel within the cavity, as by the latter stages of a test it is feasible that all of the paper face of the lining within a cavity has been burnt and is no longer a source of fuel, but there is timber stud remaining albeit protected by a char layer, thus contributing combustibles at a slower rate. This process may have happened sooner with the wider 3 mm gap, meaning the temperature within the cavity is marginally lower leading to a slightly longer Integrity failure time. Comparing the cavity temperatures for both the 1.5 and 3 mm gaps, the former is some 20°C hotter at 50 minutes (by comparing Figure 101 and Figure 102) and the exposed lining falls off at 55 minutes characterised by the rapid vertical temperature increase for 1.5 mm cracks,

irrespective of which side they are on. With the exposed lining gone there was an immediate Integrity failure (flaming) at the 1.5 mm crack on the ambient side. For the 3 mm crack the failure was more gradual and assessed at 57 minutes on the basis of the temperature indicated by the thermocouple over the crack exceeding 300°C and increasing rapidly.

Table 7: Summary of fire resistance degradation with cracks in lining

Defect	Location	Integrity	Insulation
None – control	Three locations	60 NF	60 NF
1.5 mm diagonal crack	Fire-exposed side	60 NF	57 NF
1.5 mm diagonal crack	Ambient side	55	57 NF
3 mm diagonal crack	Fire-exposed side	60 NF	60 NF
3 mm diagonal crack	Ambient side	57	60 NF

NF = no failure when test was stopped

The above results for the defects trialled only apply for small gaps and it is reasonable to assume that while appearing to marginally increase FR, it should not be taken as a comfort (increase in) but rather as some small margin by which minor damage can be considered to not reduce FRR up to a point. But beyond there, for larger openings it should be assumed the FRR may decrease away rapidly.

7.3.6 Summary of lining defects

A parallel can be drawn between the gaps in fire walls and the wall cavities with lining defects as compared in Table 8. The latter are essentially gaps with a large residence volume in the middle where slowly passing hot gases with increased residence time may heat the cavity, initiate combustion within and contribute to the breakdown of the assembly. Results depend on the location of the defect. For instance, although a crack on the exposed side may result in greater heating in the cavity due to the entry of hot gases, this is countered by the exchange of cooler 21% oxygen air with ~10% furnace gases inhibiting the continuing combustion of the paper faces of the lining within the cavity. On the other hand, a crack on the ambient side allows an exchange of cooler ambient air of 21% oxygen with hot cavity gases and this appears to assist in-cavity combustion once above a threshold, overriding the effect of the cooling. The internal cavity temperatures recorded supported the assumption of these phenomena.

Table 8: Lining defects in cavities and resultant reduction in fire resistance rating (FRR)

Defect	Location	Integrity	Insulation
None – control	Three locations	60 NF	60
Loose, 3 mm gap bottom edge	Fire-exposed side	60 NF	55
Loose, 3 mm gap bottom edge	Ambient side	60 NF	48
Loose, 3 mm gap bottom edge	Both sides	60 NF	49
Loose, 3 mm gap top edge	Fire-exposed side	49	57 NF
Loose, 3 mm gap top edge	Ambient side	54	55
Loose, 3 mm gap top edge	Both sides	49	57 NF
1.5 mm diagonal crack	Fire-exposed side	60 NF	57 NF
1.5 mm diagonal crack	Ambient side	55	57 NF
3 mm diagonal crack	Fire-exposed side	60 NF	60 NF
3 mm diagonal crack	Ambient side	57	60 NF

For the loose lining at the bottom edge, inwardly-drawn cool air supported combustion within the cavity and a reduction in the Insulation fire resistance as opposed to a loose lining on the top edge allowing one-way passage of hot gases and an earlier Integrity failure. Whereas, diagonal cracks on the ambient side permitted some flame-through and hence Integrity failure, but cracks on the fire side appeared to only have a minimal influence on the fire resistance.

7.4 Summary of failures in general

The results of the experimental trials show that there is a reduction in fire resistance with increasing earthquake damage or defects in general. In some cases, in particular with damage to plasterboard linings, there may be some tolerance to minor damage before there is a reduction in fire resistance, but eventually the fire resistance does reduce.

Some of the parameters affecting the fire resistance as discussed above are shown in Figure 109 and apply particularly for the Integrity criterion and also to Insulation, albeit indirectly. With the exception of the temperature of the furnace gases (or fire exposure), the influence of the parameters is clear cut, but for temperature the exact influence is complex. Although it is obvious that higher temperatures of hot flowing gases should be more damaging, the counter effects of density reducing and viscosity increasing with temperature reduce the heat-carrying potential of the hot gasses beyond 200^{o}C. The effects of which were suggested as being responsible for a slightly reduced reduction in fire resistance.

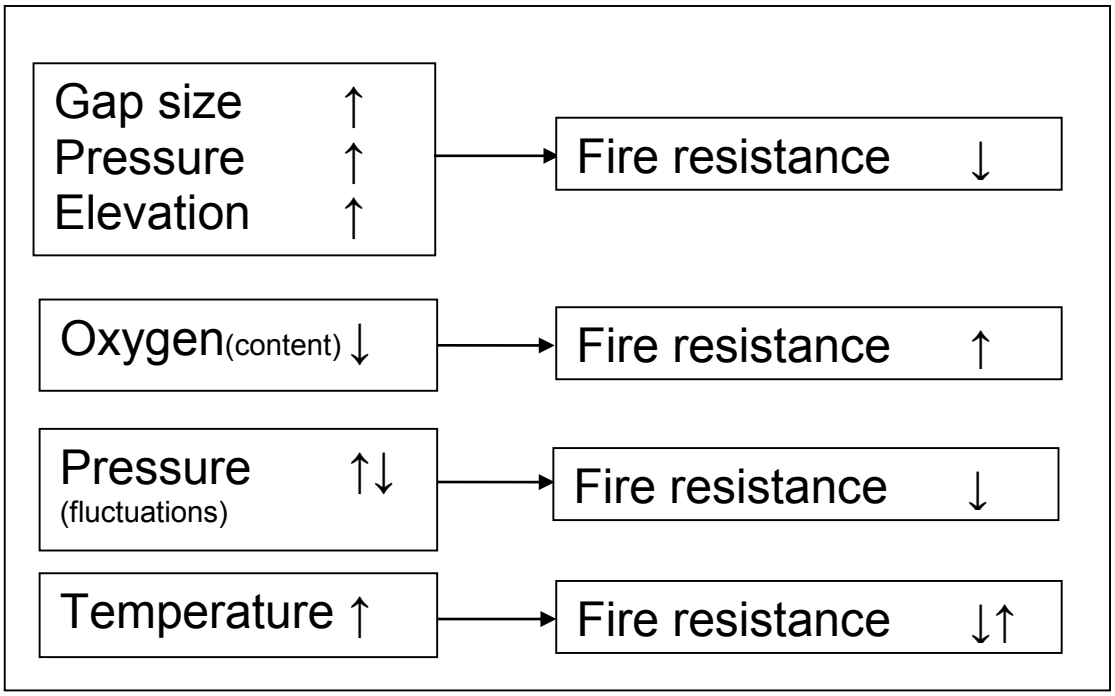

Figure 109: Factors influencing fire resistance

8. CONCLUSIONS

Following the Canterbury Earthquakes the surveys of moderately-damaged buildings that were considered structurally sound and included moderate damage to the PFP, showed the majority of the protection remained relatively intact but 5 to 10% of the PFP had sustained damage that would seriously undermine the protection to any given fire cell.

Instances of severe structural damage where the PFP was obviously ineffective, offering no protection and where clearly the condition of the PFP was a secondary consideration were omitted from the study. Similarly, superficial damage such as crazing of joints in plasterboard, where the cause may just as likely have been minor building movements over the lifetime of the building were also ignored.

Typically damage was observed in PFP in locations such as:

- Between tenancies
    - Fire-rated walls
    - Penetrations for services such as electrical cabling
- Protected paths
    - Stairwells with multiple entry points and fire-rated walls
    - Elevator shafts
    - Apartment doors to exitways.

The damage recorded mostly fell into the following categories:

- Fire-rated walls
    - Cracking and detachment of plasterboard lining from frames
    - Separation of joints in plasterboards
    - Cracking of lining around a service penetration
- Fire-rated doors
    - Movement of frame relative to leaf, clearances increased, result is a rapid decrease in fire resistance
    - Leaf and frame locked together after minor movement, move as a unit and damage plasterboard around the perimeter in particular cracking at corners
    - Frame to plasterboard lining interface develops cracks, separation and displacements from frame.

A selection of the prominent types of damage recorded in the building surveys, ranging from cracks, slots, gaps and detachments, were replicated in fire resistance tests. The damage features were instrumented with thermocouples to evaluate temperature rises and flame spread through the defects, and compared with essential physical parameters. Fluid flow theory was in turn related to the observed behaviour, in particular the magnitude and type reductions in the fire resistance.

The experimental programme has demonstrated how some types of earthquake damage to PFP systems that would be considered moderate and even superficial in some cases, do result in a reduction in fire resistance, primarily to the Integrity criterion (flaming or passage of hot gases) as the first failure. The level of reduction has loosely supported the previously-held supposition that 30-70% of the original fire resistance remains. But it has also indicated that the fire resistance may be reduced further for

higher elevations and pressures, and also at lower elevations where the pressure may oscillate such that alternating exposure to hot gas and ambient air accelerates failures. In cases where timber-framed walls have damage to the lining on one or both sides of the cavity the fire resistance was not greatly reduced for minor cracks of the order of 1.5 mm, but reduces significantly with greater openings.

The life safety implications of earthquake damage to PFP systems are twofold. Firstly, in the event of fire immediately following an earthquake, the available safe egress time (ASET) is reduced if the PFP is compromised. Secondly, buildings certified as being structurally safe for reoccupation but having unrepaired “moderate to superficial” damage to the PFP are not necessarily subjected to the same level of scrutiny, because it is not acknowledged that a seemingly small amount of damage may have resulted in significant reductions in fire resistance. Furthermore, ongoing movement and settling of buildings due to liquefaction and aftershocks may cause additional building damage, opening gaps further or initiating new ones that previously did not exist.

Either way, it is to be expected that there will be damage to the PFP post-earthquake(s) and perhaps ongoing damage due to ground settlement. The building surveys showed that approximately 10% of PFP systems were compromised in moderately-damaged buildings to a level that would cause concern and given that multiple PFP systems are protecting one firecell. As the overall protection is only as good as the weakest link, so it follows that an early failure of PFP in 5 to 10% of the systems protecting a firecell is a serious concern.

While a strategy that incorporates some risk assessment of the likely levels of compromise in the various PFP systems in a building for a given earthquake exposure is possible, an obvious and more practical solution is to lower the level of damage that is likely to be sustained by PFP systems in general by isolating them from movements of the building structure as whole. Ultimately being able to say, for example, there is a 90% probability that the PFP systems as a whole will perform to their prescribed fire resistance in a design level earthquake would be a very satisfactory statement.

Considering also the 50% reduction in FRR that is permitted in buildings where sprinklers are installed and the high rate of sprinkler system failures recorded in Christchurch, there may be a case for reviewing that reduction in high seismic risk areas and requiring 100% FRR for PFPs.

9. FURTHER WORK

Two recommendations have arisen from the project, firstly the implementation of methods to minimise damage and secondly what is the actual risk to life safety due to the outbreak of fire following an earthquake event.

9.1 Isolation of PFPs from building structure

Looking to the future, buildings are considered as heavy objects that move flexibly following ground accelerations, while the relatively lightweight PFP systems offer minimal resistance to the whole-building movement and, as a result, are damaged as the structure as a whole moves. It is proposed that isolating the non-loadbearing elements that provide the fire resistance from the building frame movements, using a range of flexible damage-resisting jointing methods, would enable the fire resisting elements to remain largely intact without repairs being required. The objective of isolating PFP systems is the prevention of damage up to a level (of earthquake drift percentage) where structural issues become the main consideration, thereafter the resistance of PFP to damage becomes less relevant.

A project undertaken at the University of Canterbury (Tasligedik, Pampanin and Palermo 2012) has shown that by simply incorporating regular relief joints, “low” and even “no damage” solutions for non-structural partitions can be designed successfully. “Shadow lines” or “negative details” at wall junctions and intersections with the main structure, and breaking up expansive areas with regular control joints, provide freedom for the non-structural elements to accommodate main structural movements. Testing has shown that incorporating such details can result in “no damage” at the **serviceability limit state** (SLS) and even ULS inter-storey drifts. Gaps can be arranged by simple calculation and can easily be made aesthetically-pleasing or hidden with sealants or trim finishes. A shift in owner and architectural expectation is required to make these details work. The challenge to the architectural profession is to incorporate and “celebrate” visible details if “low” or “no damage” solutions for non-structural gypsum plasterboard elements in commercial buildings are to be successful.

In order to protect plasterboard-lined partitions from damage, connections must be minimised and separation from the main structure must be provided so that seismic movements can be accommodated (Winstone Wallboards 2012). Figure 110 shows the principle of constructing partition framing. Metal top and bottom tracks are used with friction-fit metal or timber studs. A standard nominally 90 mm timber stud fits into a commonly-available 92 mm metal track. Plasterboard linings are fixed to studs but not to the top and bottom tracks.

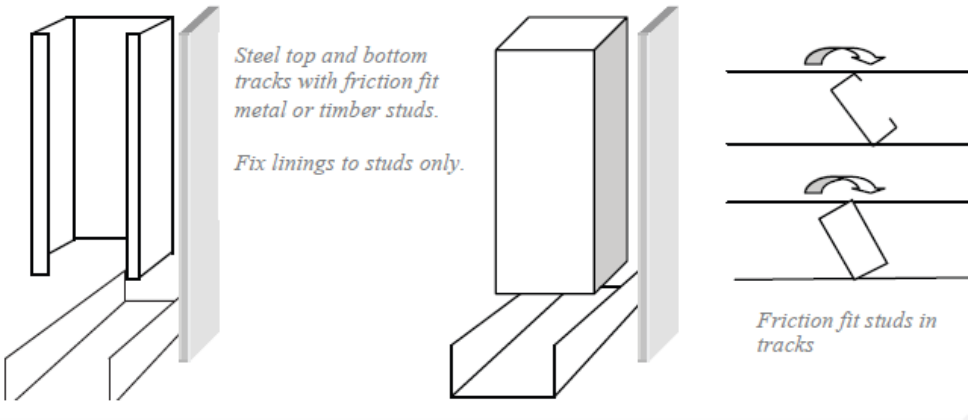

Figure 110: Framing details to minimise risk of post-earthquake damage

Figure 111 shows a sample of a number of already-available details (Winstone Wallboards 2006) that can eliminate or will significantly reduce earthquake damage to gypsum plasterboard-lined partitions in commercial construction. All details involve "disconnection" from the main structural elements and a regular pattern of intermediate control joints. Gypsum plasterboard packing strips can be provided behind joints to ensure ongoing integrity of fire or noise control separations. Proprietary trims and finishes exist to create clean shadow lines which can be left untouched, covered or sealant-filled depending on architectural preference.

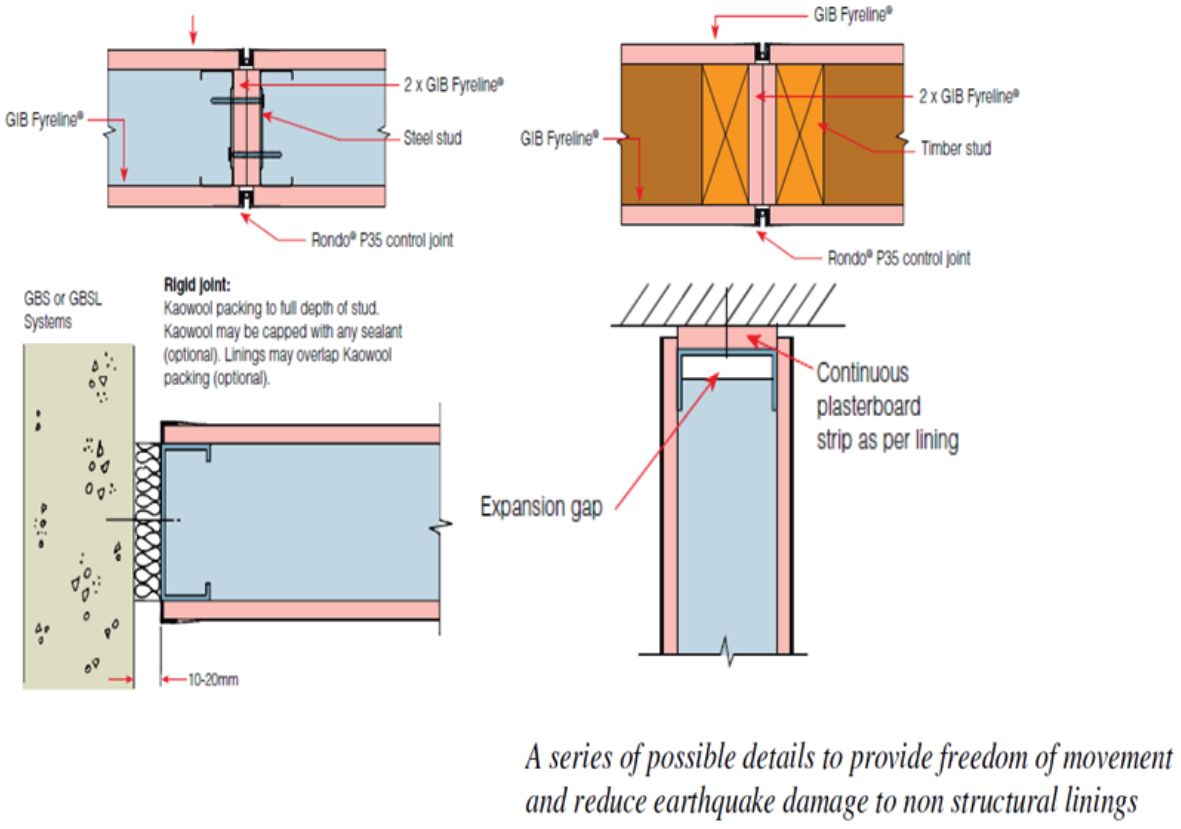

Figure 111: Simple plasterboard jointing details to minimise risk of post-earthquake damage

9.2 Risk assessment and life safety

This project has focused on the fire resistance of damaged PFP systems as determined by fire resistance testing. The FRRs determined are just that, ratings for comparative purposes, and the reductions in FRR for the damaged PFP systems tested in this project do not necessarily guarantee that is the performance in minutes that would be achieved in a real fire scenario.

To put the findings of the reductions in FRR into context some risk assessment of the reduction in life safety would be undertaken. This would include modelling the likely effects that the reduced FRR levels of the compromised PFP systems would have on the human interaction due to the spread of hot narcotic gases (FED, Fractional Effective Dose) and smoke, and how this would impact egress scenarios.

A human behaviour and tenability modelling study would trial a number of fire scenarios that include a range damaged PFP systems that result in smoke leakage and then fire spread. The resulting reductions in available safe egress time (ASET) would then be compared against the required safe egress time (RSET) to determine how much previously accepted safety margins are reduced.

Appendix A REFERENCES

Abu AK. 2012. 'Post-Earthquake Fires and Damage to Fire Safety Systems'. *Report for Natural Hazards Research Platform (NHRP)*, GNS Science, Lower Hutt, New Zealand.

Atreya A and Baum HR. 2003. 'A model for opposed flow flame spread over charring materials'. *NIST Report f03132*. Gaithersburg, MD
http://fire.nist.gov/bfrlpubs/fire03/PDF/f03132.pdf

Baker GB, Collier PCR, Abu AK and Houston BJ. 2012. 'Post-Earthquake Structural Design for Fire – A New Zealand Perspective'. *7th International Conference on Structures in Fire (SiF'12)*. Zurich, Switzerland, June 6-8, 2012.

Baker GB. 2012. 'Do Fire Protection Systems Have a Role Following Earthquakes?' *FireNZ magazine*, Fire Protection Association New Zealand (FPANZ). Issue 6 April 2012.

Borden FW. 'The 1994 Northridge Earthquake and the Fires that Followed', Thirteenth *Meeting of the UJNR Panel on Fire Research and Safety*, Vol. 2, NISTIR 6030, K.A. Beall (ed.), National Institute of Standards and Technology (NIST), Gaithersburg, MD, US, 303–312, 1997.

Cedering M. 2006. 'Effect on the charring rate of wood in fire due to oxygen content, moisture content and wood density'. *Proceedings of the Fourth International Workshop on Structures in Fire (SiF06)*. Department of Civil Engineering, University of Aveiro, Aveiro, Portugal.

Collier PCR. 1996. 'A Model for Predicting the Fire Resistance of Small-Scale Walls in Realistic Fires'. *Fire Technology* Vol. 32, No. 2 (April/May 1996), p. 120. NFPA, Quincy, MA, USA.

Collier PCR. 2005. 'Post-Earthquake Performance of Passive Fire Protection Systems'. *BRANZ Study Report 147*, Judgeford, Wellington.

Collier PCR. 2008. 'Post-Earthquake Performance of Passive Fire Protection Systems'. *5th International Conference on Structures in Fire (SiF'08)*. Singapore, 2008.

Craft ST, Desjardins R and Mehaffey JR. 2011. 'Investigation of the behaviour of CLT panels exposed to fire'. *Fire and Materials 12th International Conference*, San Francisco, USA.

DBH, 2012. New Zealand Government, "*Technical Investigation into the Structural Performance of Buildings in Christchurch – Final Report*", Department of Building and Housing (DBH), Wellington, New Zealand, 2012.

Dhakal RP. 2011 'Report to the Canterbury Earthquake Royal Commission – Structural Design for Earthquake Resistance: Past, Present and Future', *University of Canterbury*, Christchurch, New Zealand.

Drysdale D. 1998. *An Introduction to Fire Dynamics*. Wiley 2nd Edition, Chichester, England.

Frequin KL. 2011. 'Material properties and external factors influencing the charring rate of solid wood and glue-laminated timber.' *Fire and Materials Journal,* Volume 35 number 5 (pages 303–327) John Wiley & Sons, Ltd.

Gross D and Haberman WL. 1989. 'Analysis and prediction of air leakage through door assemblies'. *Fire Safety Science – Proceedings of the Second International Symposium.* Shobokaikan, Tokyo, Japan.

Hasemi Y. 2008. *Surface flame spread*. The SFPE Handbook of Fire Protection Engineering, Section 2 Chapter 12, 4th Edition, Society of Fire Protection Engineering, Bethesda, Maryland, USA.

Mikola E. 1990. 'Charring of wood'.*Technical Research Paper No. 689.* Technical Research Institute of Finland, VTT. Espoo, Finland.

Standards Association of Australia. 2005. *Methods for fire tests on building materials, components and structures. Fire resistance tests of elements of building construction*. AS1530 Part 4:2005. North Sydney, Australia.

NZS 1170.5:2004, *Structural Design Actions Part 5: Earthquake Actions – New Zealand*, Standards New Zealand (SNZ), Wellington, New Zealand, 2004.

New Zealand Government, "Compliance Document for New Zealand Building Code Clause B1 Structure (Amendment 11)", DBH, Wellington, New Zealand, 2011.

NZS 1170.5 Supp 1:2004, *Structural Design Actions Part 5: Earthquake Actions – New Zealand – Commentary*, SNZ, Wellington, New Zealand, 2004.

AS/NZS 1170.0:2002, *Australian/New Zealand Standard – Structural Design Actions Part 0: General Principles*, SNZ, Wellington, New Zealand, 2002.

Scawthorn C. 'Fire Following Earthquake', *Fire Safety Science – Proceedings of the First International Symposium,* IAFSS, 971–979, 1984.

Nightingale TRT and Sultan MA. 1998. 'Sound Isolation and Fire Resistance of Assemblies with Firestops'. *Construction Technology Update 16*, IRC, National Research Council of Canada, Ottawa, Canada.

Tasligedik AS, Pampanin S and Palermo A. 'Damage States and Cyclic Behaviour of Drywalls infilled within RC Frames'. *Bulletin of the New Zealand Society for Earthquake Engineering*, Vol. 45, No.2, June 2012.

Winstone Wallboards, 'GIB® Fire Rated Systems', 2006, CBI 5113 Winstone Wallboards Ltd.

Winstone Wallboards, 'GIB® Information Bulletin', 2012. Gypsum plasterboard lined partitions in commercial construction update. Winstone Wallboards Ltd. http://gib.co.nz/assets/PDFs/03092GIBGypsumLinedPartitionsManual.pdf accessed 11/3/2013.

Appendix B FIRE TEST 1

The following photographs (Figure 112 to Figure 119) are of the charring progression in the holes at the end of Test 1. The test was stopped at 118 minutes but it was closer to 120 minutes by the time the test specimen was removed from the furnace and burning extinguished. In the samples denoted by an alphabetical character A-X, the key to the locations can be found in Table 2 and Table 3. Where a particular sectioned sample is not shown it was totally consumed (charred) in the test.

Figure 112: Charring in 3 mm holes after 120 minutes (left to right A, E, I, M, Q and U)

Figure 113: Charring in 6 mm holes after 120 minutes (left to right holes B, F, J, N, R and V)

Figure 114: Charring in 12 mm holes after 120 minutes (left to right holes K, O, S and W)

Figure 115: Charring in 24 mm hole after 120 minutes (X)

Figure 116: Charring in 3 to 12 mm holes at 2.2 Pa after 120 minutes (left to right I, J and K)

Figure 117: Charring in 3 to 12 mm holes at -2.52 Pa after 120 minutes (left to right M, N and O)

Figure 118: Charring in 3 to 24 mm holes at -7.24 Pa after 120 minutes (left to right Q, R, S and T)

Figure 119: Charring in 3 to 24 mm holes at -11.96 Pa after 120 minutes (left to right U, V, W and X)

DISCLAIMER

The results obtained in this study relate only to the un-named products tested and not to any other item of the same or similar description. BRANZ Ltd does not necessarily test all brands or types available within the class of items tested and exclusion of any brand or type is not to be taken as any reflection upon it.

Furthermore, construction methods and specifications of the tested samples may deviate from those specified by the manufacturers, not to mention artificial and deliberate defects that were included for the purposes of gaining knowledge of the relative rather than absolute performances and does not imply the performance is better or worse than any other available product.

A laboratory test may not be exactly representative of the performance of the item in general use. Also, certain parameters in this set of experiments may have altered the performance. Therefore, any conclusion drawn should only be in relative terms and not taken as absolute, some construction details may differ from actual practice.

This work was carried out for specific research purposes and BRANZ may not have assessed all aspects of the products which would be relevant in any specific use. For this reason, BRANZ disclaims all liability for any loss or other deficit following use of the products, which is claimed to be based on reliance on the results published here.